

CENTRAL RESEARCH LIBRARY.

ORNL-4918

LOCKHEED MARTIN ENERGY RESEARCH LIBRARIES



3 4456 0515605 0

Cy 1

HEAVY-SECTION STEEL TECHNOLOGY PROGRAM
SEMIANNUAL PROGRESS REPORT
FOR PERIOD ENDING FEBRUARY 28, 1973

OAK RIDGE NATIONAL LABORATORY
CENTRAL RESEARCH LIBRARY
DOCUMENT COLLECTION

LIBRARY LOAN COPY

DO NOT TRANSFER TO ANOTHER PERSON

If you wish someone else to see this
document, send in name with document
and the library will arrange a loan.

UCN-7969
(3 3-67)



OAK RIDGE NATIONAL LABORATORY

OPERATED BY UNION CARBIDE CORPORATION • FOR THE U.S. ATOMIC ENERGY COMMISSION

Printed in the United States of America. Available from
the U.S. Atomic Energy Commission, Technical Information Center
P.O. Box 62, Oak Ridge, Tennessee 37830
Price: Printed Copy \$5.45 ; Microfiche \$1.45

This report was prepared as an account of work sponsored by the United States Government. Neither the United States nor the United States Atomic Energy Commission, nor any of their employees, nor any of their contractors, subcontractors, or their employees, makes any warranty, express or implied, or assumes any legal liability or responsibility for the accuracy, completeness or usefulness of any information, apparatus, product or process disclosed, or represents that its use would not infringe privately owned rights.

ORNL-4918
UC-78 - Light-Water
Reactor Technology

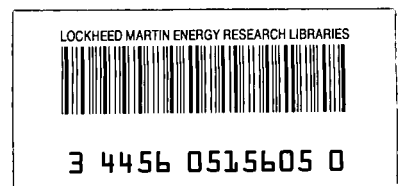
Contract No. W-7405-eng-26

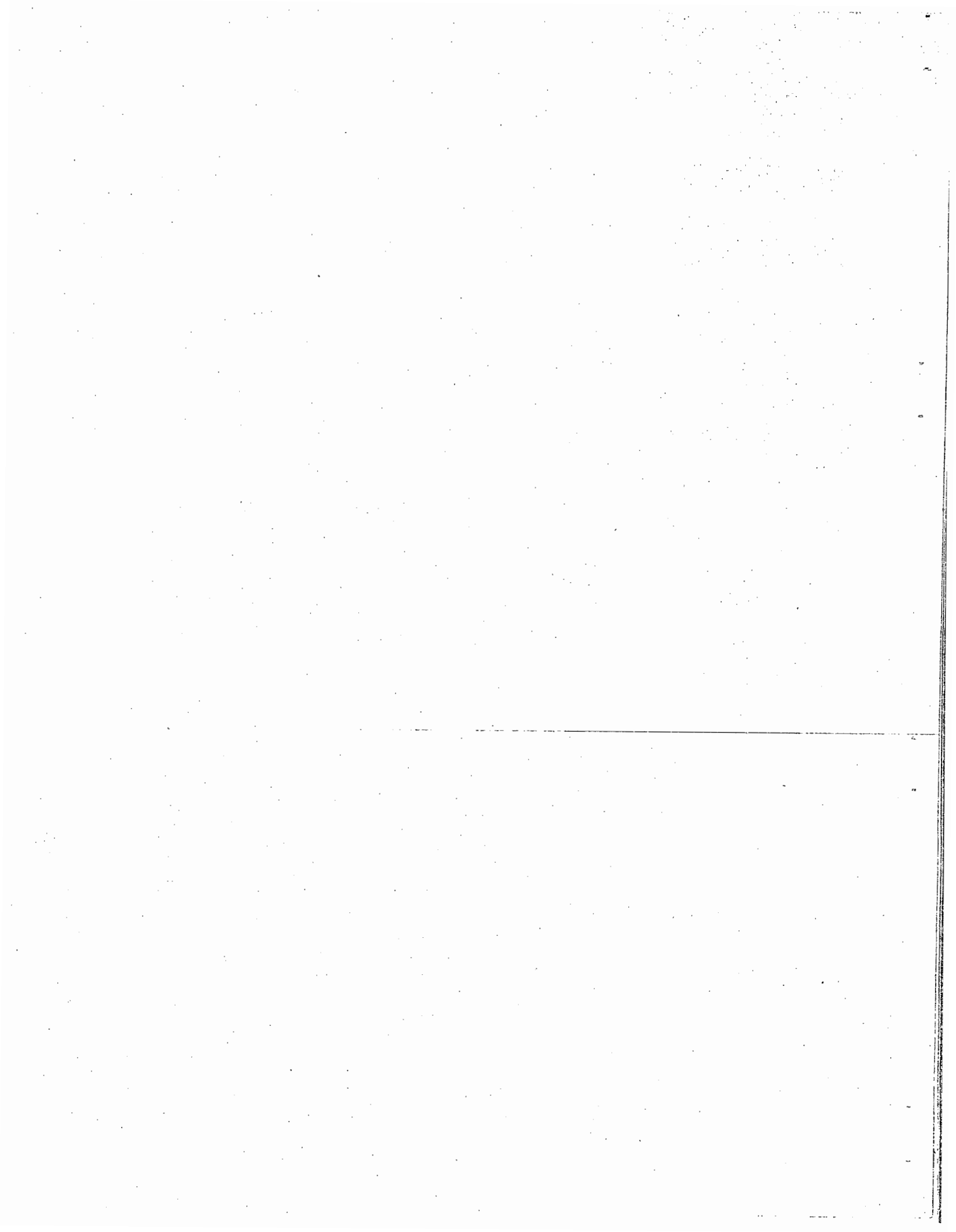
HEAVY-SECTION STEEL TECHNOLOGY PROGRAM
SEMIANNUAL PROGRESS REPORT
For Period Ending February 28, 1973

F. J. Witt, Program Director

FEBRUARY, 1974

OAK RIDGE NATIONAL LABORATORY
Oak Ridge, Tennessee 37830
operated by
UNION CARBIDE CORPORATION
for the
U.S. ATOMIC ENERGY COMMISSION





CONTENTS

	<u>Page</u>
FOREWORD	v
SUMMARY	vii
1. PROGRAM ADMINISTRATION AND PROCUREMENT	1
2. INVESTIGATIONS OF UNIRRADIATED MATERIALS	3
FRACTURE TOUGHNESS CHARACTERIZATION OF HSST WELDMENT MATERIAL	3
Introduction	3
Specimen Fabrication	4
Test Program	4
Test Results	7
INVESTIGATION OF WELD METAL HEAT-AFFECTED ZONE	9
CRACK INITIATION IN TESTING PRECRACKED CHARPY SPECIMENS	10
EXPERIMENTAL AND ANALYTICAL ELASTIC-PLASTIC FRACTURE THEORIES EVALUATION PROGRAM	10
Introduction	10
Experimental Program	13
Analytical Program	21
EFFECT OF HIGH-TEMPERATURE PRIMARY REACTOR WATER ON THE SUBCRITICAL CRACK GROWTH OF REACTOR VESSEL STEEL	27
Experimental Procedure	27
Experimental Results	28
Ad Hoc Task Group on Fatigue	28

3.	INVESTIGATIONS OF IRRADIATED MATERIALS	31
	IRRADIATION EFFECTS ON THE FRACTURE OF HEAVY-SECTION PRESSURE VESSEL STEELS	31
	The Effect of Irradiation on the Fracture Toughness of A533-B; Lower-Bound Evaluation Using C_V CT Specimens	31
	Fatigue-Crack Propagation of ASTM A533, Grade B, Class 1 Steel	36
	Effect of cyclic frequency	39
	Effect of stress ratio	39
	Fracture Toughness Characterization of Irradiated A533, Grade B, Class 1 Steel Using $4T$ Compact-Tension Specimens	41
	Specimen encapsulation	41
	Specimen irradiation	45
4.	PRESSURE VESSEL AND PIPING INVESTIGATIONS	53
	CHARACTERIZATION OF INTERMEDIATE TEST VESSEL MATERIALS	53
	FRACTURE TOUGHNESS CHARACTERIZATION OF HSST INTERMEDIATE PRESSURE VESSEL MATERIAL	60
	Introduction	60
	Specimen Fabrication	61
	Test Program	61
	Test Results	64
	FRACTOGRAPHY STUDY OF FAILURE IN INTERMEDIATE TEST VESSEL V-1	68
	Fracture Propagation	69
	Fractography Study	71
	PROCUREMENT OF INTERMEDIATE TEST VESSELS	73
	TESTING OF 6-IN.-THICK INTERMEDIATE TEST VESSELS	77
	Vessel V-2	77
	Vessel V-3	82
	Vessel V-4	87
	Summary of Results and Future Plans	93
	INVESTIGATION OF MODE III CRACK EXTENSION IN REACTOR PIPING	93
	Introduction	93
	Results of Experiments 37 and 38	96
	Future Work	99

FOREWORD

The Heavy-Section Steel Technology (HSST) Program is a USAEC-sponsored effort for investigating the effects of flaws, variations of properties, stress raisers, and residual stress on the structural reliability of present and contemplated water-cooled reactor pressure vessels. The cognizant engineer for the USAEC is J. R. Hunter, and at ORNL the program is under the Pressure Vessel Technology Program, of which G. D. Whitman is Director. The program is being carried out in very close cooperation with the nuclear power industry. Prior reports in this series are ORNL-4176, ORNL-4315, ORNL-4377, ORNL-4463, ORNL-4512, ORNL-4590, ORNL-4653, ORNL-4681, ORNL-4764, ORNL-4816, and ORNL-4855.

SUMMARY

The Heavy-Section Steel Technology (HSST) Program is one of the major USAEC safety engineering research programs devoted to extending and developing the technology for quantitatively assessing the margins of safety against fracture of the primary containment systems of civilian water reactors. Emphasis is on the massive pressure vessels of these sophisticated systems. Practically all areas of materials technology as related to the pertinent steels and weldments have been or are being investigated. The investigations in progress are discussed in this report; prior reports in this series are identified in the Foreword.

Eight technical reports were issued during this reporting period. The fifth and sixth 6-in.-thick intermediate test vessels were received, and four additional vessels are in various stages of fabrication.

Weldment material from HSST weldment 57E has been fabricated into 1T and 6T compact-tension specimens. Twelve of these specimens have been tested at temperatures between -150 and 540°F in order to characterize the fracture toughness of this weldment using the equivalent-energy concept.

A continuation of the investigation of possible heat-affected zone cracking of submerged-arc welds of ASTM A508, class 2 steel has disclosed no evidence of sensitivity to cracking.

An investigation of crack growth of Charpy V specimens during the slow-bend mode of testing and at a deflection rate of 0.100 in./min indicated that the crack growth initiates at the initial peak load.

A combined experimental and analytical program is in progress to evaluate the engineering usefulness of the two leading theories of elastic-plastic fracture: the equivalent-energy approach and the J -integral approach. Under the experimental portion of the program, six compact-tension specimens have been tested, and fracture toughness values obtained using both theories were shown to be in good agreement. The first center-cracked (fracture theories evaluation) specimen was tested during this report period, and an additional 50 fracture toughness specimens have been machined.

A full elastic-plastic analysis of the fracture theories evaluation specimen was completed, and the agreement between the analytical and experimental load-displacement records was reasonably good. Fracture predictions made from the analytical data using both fracture theories were also in good agreement.

The program to attain fatigue-crack-growth data in PWR and BWR primary coolant water continued. Data from three low-frequency fatigue-crack-growth tests in PWR and BWR environments were evaluated in terms of da/dn vs ΔK . The results indicate a significantly higher growth rate than was expected from high-frequency tests. A low-frequency test in an air environment was run to determine if the indicated frequency sensitivity is strictly a corrosion effect.

Charpy thickness compact-tension specimens were used to determine lower-bound fracture toughness, $K_{Ic.394}$, for ASTM A533, grade B, class 1 steel irradiated to 5.3 to 5.7×10^{19} neutrons/cm² ($E > 1$ MeV) at 550°F and 8×10^{19} neutrons/cm² ($E > 1$ MeV) at 540°F. Compared with unirradiated data, the irradiation shift in transition was 180 and 290°F for the low and high fluences respectively. No degradation of upper-shelf behavior was observed after irradiation.

The effect of cyclic frequency on crack propagation was compared at 1 and 600 cpm at room temperature and at 500°F in air. The fatigue-crack propagation behavior of A533-B was essentially the same at both temperatures and cyclic frequencies.

The stress ratio effect on fatigue-crack propagation was correlated for A533-B using an effective stress ratio. Data over a stress ratio range from $R = 0$ to $R = 0.8$ were correlated for tests conducted at 550°F.

Six 4T compact-tension (CT) specimens are being irradiated in the Battelle Research Reactor (BRR) to midthickness fluence levels of 5×10^{19} neutrons/cm² ($E > 1$ MeV). Three irradiation capsules were fabricated and six 4T CT specimens, two per capsule, were encapsulated. Additional smaller specimens, Charpy V-notch, tensile, and 0.4T CT specimens, were also encapsulated. The three capsules were inserted into the BRR and presently are undergoing neutron bombardment.

Prolongations of intermediate vessels V-2, V-3, and V-4 were studied to obtain tensile, Charpy-V impact, and static lower-bound fracture toughness data. These data were used to assist in setting the fracture criteria and in predicting failure as was done for vessel V-1 prior to rupturing the vessel.

Weldment and base-metal material from the third and fourth HSST intermediate pressure vessels was fabricated into 0.394T, 0.85T, 3T, and 4T CT specimens. These specimens were tested over a temperature range of 0 to 200°F to establish a lower-bound curve of the fracture toughness of the pressure vessel material using the equivalent-energy concept.

A study of the fracture surface of intermediate test vessel V-1 revealed a mixed mode of fracture. Initial crack growth is by ductile tearing. The growth is by tunneling and continues until the flaw size is such that unstable crack growth can occur. This results in a transition from a dimpled fracture mode to one wherein cleavage was the mode of failure.

Difficulty was experienced by Taylor Forge in producing welds free of any rejectable indications on intermediate test vessels V-4, V-5, and V-6 as inspected ultrasonically by the stringent conditions imposed. After vessel V-4 was repaired, the welds were found to be acceptable on final inspection. After several repair attempts on vessels V-5 and V-6, rejectable indications remained. These indications were located in such a position that they could be tolerated during testing. Therefore, these vessels were accepted with these imperfections.

During this reporting period, three intermediate test vessels (V-2, V-3, and V-4) were flawed, instrumented, and pressurized to destruction. Pressure, strain, and crack-opening-displacement measurements were successfully obtained from all the tests. Inaccuracies in monitoring crack

growth during the sharpening of the flaws in vessels V-3 and V-4 led to fracture behavior somewhat different than anticipated.

Work continued on the investigation of mode III - tearing shear fracture in nuclear reactor piping. To date, four full-scale rupture experiments have been conducted. Based upon the last two tests, it appears that reservoirs as employed on experiment 32 will be required to obtain extensive mode III fracture propagation.

1. PROGRAM ADMINISTRATION AND PROCUREMENT

The Heavy-Section Steel Technology (HSST) Program is one of the major safety engineering programs concerned with the structural integrity of the primary containment systems of civilian water-reactor power stations. The main effort in the program is to extend and develop the technology for quantitatively assessing the margins of safety against fracture of these sophisticated systems, with emphasis on the massive pressure vessels. Practically all areas of materials technology relating to the steels and weldments used in fabricating the vessels of present and contemplated plants in the United States have been or are being investigated.

While very substantial efforts have been directed to the variability of properties among and within various product forms, metallurgical studies, the variables that affect fatigue-crack growth behavior, and the effect of fast-neutron irradiation on the steels, the paramount emphasis has been on the load-flaw size-toughness relationships from which fracture will initiate and/or propagate. The program is coordinated with efforts by other government agencies and the manufacturing and utility sectors of the nuclear power industry both in the United States and abroad. These total efforts should result in the quantification of safety assessments which are needed by the USAEC regulatory bodies, the professional code-writing bodies, and the nuclear power industry.

The activities of the program are carried out under 12 separate tasks. Several of the task activities are performed under subcontract by research facilities throughout the United States and through informal cooperative

efforts abroad. Currently there are eight research and development sub-contracts in force.

Eight technical reports were issued during this reporting period.¹⁻⁸ The major procurement items of the HSST program are the intermediate test vessels; six have been received and four more are in various stages of fabrication.

Administratively, the HSST program is carried out as task activities; however, for reporting purposes here, the research areas are discussed under investigations of unirradiated materials, investigations of irradiated materials, and pressure vessel and piping investigations.

1. S. C. Grigory, *Tests of Six-Inch-Thick Flawed Tensile Specimens, Third Technical Summary Report, Longitudinal Specimens Numbers 14 through 16, Unflawed Specimen Number 17*, HSSTP-TR-22, Southwest Research Institute (August 1972).

2. L. A. James and J. A. Williams, *The Effect of Temperature and Neutron Irradiation upon the Fatigue-Crack Propagation Behavior of ASTM A 533-B Steel*, HEDL-TME-72-132, Hanford Engineering Development Laboratory (September 1972).

3. F. J. Witt and T. R. Mager, *A Procedure for Obtaining Bounding Values on K_{Ic} at Any Temperature*, ORNL-TM-3894 (October 1972).

4. A. A. Abbatiello and R. W. Derby, *Notch Sharpening in the Large Tensile Specimens by Local Fatigue*, ORNL-TM-3925 (November 1972).

5. S. P. Ying and S. C. Grigory, *Tests of 6-inch-thick Tensile Properties, Fifth Technical Summary Report, Acoustic Emission Monitoring of one-inch-thick and six-inch-thick Tensile Specimens*, HSSTP-TR-24, Southwest Research Institute (November 1972).

6. S. A. Legge, *Analysis and Experimental Verification of the Thermal Behavior of a four-inch Steel Section Undergoing Nuclear Heating*, WCAP-8022, Westinghouse Electric Corporation (December 1972).

7. J. G. Merkle, *An Elastic-Plastic Thick-Walled Hollow Cylinder Analogy for Analyzing the Strains in the Plastic Zone Just ahead of a Notch Tip*, ORNL-TM-4071 (January 1973).

8. P. B. Crosley and E. J. Ripling, *Crack Arrest in an Increasing K -Field*, HSSTP-TR-27, Materials Research Laboratory (January 1973).

2. INVESTIGATIONS OF UNIRRADIATED MATERIALS

The materials investigations under the HSST program are divided into studies of unirradiated materials and studies of irradiation effects. The studies of unirradiated materials, which include inspection, characterization, metallurgy, variability determinations, transition temperature investigations, fracture mechanics studies, and fatigue-crack propagation tests, are discussed here. No work specifically under the transition temperature task is in progress. Additional results for unirradiated materials are presented in Chapter 3, and inspections and material properties results related to the intermediate vessel tests are presented in Chapter 4.

FRACTURE TOUGHNESS CHARACTERIZATION OF HSST WELDMENT MATERIAL¹

P. C. Riccardella L. R. Singer

Introduction

Extensive fracture toughness data have been obtained on reactor vessel plate and forging materials as part of the HSST program.²⁻⁵ However,

1. Work sponsored by the HSST program under UCCND Subcontract No. 3196 between Union Carbide and Westinghouse Electric Corporation.

2. F. J. Witt, "A Procedure for Determining Bounding Values on Fracture Toughness K_{Ic} at Any Temperature," HSST 5th Annual Information Meeting, Paper 13, March 1971.

3. T. R. Mager, *Fracture Toughness Characterization Study of A533, Grade B, Class 1 Steel*, HSST Program Technical Report No. 10 (October 1970).

only limited data are available for weldment materials used in fabricating reactor vessels.⁵ The objective of this program is to study the fracture toughness characteristics of a plate weldment which was prepared using procedures analogous to those used in reactor vessel fabrication (HSST weldment 57E).

Specimen Fabrication

Nineteen compact-tension (CT) specimens have been fabricated from HSST weldment 57E. These specimens include three 6T CT (6-in.-thick, compact-tension) specimens which were machined from the main weld as shown in Fig. 2.1. The remaining 16 specimens are 1T CT specimens machined from the weld intersection region as shown in Fig. 2.2. Five of these specimens were taken directly from the weld intersection, and eleven were taken from the main weld in the vicinity of that intersection. The five specimens from the intersection were taken in two different orientations to determine the effect of crack orientation on the data.

Test Program

Twelve of these nineteen specimens have been tested at temperatures ranging between -150 and $+540^{\circ}\text{F}$ during this report period. The fracture toughness of this weldment is so high in this temperature range that very large specimens would be necessary to perform valid fracture toughness testing according to the ASTM recommended procedure.⁶ Therefore the equivalent-energy concept² was used to interpret the data in terms of lower-bound values of actual fracture toughness.

4. T. R. Mager, "Experimental Verification of Lower Bound K_{IC} Values Utilizing the Equivalent Energy Concept," HSST 6th Annual Information Meeting, Paper 23, April 1972.

5. W. O. Shabbits, W. H. Pryle, and E. T. Wessel, *Heavy Section Fracture Toughness Properties of A533 Grade B, Class 1 Steel Plate and Submerged Arc Weldment*, HSST Program Technical Report No. 6 (December 1969).

6. Tentative Method of Test for Plane-Strain Fracture Toughness of Metallic Materials, ASTM E399-70T.

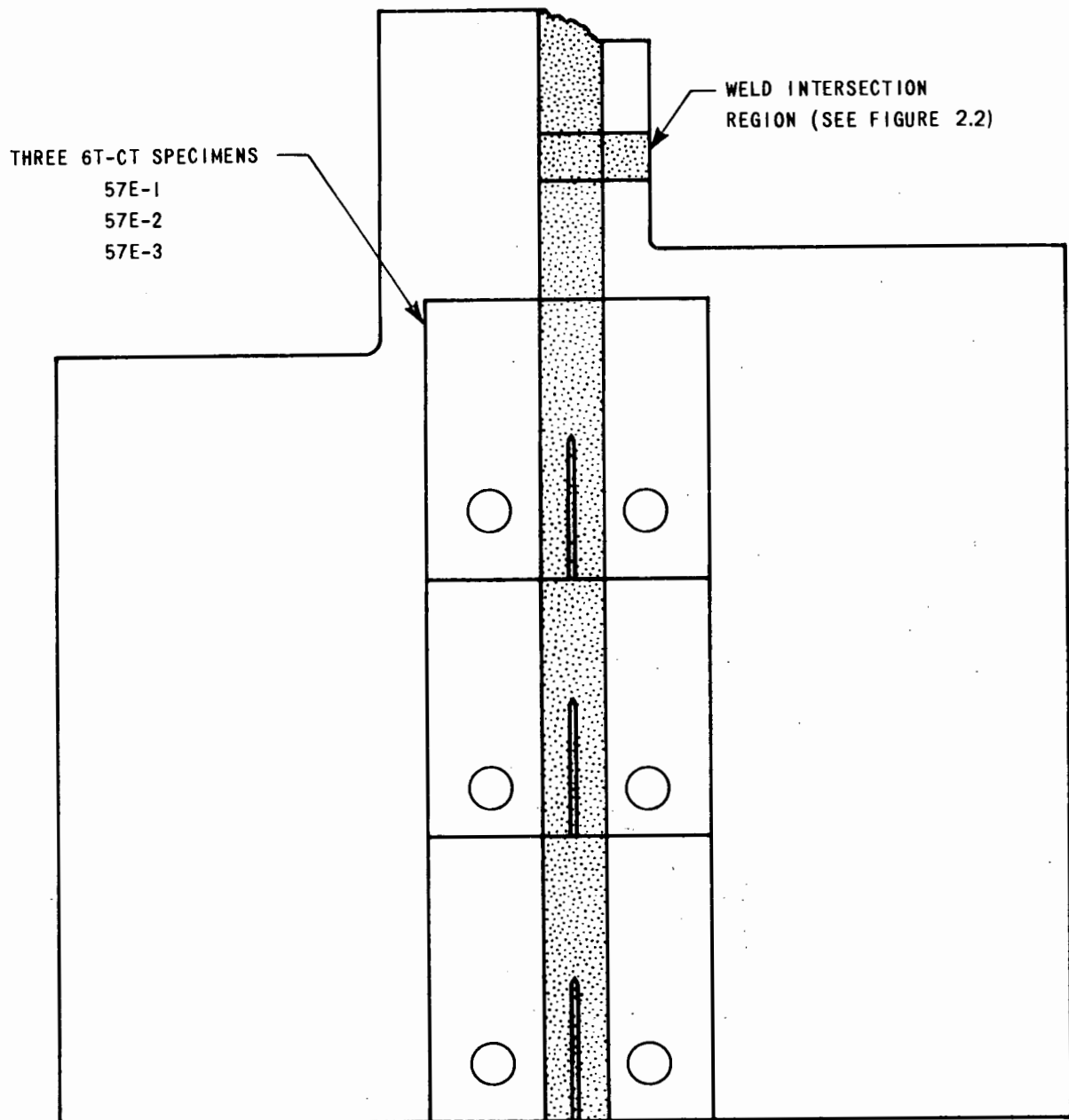


Fig. 2.1. Machining of fracture toughness specimens from HSST weldment 57E.

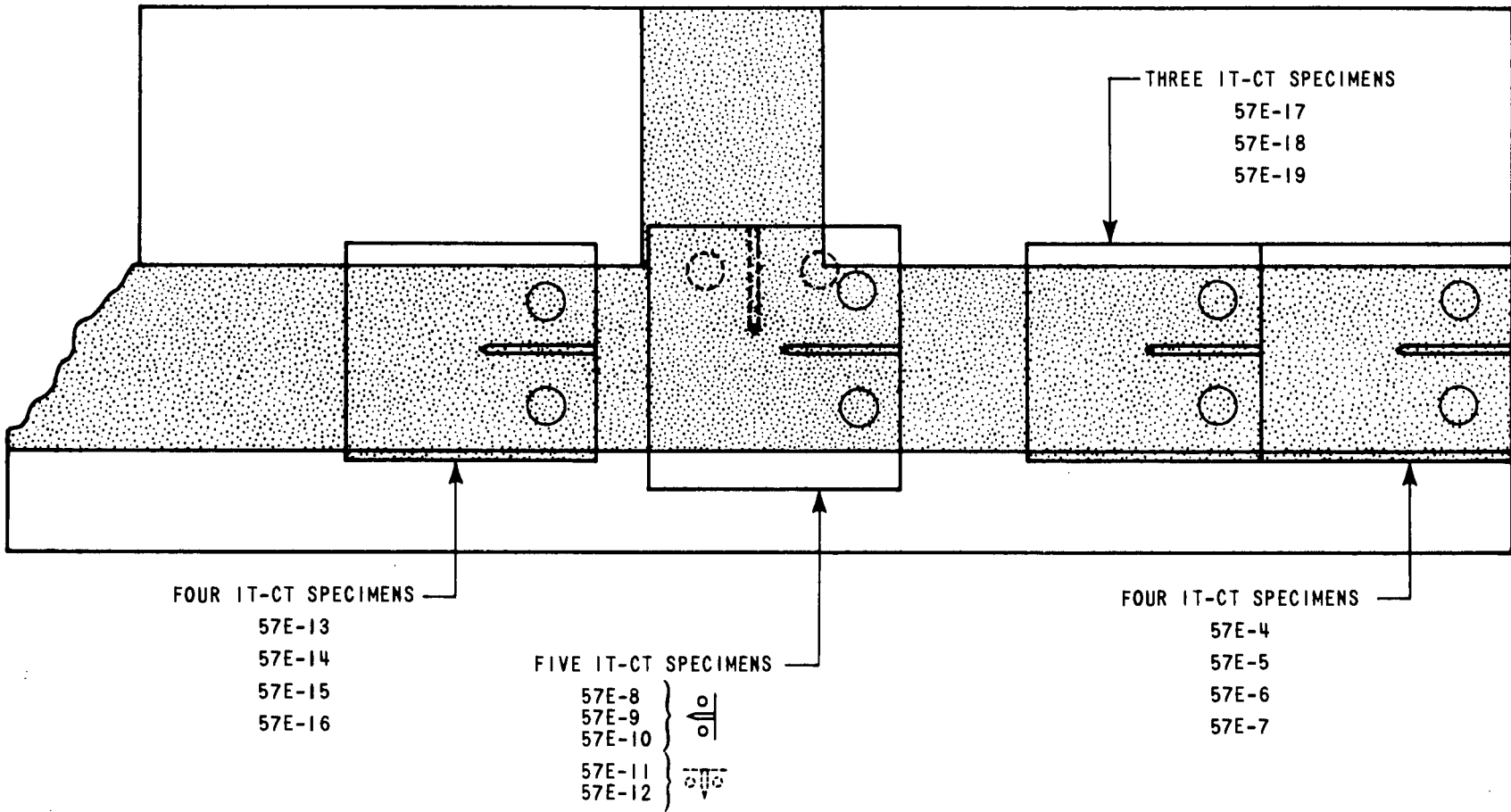


Fig. 2.2. Machining of fracture toughness specimens from weld inter-section region of HSST weldment 57E.

Test Results

The resulting fracture toughness data from these tests are summarized in Table 2.1 and are illustrated graphically in Fig. 2.3. Comparisons of these data with previous fracture toughness data for base metal^{3,4} indicate that this weldment is significantly tougher. Furthermore, these tests indicate that the toughness of the weld intersection is not significantly different than that of the main weld. Temperatures have been chosen for testing the remaining seven specimens to fill in the gaps in the data presented in Fig. 2.3.

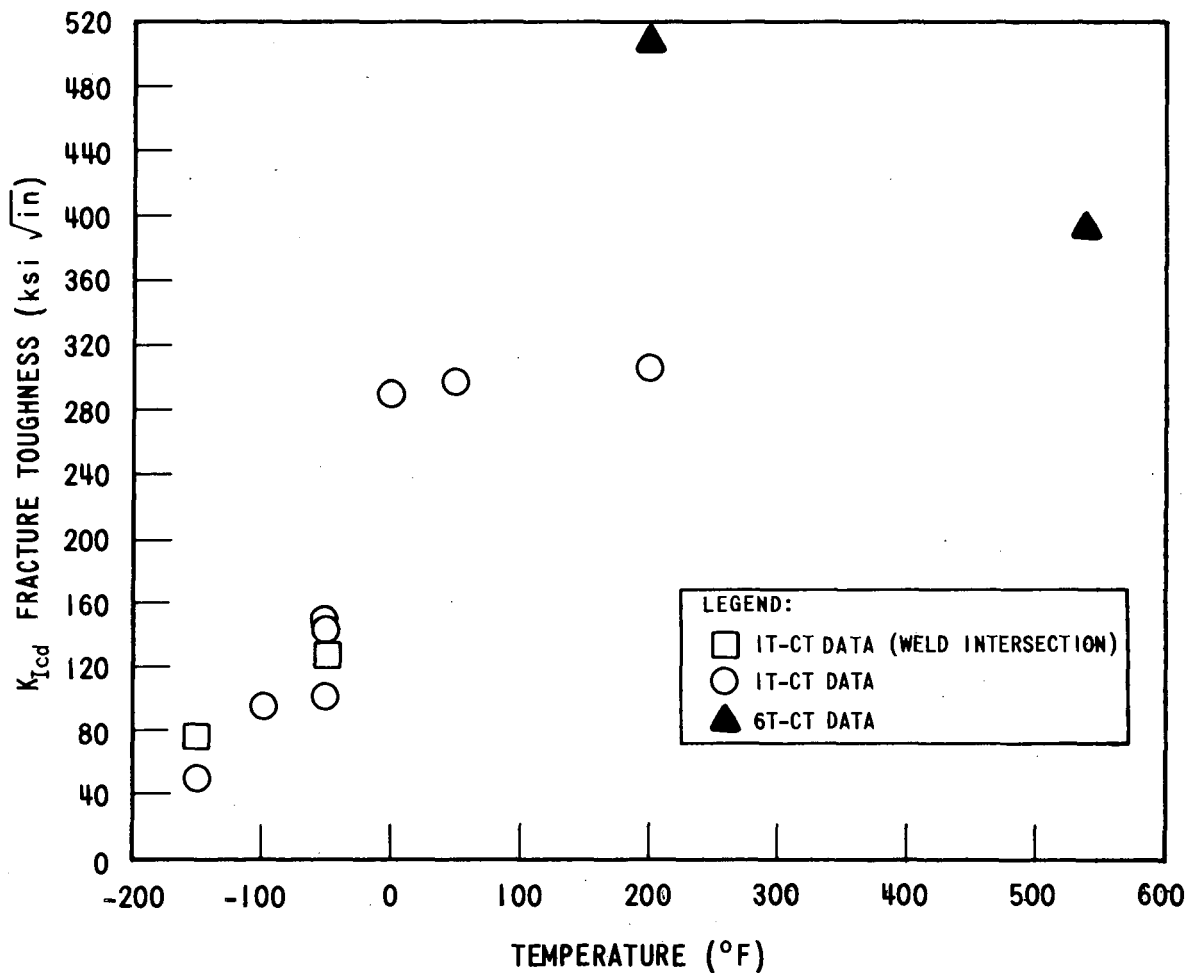


Fig. 2.3. Fracture toughness data for HSST weldment 57E.

Table 2.1. Fracture toughness results determined from testing 1T and 6T compact-tension specimens from HSST weldment 57E

Specimen No.	Test temp. (°F)	Crack length (in.)	Maximum load (lb)	Energy to maximum load (in.-lb)	P_Q (lb)	Energy to P_Q (in.-lb)	K_{Icd} (ksi $\sqrt{\text{in.}}$)
1T Compact-tension specimens							
57E-17	-150	1.037	6,800	48.0	4,000	16.5	49.0
57E-8	-150	1.027	10,390	116.6	4,000	16.0	76.3
57E-4	-100	1.038	12,200	194.8	4,000	16.0	97.5
57E-11	-50	1.040	12,440	199.7	4,000	16.0	102.0
57E-9	-50	1.037	14,120	320.3	4,000	16.0	128.5
57E-18	-50	1.023	15,100	445.1	4,000	17.0	144.0
57E-13	-50	1.047	14,570	432.0	4,000	16.5	149.3
57E-5	±0	1.038	15,530	1,573.0	4,000	15.5	290.1
57E-14	+50	1.055	14,930	1,612.8	4,000	16.0	297.0
57E-15	+200	1.043	15,180	1,993.2	4,000	18.0	305.4
6T Compact-tension specimens							
57E-2	+200	6.133	512,000	197,050.0	100,000	1550.0	511.0
57E-3	+540	6.133	490,000	118,460.0	100,000	1760.0	391.0

INVESTIGATION OF WELD METAL HEAT-AFFECTED ZONE

D. A. Canonico

In the last HSST semiannual report,⁷ we described the investigation being conducted on the heat-affected zone of welds made between two plates of ASTM A533, grade B, class 1 steel. No evidence of cracking in the heat-affected zone was reported. We have continued the investigation of those welds and have as yet to uncover any evidence of cracking.

During this report period, we initiated a study of the heat-affected zone of a longitudinal weld in the prolongation from the intermediate test vessel V-3. The vessel is fabricated from ASTM A508, class 2 steel, which has been identified as having a higher sensitivity to heat-affected zone cracking.⁸ We have longitudinally sectioned a piece of the weld and prepared it for study, as shown in Fig. 2.4. The individual specimens are

7. D. A. Canonico, *HSST Program Semiannu. Progr. Rep. Aug. 31, 1972*, ORNL-4855, pp. 3-6.

8. Private communication, K. Kussmaul, MPA Stuttgart, West Germany, 1972 annual information meeting of the HSST program.

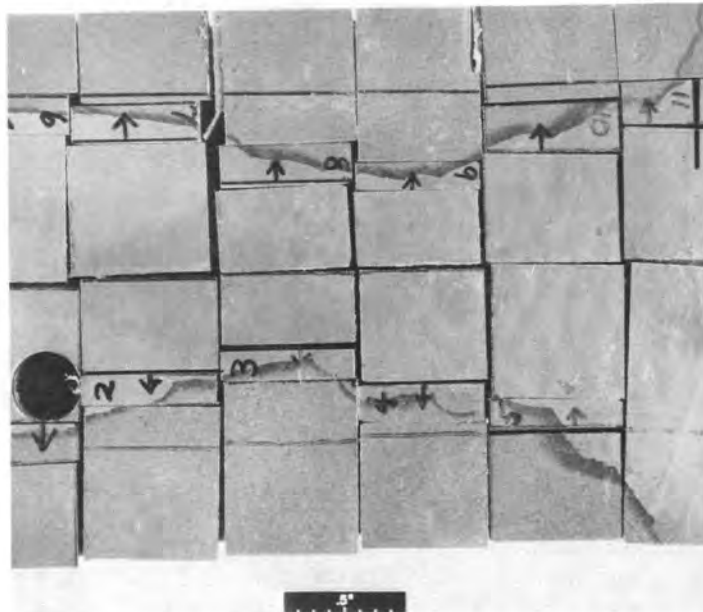


Fig. 2.4. Photograph of a weld section from the prolongation of intermediate test vessel 3. The numbers identify each specimen, which is mounted, polished, and metallographically studied on the surface identified by the arrows.

numerically identified, and the arrows point to the surface being investigated. Considerable time and effort have been spent in preparing and metallographically viewing the specimens. Figure 2.5 contains two typical metallographic mounts. No evidence of cracks in the heat-affected zone of any of the 11 specimens has been detected.

CRACK INITIATION IN TESTING PRECRACKED CHARPY SPECIMENS

W. J. Stelzman

A study was made to determine when crack growth initiates in pre-cracked Charpy specimens during slow-bend testing. The slow-bend test was interrupted at various stages of bending and immediately unloaded. Figure 2.6 shows a typical load-deflection (time) trace, the test interruptions, and subsequent extension. The partially bent specimen was placed in a 900°F furnace for 2 hr, during which the fatigue crack and extension, if any, were blue tinted. After the specimen was removed and cooled to room temperature, it was immersed in liquid nitrogen and fractured. The extension was then measured on a traveling stage microscope. This method of investigation shows that crack growth during the slow-bend mode of testing and at a deflection rate of 0.100 in./min initiates at the initial peak load. At the test temperature (75°F), the tip of the fatigue crack deformed plastically prior to crack initiation. This crack elongation, usually referred to as "the stretch zone," was from 0.002 to 0.005 in. prior to peak load.

EXPERIMENTAL AND ANALYTICAL ELASTIC-PLASTIC FRACTURE THEORIES EVALUATION PROGRAM⁹

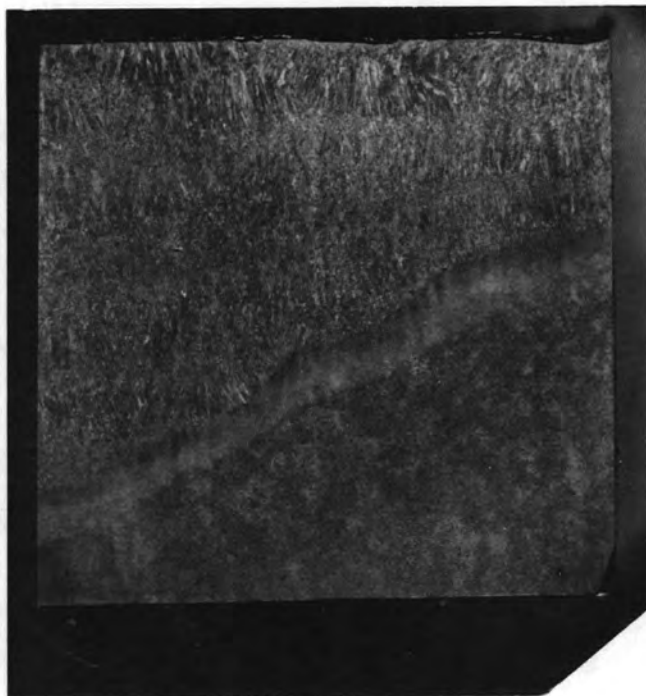
P. C. Riccardella J. L. Swedlow

Introduction

The two leading theories of elastic-plastic fracture (J -integral and equivalent-energy) have not yet been subjected to a critical evaluation to demonstrate their applicability to complex loading and geometric

9. Work sponsored by HSST program under UCCND Subcontract No. 3196 between Union Carbide and Westinghouse Electric Corporation.

PHOTO Y-II7470



Specimen No. 4

PHOTO Y-II7475



Specimen No. 9

Fig. 2.5. Photomicrographs (original magnification, 3.5 \times) of metallographic specimens identified as Nos. 4 and 9 in Fig. 2.4. These photomicrographs represent the specimens under study. Extensive microscopic studies are conducted at the weld metal-base metal junction.

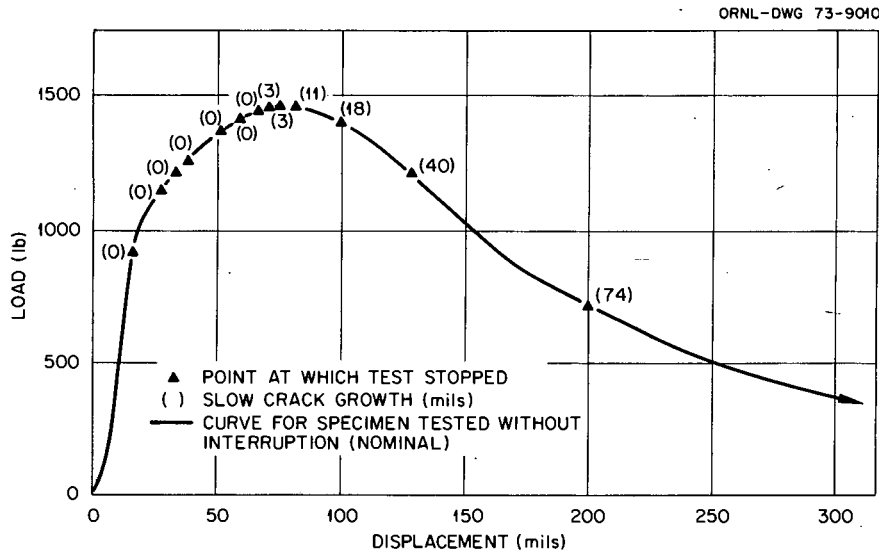


Fig. 2.6. Slow stable crack growth in precracked Charpy specimens obtained by interrupting the load at various deflections. Specimens tested in the slow-bend mode.

configurations typical of those that exist in nuclear reactor pressure vessels. Both theories rely heavily on the experimental load-deflection curve of a test specimen to predict failure. However, in a reactor vessel, no single parameter represents applied load and no single displacement value is pertinent to the overall problem. The degree of loading can only be estimated using sophisticated, two-dimensional analysis techniques, such as the finite-element technique, which are capable of considering geometric discontinuities, pressure stresses, and complex thermal gradients.

The objective of this program was to apply both fracture theories to a relatively simple test specimen using a two-dimensional, finite-element computer program which has enough generality that it can later be applied to more complex reactor vessel problems. The test specimen chosen was a center-cracked plate geometry [hereafter referred to as the fracture theories evaluation (FTE) specimen].¹⁰ Critical failure parameters (load and deflection) were predicted by both fracture theories

10. P. C. Riccardella and J. L. Swedlow, *HSST Program Semiannu. Progr. Rep. Aug. 31, 1972*, ORNL-4855, pp. 7-12.

from the analysis and the accuracy of the predictions evaluated by comparison with actual experimental results.

To ensure a meaningful evaluation of the two theories, the tests were performed in the transition range between linear-elastic (frangible) behavior and limit-load (fully ductile) behavior. To satisfy this constraint, a test temperature of +50°F was chosen.

Experimental Program

Two 4T CT specimens and four 2T CT specimens were machined from HSST plate section 04-A.¹⁰ The specimens were all oriented in the longitudinal (RW) direction and were all taken from approximately the center thickness location. These specimens were tested at +50°F, and fracture toughness evaluations were performed using both the J -integral (J_{Ic})¹¹ and the equivalent-energy (K_{Icd})¹² interpretations as shown in Table 2.2. Note

11. R. J. Bucci et al., "J-Integral Estimation Procedures," in *Fracture Toughness*, Proceedings of the 1971 National Symposium on Fracture Mechanics, part II, ASTM STP-514 (1972).

12. T. R. Mager, "Experimental Verification of Lower Bound K_{Ic} Values Utilizing the Equivalent Energy Concept," HSST Program 6th Annual Information Meeting, Apr. 25-26, 1972.

Table 2.2. Results of compact-tension tests

Specimen designation	Size, B	J -integral interpretation		Equivalent-energy interpretation	
		J_{Ic} (in.-lb/in. ²)	K_{Ic} (ksi $\sqrt{\text{in.}}$)	J_{Icd} (in.-lb/in. ²)	K_{Icd} (ksi $\sqrt{\text{in.}}$)
04A-1	4T	339.4	105.8	382.5	112.3
04A-2	4T	289.2	97.6	347.3	107.0
04A-3	2T	359.5	108.9	400.5	114.9
04A-4	2T	315.5	102.0	353.8	108.0
04A-5	2T	466.5	124.0	458.2	122.9
04A-6	2T	391.0	113.5	383.2	112.4
Average		360.2	108.6	387.6	112.9
Std. dev., σ		62.8	9.3	39.9	5.7
3 σ		188.4	27.9	119.7	17.1

that the average values of fracture toughness, as evaluated by both interpretations, are approximately the same. However, the standard deviation of the data is significantly greater for the J -integral interpretation. The greater scatter in the J -integral data can be attributed to the fact that it utilizes total energy to fracture to measure toughness and as such is sensitive to variations in the displacement calibration of the test. On the other hand, the equivalent-energy interpretation utilizes only energy ratios to measure toughness and therefore is insensitive to displacement calibration. (In fact, none is required.)

The K_{Icd} values from Table 2.2, along with $\pm 3\sigma$ scatter band for the data, are plotted as a function of specimen size in Fig. 2.7. Similar data from the J -integral interpretation are given in Fig. 2.8. The valid linear-elastic fracture mechanics specimen size requirement¹³ and the proposed J -integral specimen size requirement¹⁴ are included on these figures. The specimens which were tested are significantly smaller than the linear-elastic requirement but larger than the proposed J -integral requirements.

To further evaluate the statistical variability of the two toughness measurement schemes, a series of additional fracture toughness specimens were machined from HSST plate 04-A in the same orientation and location. These included ten 1T compact-tension, twenty 0.4T compact-tension, and twenty precracked Charpy V-notch specimens (Fig. 2.9). These specimens were also tested at +50°F.

The first fracture theories evaluation (FTE) specimen¹⁰ was tested at +50°F. This was the thinnest (1 in.) of those to be tested. Experimental load vs gage displacement data for this specimen are plotted in Fig. 2.10, and the fracture surface is shown in Fig. 2.11. Two important items of information can be discerned from the appearance of the fracture surface: (1) very large shear lips were present, which indicates that

13. "Tentative Method of Test for Plane Strain Fracture Toughness of Metallic Materials," ASTM-E399-70T, *Annual Book of ASTM Standards*, 1970.

14. J. R. Rice, "A Path Independent Integral and the Approximate Analysis of Strain Concentration by Notches and Cracks," *Trans. ASME, J. Appl. Mech.* (June 1968).

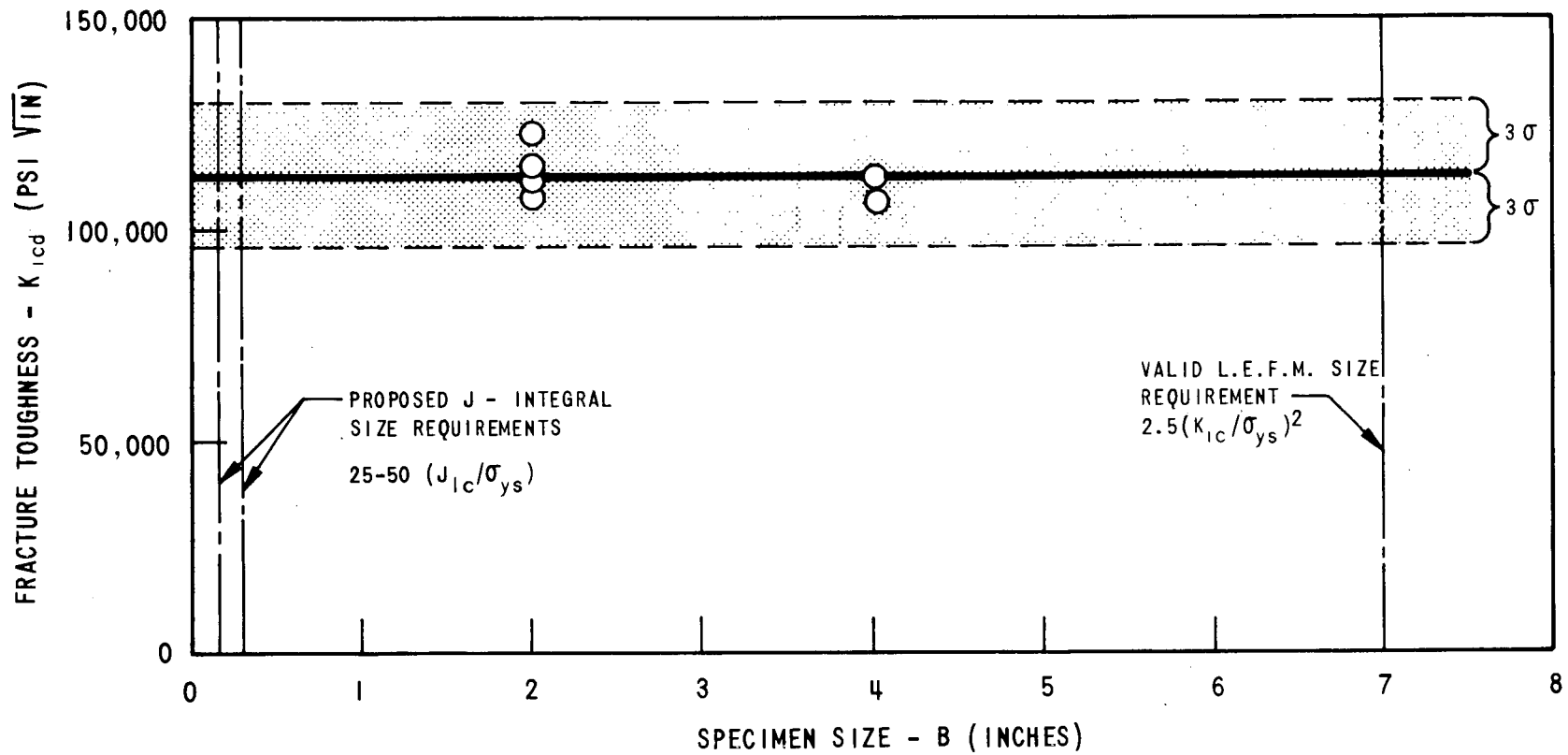


Fig. 2.7. Fracture toughness data from HSST plate 04-A using the equivalent-energy interpretation.

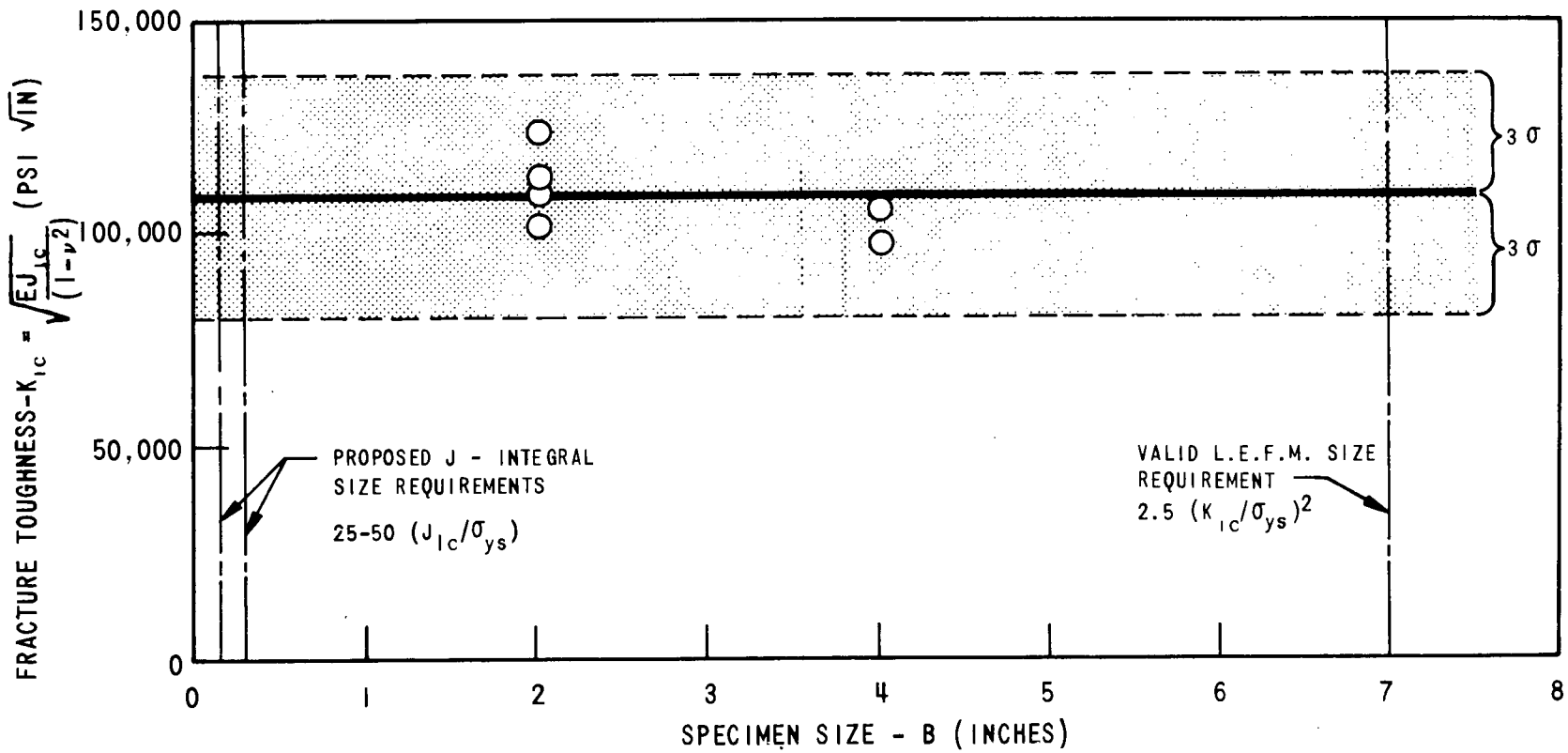


Fig. 2.8. Fracture toughness data from HSST plate 04-A using the J -integral interpretation.

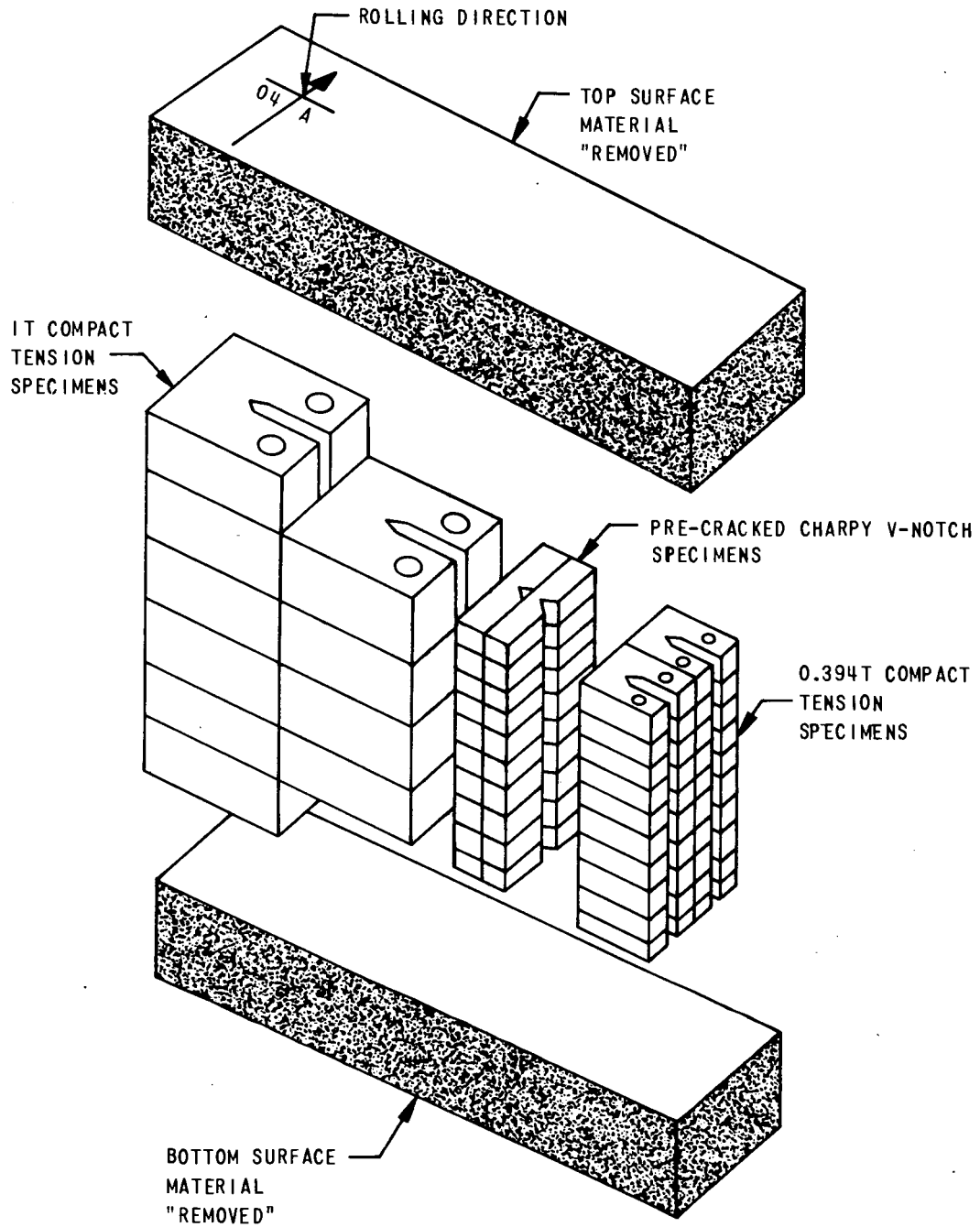


Fig. 2.9. Additional fracture toughness specimens from HSST plate 04-A for statistical study.

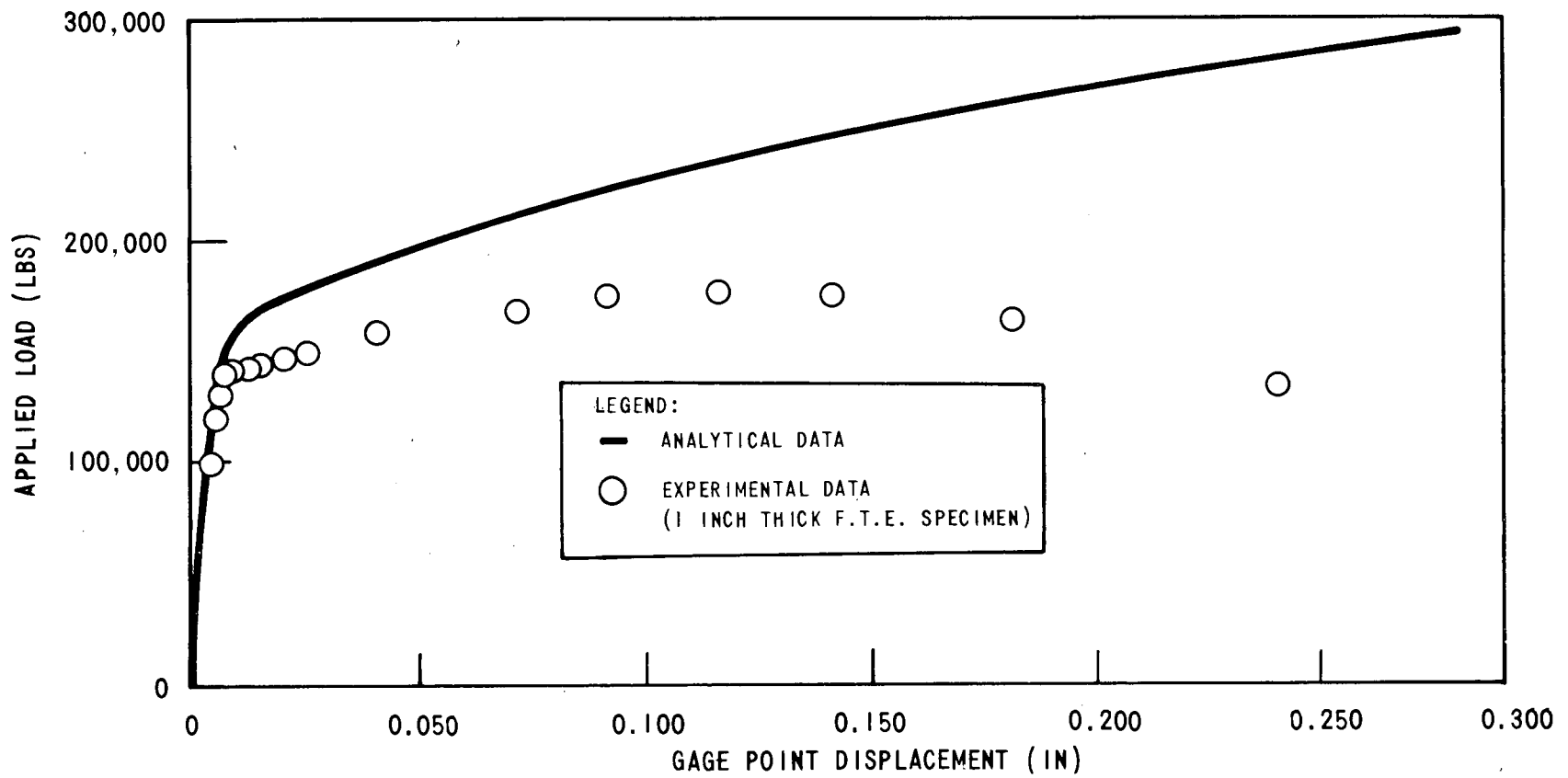


Fig. 2.10. Analytical and experimental compliance data for fracture theories evaluation specimen.

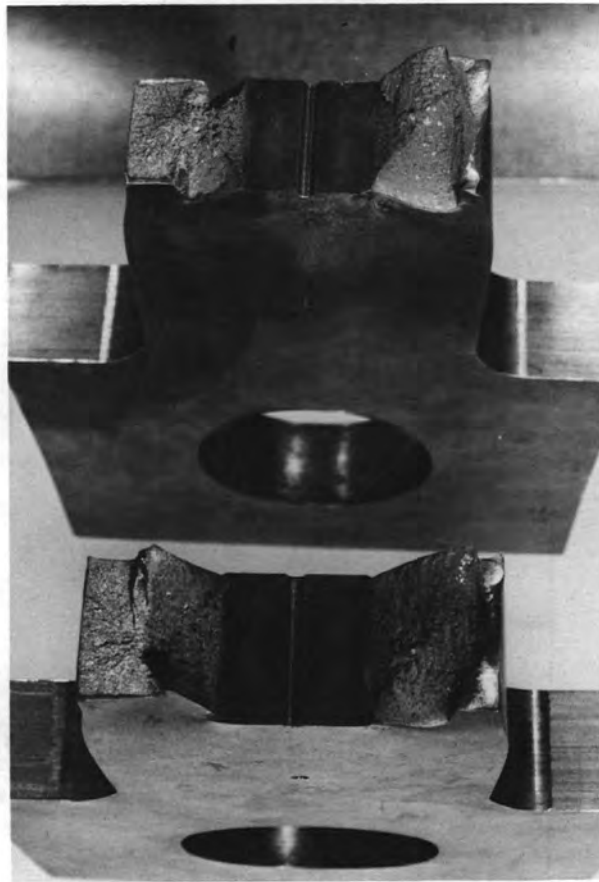


Fig. 2.11. Fracture surface from first (1-in.-thick) fracture theories evaluation specimen.

the state of stress was closer to plane stress than to plane strain; and (2) a significant amount of subcritical crack growth occurred prior to fracture. Because of these two factors, fracture predictions for the first FTE specimen are not expected to be accurate.

The remaining FTE tests will include specimens with thicknesses of 2.0 and 4.0 in., the latter of which should approach a plane strain state of stress, and a 1.0-in.-thick specimen with rounded crack tips (Fig. 2.12), which should indicate the point at which subcritical crack growth occurs in the cracked specimens.

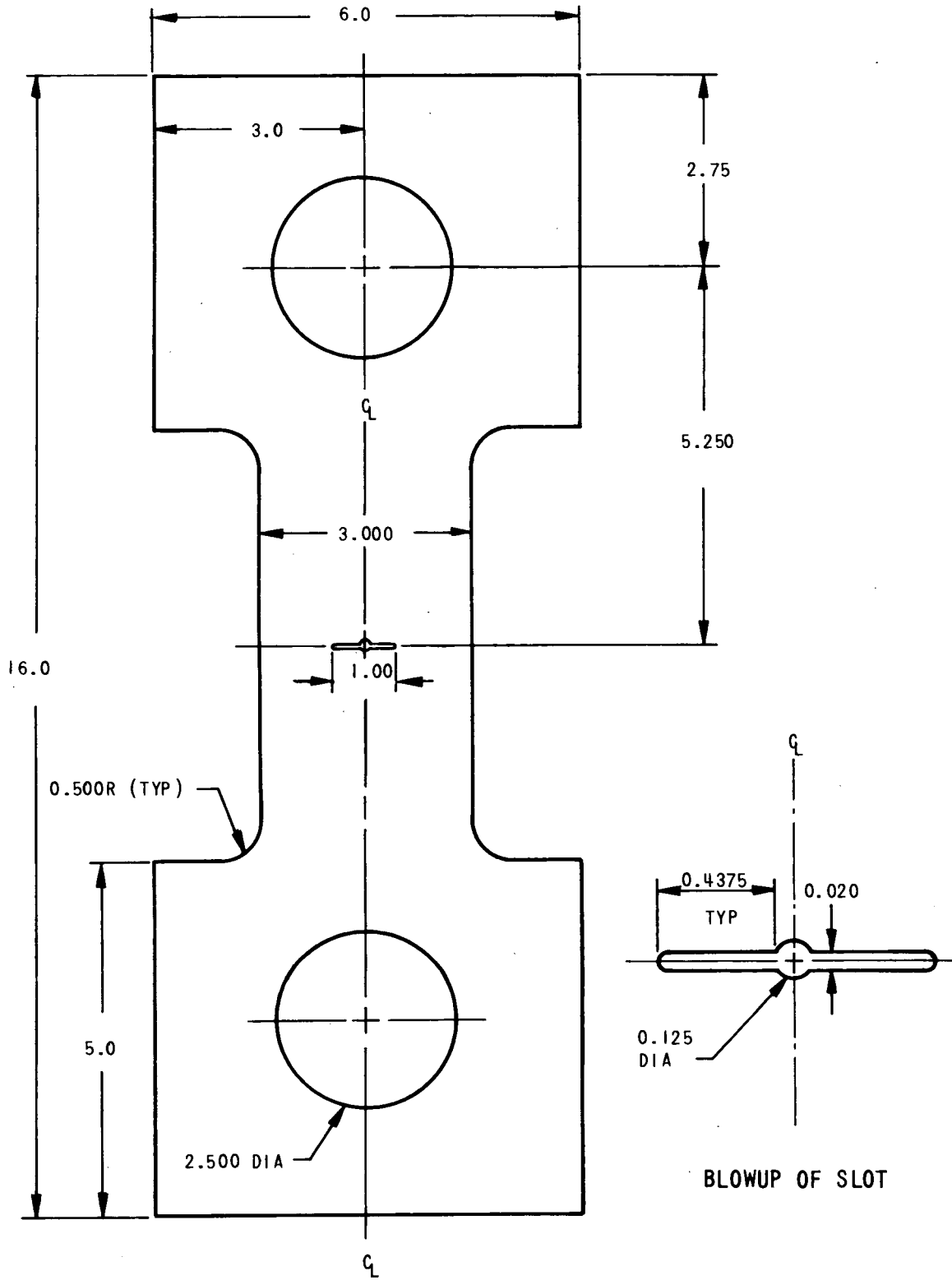


Fig. 2.12. Fracture theories evaluation specimen with rounded crack ends.

Analytical Program

A finite-element model of the gage length region of the FTE specimen was set up to perform a detailed elastic-plastic analysis of the specimen.¹⁰ The resulting analytical load vs displacement curve is shown compared with the experimental data for the first FTE test in Fig. 2.10. The agreement between the experimental and analytical results is within approximately 25% up to the maximum load point in the experiment. Since the analysis was based on small strain theory, it could not be expected to predict load reversal beyond the maximum load point. The 25% difference between the analytical and experimental data can be explained by the fact that the analysis was performed for plane strain, and the test was closer to plane stress. This difference should reduce as the thicker FTE specimens are tested. In the analysis, 140 load steps were used, and the total running time on the CDC-7600 computer was less than 6 min.

Values of the path integral J were computed¹⁴ over 13 different paths at each load step ranging from very small bands (mean radius = 0.0013 in.) to very large bands (mean radius = 0.637 in.). Normalized values of the J -integral as a function of path radius are shown in Fig. 2.13 for several selected load steps, ranging from the first (elastic) load step to load steps in the highly plastic regime. The path independence of the J -integral is illustrated by this figure. In the elastic step, the J -integral was essentially path independent except for the three paths nearest the crack tip which were disregarded due to numerical noise. As the loading increases into the plastic range, the path independence is maintained; however, the variability from path to path and the number of paths which must be disregarded due to numerical noise increase.

The average values of J over the paths, disregarding the anomalous paths near the crack tip, are plotted as a function of gage length displacement in Fig. 2.14. The J -integral fracture toughness data from Table 2.2, including the $\pm 3\sigma$ scatter band for the data, are also plotted on this figure. The intersection of the fracture toughness lines with the computed J -integral curve yields a predicted fracture displacement of 0.010 in., with a $\pm 3\sigma$ range of 0.007 to 0.013 in. for the J -integral approach.

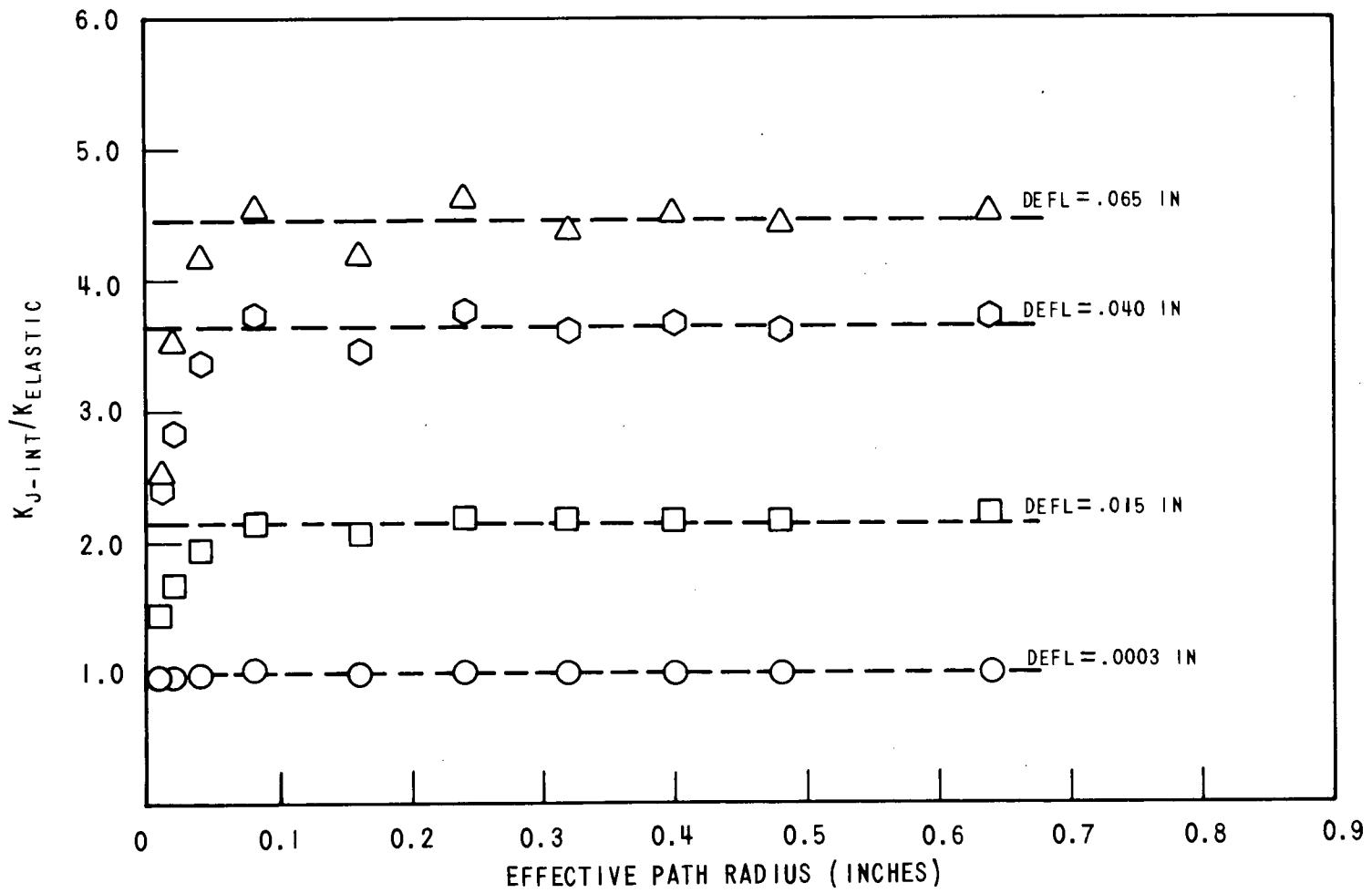


Fig. 2.13. Path dependence of analytical J -integral data.

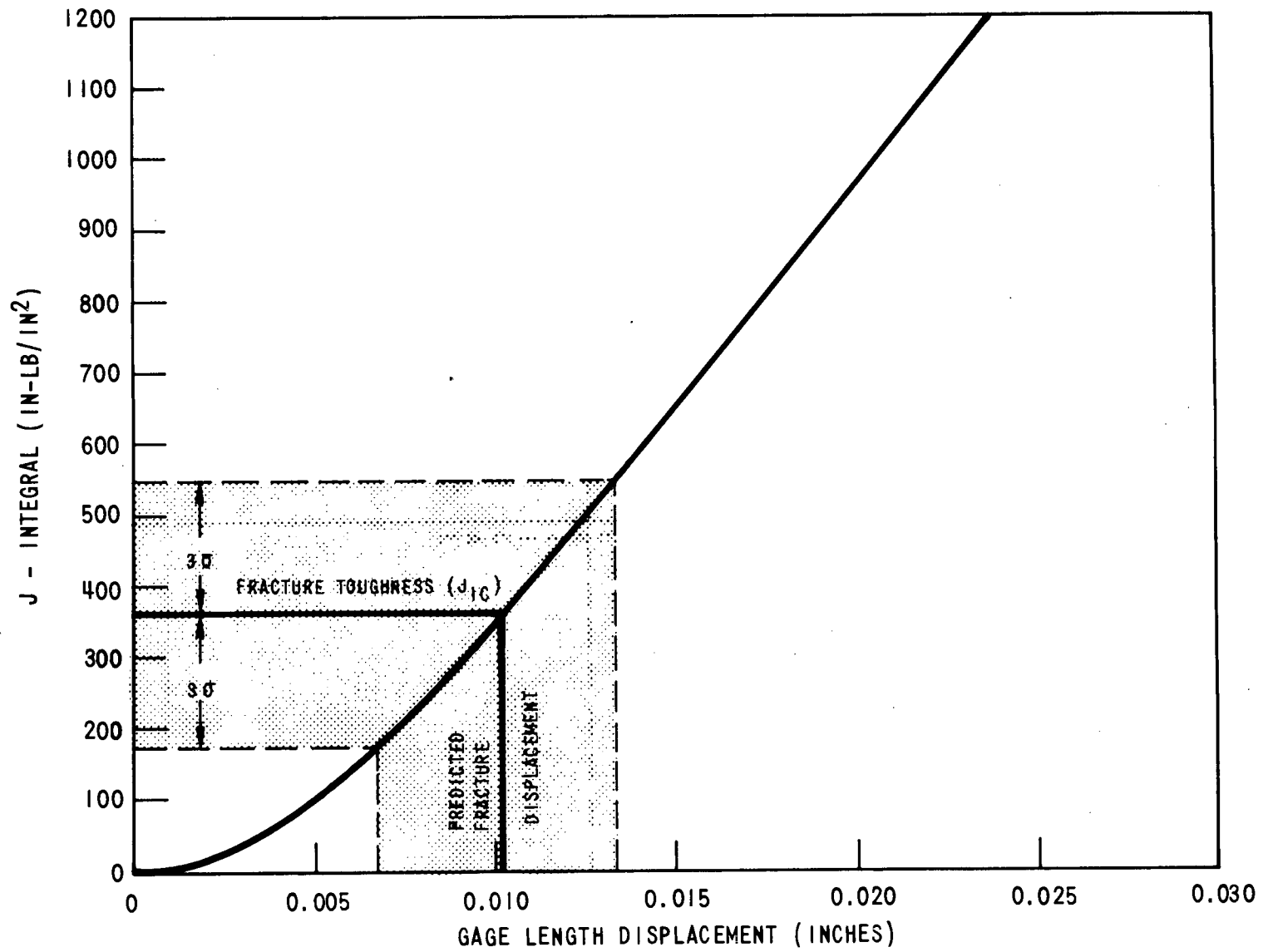


Fig. 2.14. Predicted fracture displacement of FTE specimen using the J -integral approach.

To obtain a fracture prediction using the equivalent-energy approach, values of total energy input to the model were computed at each load step by summing the work done on each element in the model during that load step. Values of total energy input, computed in this manner, are shown as a function of gage length displacement in Fig. 2.15. In order to determine the critical value of energy to fracture, two geometrically similar specimens must be considered (see Fig. 2.16).¹⁵ Let specimen 1 be the 4-in.-thick FTE specimen and specimen 2 be a geometrically similar specimen large enough to fracture in a brittle manner (assumed thickness = 20 in.). The total energy to fracture for specimen 2 can be calculated using linear-elastic fracture mechanics and the equivalent-energy fracture toughness data of Table 2.2. Assuming that the volumetric energy ratio for specimens 1 and 2 is equal to the ratio of their dimensions, the total energy to fracture for specimen 1 can be calculated as outlined in Fig. 2.16. The results of this calculation are summarized in Table 2.3 and

Table 2.3. Fracture energy calculations

	K_{Icd} (ksi $\sqrt{\text{in.}}$)	Energy to fracture (in.-lb)
3 σ upper bound	130.0	6515.4
Mean value	112.9	4914.1
3 σ lower bound	95.8	3538.2

are also plotted on Fig. 2.15, including the $\pm 3\sigma$ scatter band for the data. Using the intersection of the fracture toughness energy lines with computed energy input curve to predict fracture yields a fracture displacement of 0.011 in., with a $\pm 3\sigma$ range of 0.009 to 0.013 in. for the equivalent-energy approach.

15. W. F. Brown and J. R. Srawley, Plane Strain Crack Toughness Testing of High Strength Metallic Materials, ASTM STP-410 (1967).

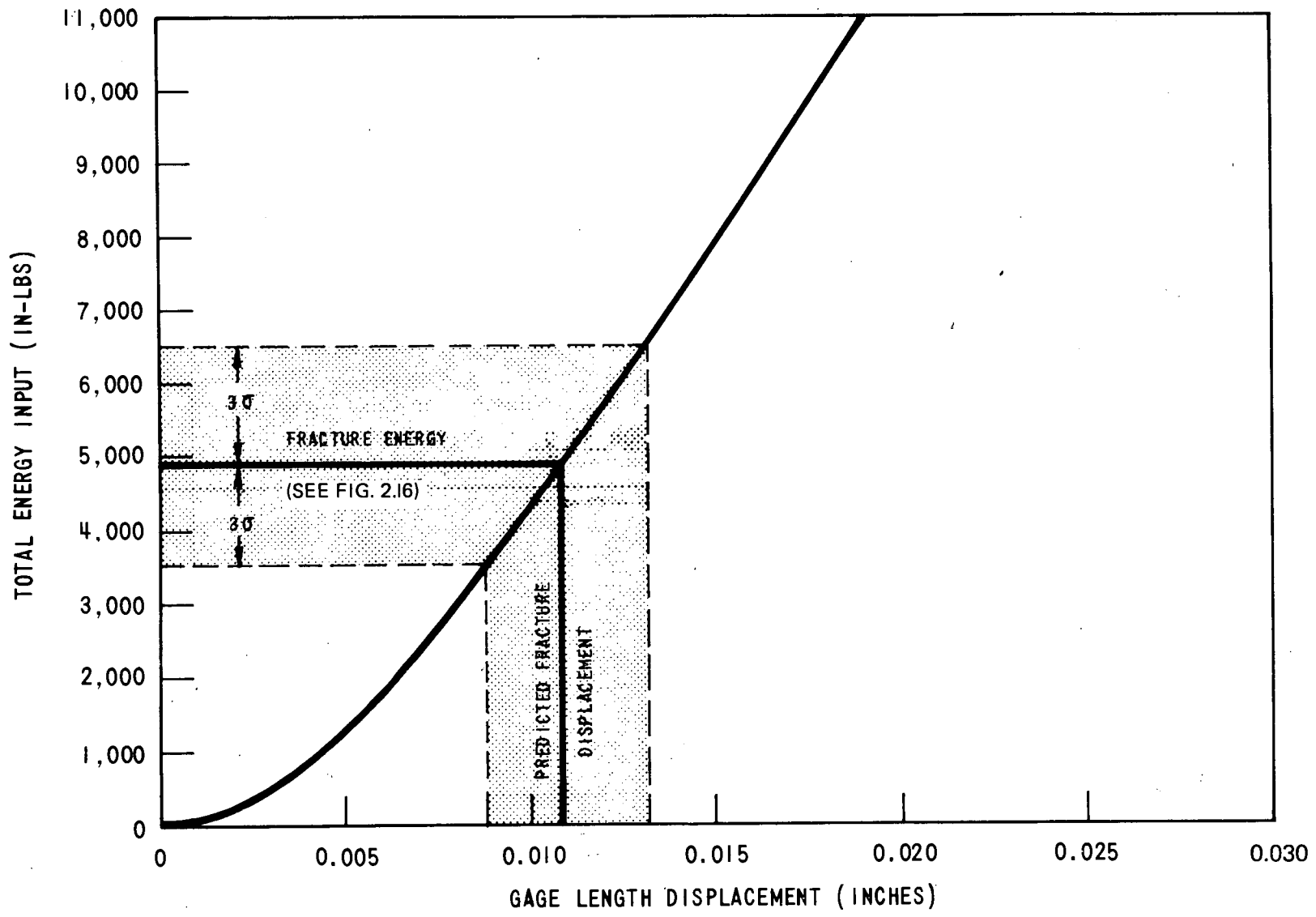
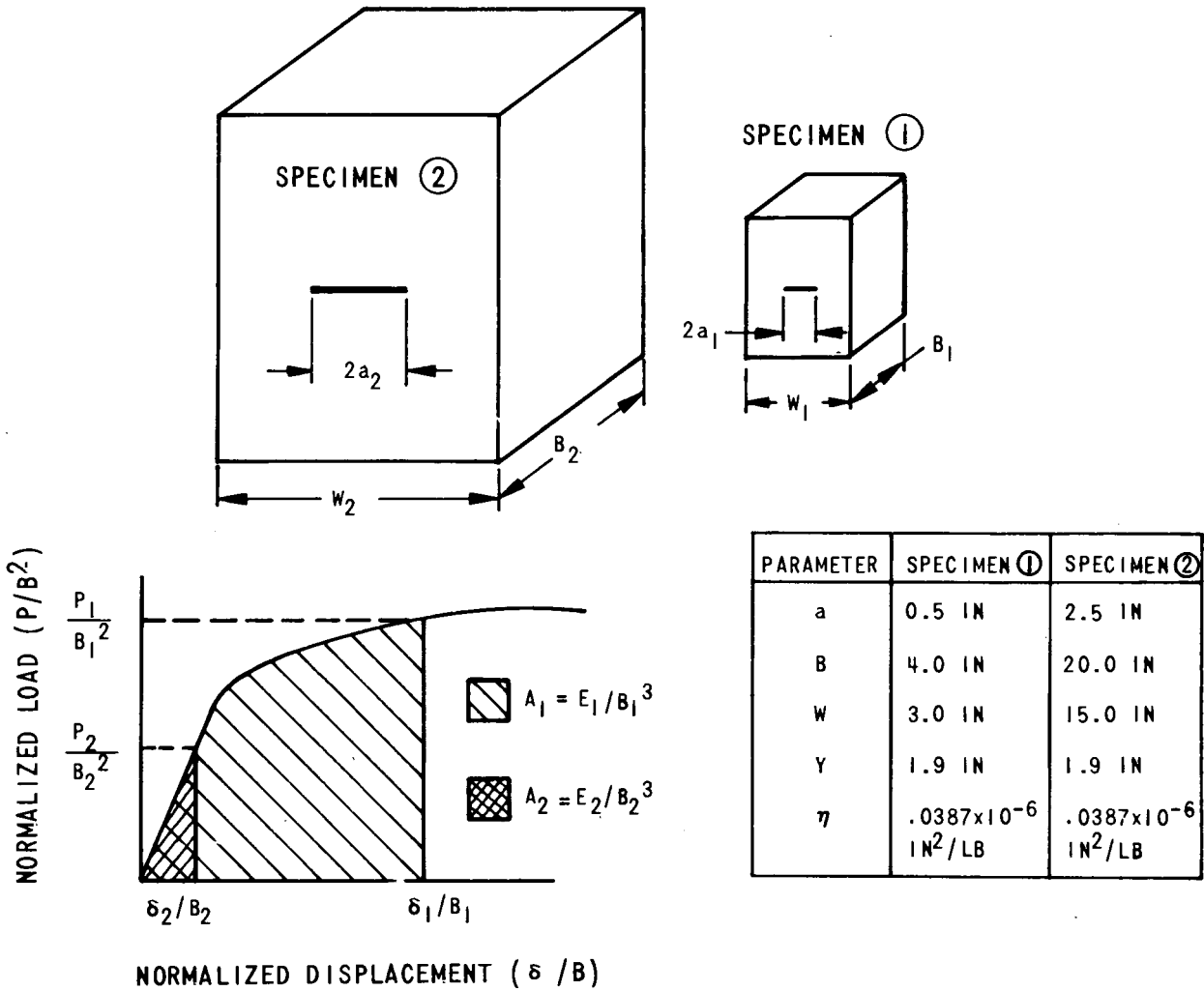


Fig. 2.15. Predicted fracture displacement of FTE specimen using the equivalent-energy approach.



FROM LEFM:

$$E_2 = \frac{1}{2} P_2 \delta_2$$

WHERE: $P_2 = \frac{B_2 W_2}{Y \sqrt{a_2}} K_{1C}$ (REF. 15)

$\delta_2 = \eta (P_2 / B_2)$ (ELASTIC COMPLIANCE)

THEREFORE: $E_2 = \frac{1}{2} \left(\frac{\eta B_2 W_2^2 K_{1C}^2}{Y^2 a_2} \right)$

FROM EQUIV. ENERGY:

$$\frac{A_1}{A_2} = \frac{B_2}{B_1}$$

$$\frac{(E_1 / B_1^3)}{(E_2 / B_2^3)} = \frac{B_2}{B_1}$$

THEREFORE: $E_1 = \left(\frac{B_1}{B_2} \right)^2 E_2$

Fig. 2.16. Development of fracture energy from the equivalent-energy approach.

EFFECT OF HIGH-TEMPERATURE PRIMARY REACTOR WATER ON THE
SUBCRITICAL CRACK GROWTH OF REACTOR VESSEL STEEL¹⁶

T. R. Mager V. J. McLoughlin

Experimental Procedure

Six precracked 2T CT specimens (RW orientation) were fabricated from HSST plate 02 for the study. The load cycle was held constant at a frequency of 1 cpm with maximum load at 20,000 lb. Two specimens were tested in a PWR environment (2000 psi, 550°F) and one in a BWR environment (1200 psi, 550°F). The water chemistries were controlled to the specifications in Table 2.4. A fourth specimen was tested in an air environment at a frequency of 1 cpm (2000 psi, 550°F).

Table 2.4. Environmental water chemistry

	Pressurized-water reactor	Boiling-water reactor
Oxygen, ppm	<0.1	<0.3
Chloride, ppm	<0.15	<0.1
Fluoride, ppm	<0.15	<0.1
Total suspended solids, ppm	<1.0	<0.2
Boron, ppm	0-4000	
Solution pH	4.2-10.5	Neutral
Electrical conductivity, μ mhos/cm	<1-40	0.1
Hydrogen, cc (STR)/kg	25-35	0.037
Li(OH), <i>m</i>	0.3×10^{-4} - 3.2×10^{-4}	

A fifth test is currently under way in a PWR environment at 550°F. The test is being conducted in accordance with the recommendations of the HSST ad hoc task group on fatigue. The 2T WOL specimen was precracked at a K_{If} less than 10 ksi $\sqrt{\text{in.}}$. Thus, the fifth test was started at a ΔK of 10 ksi $\sqrt{\text{in.}}$ at a frequency of 1 cpm. When the ΔK reaches approximately 25 ksi $\sqrt{\text{in.}}$, the frequency will be reduced to 0.5 cpm.

16. Work sponsored by HSST program under UCCND Subcontract No. 3290 between Union Carbide and Westinghouse Electric Corporation.

Experimental Results

The resultant crack length vs cycle data were reduced to fracture mechanics parameters. The results for the first three tests were reported in the previous semiannual report¹⁷ and are reproduced in Fig. 2.17, where the crack growth rate (da/dn) is plotted as a function of the independent variable, stress intensity factor (ΔK). For convenience, a reference line has been included on the plot representing an upper bound for all previous crack growth rate data generated on HSST plate 02 at frequencies of 60 and 600 cpm.¹⁸ The results of the test in air at a frequency of 1 cpm are also given in Fig. 2.17.¹⁹ The data fall within the upper scatter band for the 60- and 600-cpm data. It is apparent that at the lower frequencies and in an environment of primary-grade reactor water, the crack growth rates are accelerated for the stress intensity range studied (30 to 100 ksi $\sqrt{\text{in}}$).

Ad Hoc Task Group on Fatigue

An HSST ad hoc task group reviewed the available test data and made the following recommendations:

1. Evaluate the effect of the R ratio ($R = K_{\min}/K_{\max}$) on low-frequency fatigue-crack growth rates. The R ratio is generally more important in aggressive environments than in ordinary air. The two recommended ratios were 0.2 and 0.8.
2. Evaluate the effect of low frequency on fatigue-crack growth rates in the lower range of ΔK . The recommended minimum ΔK was 10 ksi $\sqrt{\text{in}}$.
3. Evaluate the effect of frequencies of less than 1 cpm on the fatigue-crack growth rates. The recommended frequency was 0.1 cpm.

17. S. A. Legge and T. R. Mager, *HSST Program Semiannu. Progr. Rep. Aug. 31, 1972*, ORNL-4855, pp. 12-15.

18. T. R. Mager and V. J. McLoughlin, *The Effect of an Environment of High Temperature Primary Grade Nuclear Reactor Water on the Fatigue Crack Growth Characteristics of A533 Grade B Class 1 Plate and Weldment Material*, Heavy Section Steel Technology Program Technical Report No. 16 (October 1971).

19. P. C. Paris et al., "Extensive Study of Low Fatigue Crack Growth Rates in A533 and A508 Steels," *Stress Analysis and Growth of Cracks*, Proceedings of the 1971 National Symposium on Fracture Mechanics, part I, ASTM-STP-513, 1972, pp. 141-76.

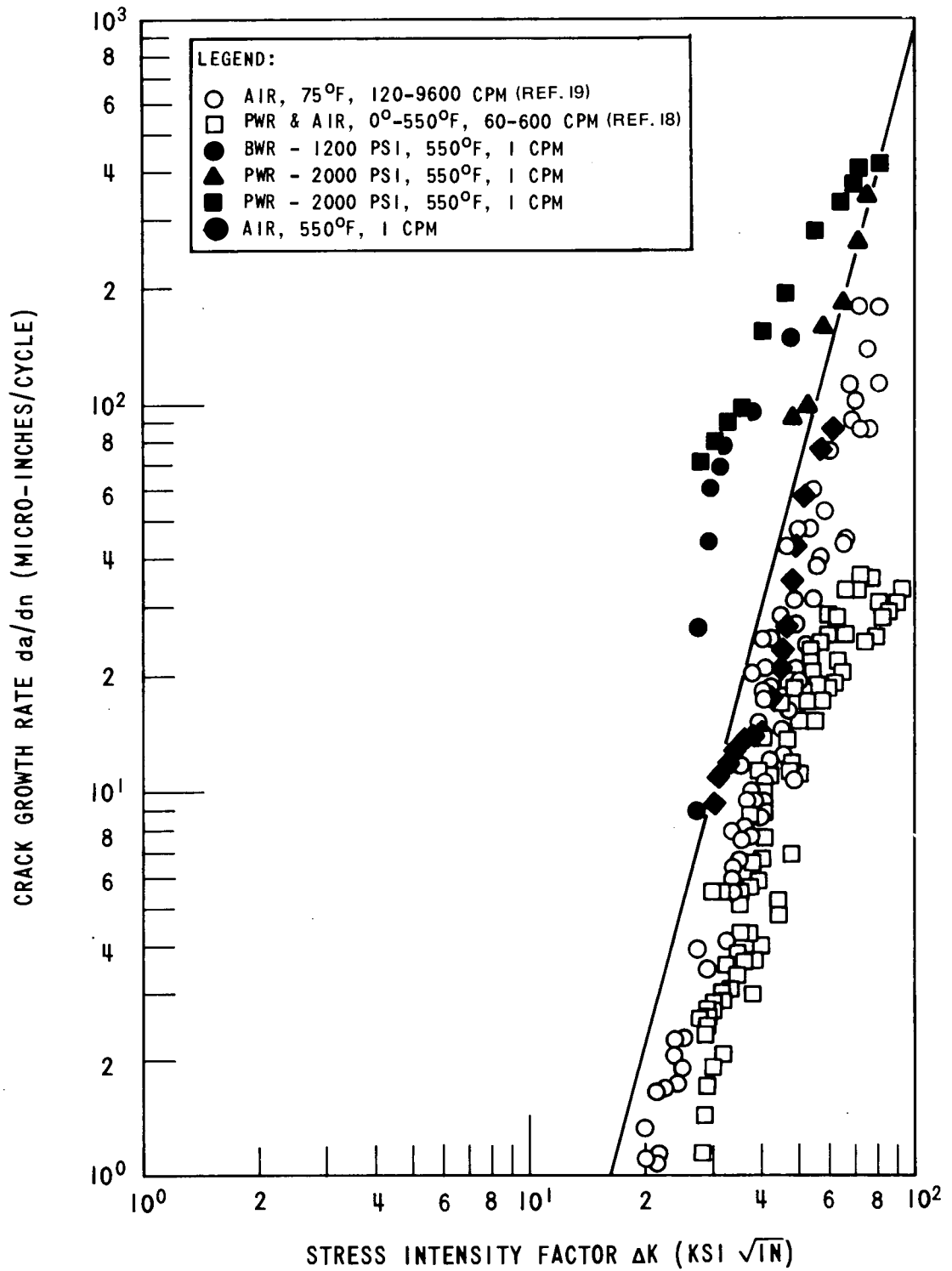


Fig. 2.17. Crack growth rates for HSST 02 material at 1 cpm frequency in PWR and BWR environments.

3. INVESTIGATIONS OF IRRADIATED MATERIALS

One of the environmental factors that must be considered in safety evaluations of reactor pressure vessels is irradiation, because the mechanical properties of metals may be modified thereby to a degree that is of considerable engineering significance. Irradiation effects have been recently investigated by Hanford Engineering Development Laboratory (HEDL) and by Westinghouse Electric Corporation. Most of the irradiated specimens being tested by HEDL were machined by ORNL from broken halves of previously tested specimens. The areas of primary interest to the HSST program are the temperature range 450 to 600°F and the fast-neutron ($E > 1$ MeV) fluence range 1 to 8×10^{19} neutrons/cm².

This chapter summarizes the research performed by HEDL and Westinghouse.

IRRADIATION EFFECTS ON THE FRACTURE OF HEAVY-SECTION PRESSURE VESSEL STEELS¹

J. A. Williams L. A. James
Hanford Engineering Development Laboratory

The Effect of Irradiation on the Fracture Toughness of A533-B; Lower-Bound Evaluation Using C_v CT Specimens

The lower-bound fracture toughness K_{Icd} of irradiated ASTM A533, grade B, class 1 steel, HSST plate 02, was evaluated between 0 and 550°F.

1. Research sponsored under Purchase Order No. 11Y-50917V between Union Carbide Corporation and Hanford Engineering Development Laboratory.

Compact-tension specimens of the same thickness as Charpy impact specimens, 0.394 in., were used; the fracture toughness measurement is designated $K_{Ic.394}$.

Irradiation levels were 5.3 to 5.7×10^{19} and 8×10^{19} neutrons/cm² ($E > 1$ MeV). All specimens were remachined by ORNL from previously irradiated and tested specimens. The 5.3 to 5.7×10^{19} neutron/cm² specimens were from material irradiated at 550°F reported by Mager.² The 8×10^{19} neutron/cm² specimens were from material irradiated at 540°F and tested by HEDL.³ The lower-bound fracture toughness $K_{Ic.394}$ was determined for longitudinal (RW) and transverse (WR) orientations at the lower fluence level and for the RW orientation at the higher fluence. The testing procedures, crack preparation, and validity criteria of compact-tension specimens for K_{Ic} plane strain fracture toughness measurements⁴ were applied to the $K_{Ic.394}$ evaluation. The results of all the test specimens are reported in Table 3.1. The lower-bound toughness was determined by the procedure proposed by Witt and Mager.⁵

The primary effect of irradiation on the lower-bound fracture toughness was to cause the transition from low to high toughness to occur at a higher temperature. No criteria for fracture toughness transition (i.e., such as C_V of 30 ft-lb energy) have been established, so an arbitrary value of 100 ksi $\sqrt{\text{in.}}$ is chosen as a basis of comparison. This value is also approximately midrange between high and low $K_{Ic.394}$ toughness.

The 100-ksi $\sqrt{\text{in.}}$ level lower-bound fracture toughness of the RW orientation of A533-B irradiated to 5.3 to 5.7×10^{19} neutrons/cm² ($E > 1$ MeV), Fig. 3.1, occurs at approximately 180°F. The transition to full upper-shelf lower-bound toughness is complete at approximately 300°F.

2. T. R. Mager, *Postirradiation Testing of 2T Compact Tension Specimens*, WCAP-7561, Westinghouse Electric Corporation (August 1970).

3. C. W. Hunter and J. A. Williams, "Irradiation Effects on the Fracture of Heavy Section Pressure Vessel Steels," *HSSST Program Semiannu. Progr. Rep. Feb. 28, 1971*, ORNL-4681.

4. ASTM Standard E399-70T, Tentative Method of Test for Plane-Strain Fracture of Metallic Materials, ASTM Standards, Part 31, 1970.

5. F. J. Witt and T. R. Mager, "A Procedure for Determining Bounding Values on Fracture Toughness K_{Ic} at any Temperature," paper presented at Fifth National Symposium on Fracture Mechanics, University of Illinois, Aug. 28-Sept. 1, 1971.

Table 3.1. Irradiated fracture toughness of ASTM A533-B measured with 0.394 compact-tension specimens

Specimen identification (orientation)	Test temp. (°F)	Fluence ($\times 10^{19}$ neutrons/cm ²) ($E > 1$ MeV)	Yield strength ($\times 10^3$ psi)	Crack length (in.)	$K_{fatigue}$ (ksi $\sqrt{\text{in.}}$)	K_Q (ksi $\sqrt{\text{in.}}$)	$K_{Ic.394}$ (ksi $\sqrt{\text{in.}}$)
02D0009 (RW)	0	5.3-5.7	120	0.381	18.9	40.2	40.2 ^a
02D0008 (RW)	80	5.3-5.7	114	0.386	18.9	52.7	52.7
02D0005 (RW)	150	5.3-5.7	109	0.379	20.2	56.5 ^b	88.9
02D0022 (RW)	250	5.3-5.7	104	0.369 ^e	20.0	56.4 ^b	164.6
02D0004 (RW)	300	5.3-5.7	101	0.397 ^e	18.4	45.9 ^b	164.1
02D0007 (RW)	300	5.3-5.7	101	0.366 ^e	17.9	60.8 ^b	138.2
02D0021 (RW)	550	5.3-5.7	94	0.354 ^e	23.9	52.6 ^b	152.0
02D0003 (RW)	550	5.3-5.7	94	0.380 ^e	18.4	61.2 ^b	144.9
02E0010 (WR)	0	5.3-5.7	120	0.393	22.1	34.1	34.1 ^d
02E0005 (WR)	80	5.3-5.7	114	0.371	20.2	51.6	51.6 ^e
02E0018 (WR)	175	5.3-5.7	108	0.392	21.9	56.2 ^b	125.7
02E0004 (WR) ^f	200	5.3-5.7	107	0.385	27.7	71.8 ^b	92.4
02E0009 (WR) ^g	250	5.3-5.7	104	0.383	27.4	52.2 ^b	110.7
02E0023 (WR)	300	5.3-5.7	101	0.389	18.7	55.7 ^b	157.7
02E0017 (WR)	300	5.3-5.7	101	0.368 ^e	20.0	58.9 ^b	142.0
02E0019 (WR)	300	5.3-5.7	101	0.370 ^e	20.2	52.4 ^b	161.1
02E0022 (WR)	400	5.3-5.7	97	0.412 ^e	20.9	55.1 ^b	134.5
02E0024 (WR)	550	5.3-5.7	94	0.404	19.9	52.8 ^b	128.7
02E0003 (WR)	550	5.3-5.7	94	0.362 ^e	19.5	58.6 ^b	143.2
02E0008 (WR)	550	5.3-5.7	94	0.387 ^e	20.9	59.6 ^b	136.7
02GA44A2 (RW)	200	8.2	112	0.398	20.7	49.3 ^h	49.3 ^e
02GA43B2 (RW)	245	8.3	109	0.380	19.4	55.7 ^b	86.7
02GA44A1 (RW)	300	8.2	106	0.357 ^e	16.9	68.7 ^b	105.7
02GA44B2 (RW)	400	8.2	101	0.386 ^e	18.7	70.9 ^b	153.9
02GA43A2 (RW)	245	8.3	109	0.427 ^e	21.9	69.1 ⁱ	69.1
02GA43A1 (RW)	350	8.3	104	0.346 ^e	19.4	48.3 ^b	138.4
02GA43B1 (RW)	550	8.3	95	0.392 ^e	19.0	66.6 ^b	145.7

^a K_{Ic} .^b P_5 secant offset load.^cIrregular crack shape.^d K_f too high, so reported as $K_{Ic.394}$.^eDoes not meet $B, \geq 2.5(K_Q/\sigma_y T)^2$, so recorded as $K_{Ic.394}$.^fSpecimen thin, $B = 0.301$ in.^gSpecimen thin, $B = 0.302$ in.^hPop-in load.ⁱ K_{Ic} .

The same interpretation of results can be made for the WR orientation data shown in Fig. 3.2.

The results of ASTM A533-B, RW orientation, irradiated to a fluence of 8×10^{19} neutrons/cm² ($E > 1$ MeV) are shown in Fig. 3.3. A lower-bound $K_{Ic.394}$ fracture toughness of 100 ksi $\sqrt{\text{in.}}$ is reached at 290°F, and the $K_{Ic.394}$ upper shelf is fully developed at 400°F.

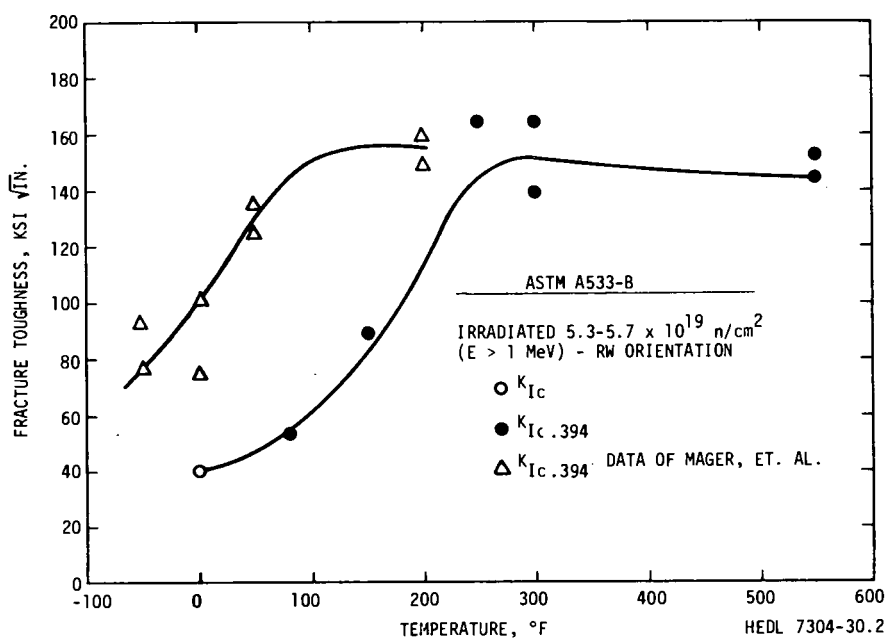


Fig. 3.1. Lower-bound $K_{Ic.394}$ toughness of ASTM A533-B, RW orientation, irradiated to 5.3 to 5.7×10^{19} neutrons/cm² ($E > 1$ MeV) at 550°F . The unirradiated data of Mager et al. are given in Ref: 6.

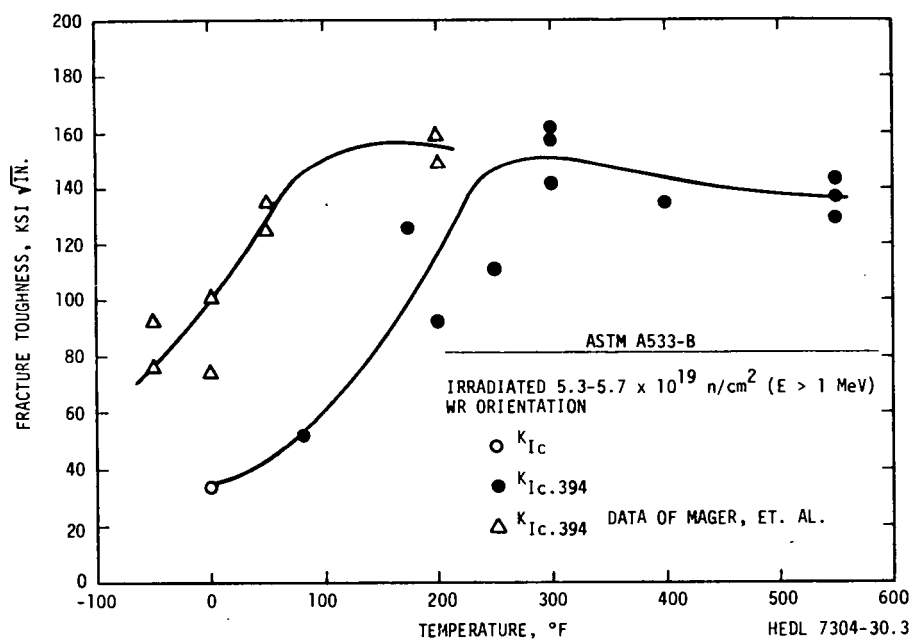


Fig. 3.2. Lower-bound $K_{Ic.394}$ toughness of ASTM A533-B, WR orientation, irradiated to 5.3 to 5.7×10^{19} neutrons/cm² ($E > 1$ MeV) at 550°F . The unirradiated data of Mager et al. are given in Ref. 6 and are from the RW orientation.

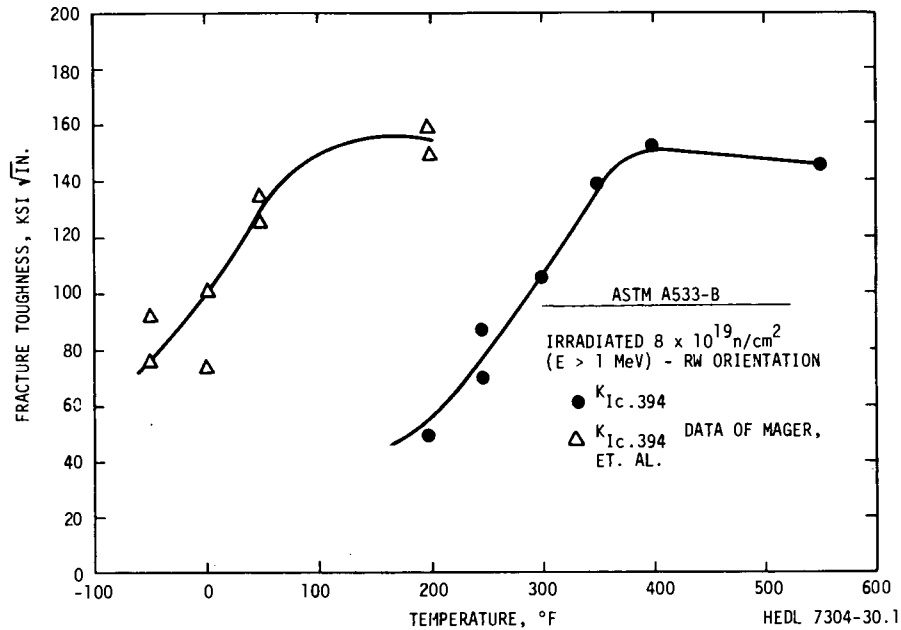


Fig. 3.3. Lower-bound $K_{Ic.394}$ toughness of ASTM A533-B, RW orientation, irradiated to 8×10^{19} neutrons/cm² ($E > 1$ MeV) at 540°F. Unirradiated data of Mager et al. are given in Ref. 6.

A $K_{Ic.394}$ toughness of 100 ksi $\sqrt{\text{in.}}$ at 0°F is exhibited by the data of Mager et al.⁶ on unirradiated specimens. By comparison, irradiation at 5.3 to 5.7×10^{19} and 8×10^{19} neutrons/cm² causes a shift in toughness of 180°F for the RW and WR orientations and 290°F for RW orientation respectively. For all practical purposes no degradation in upper-shelf $K_{Ic.394}$ toughness results from irradiation to the highest level of 8×10^{19} neutrons/cm². Previous results reported⁷ for $K_{Ic.394}$ fracture toughness of ASTM A533-B irradiated to approximately 2×10^{19} neutrons/cm² ($E > 1$ MeV) show the 100-ksi $\sqrt{\text{in.}}$ toughness level to exist at 200°F for both RW and WR orientations; the upper shelf of these data was complete at approximately 300°F and reached a value of 150 ksi $\sqrt{\text{in.}}$. The upper-shelf

6. T. R. Mager, S. A. Legge, and D. J. Lege, "Experimental Verification of Lower-Bound K_{Ic} Values Using the Equivalent Energy Concept," *HSST Program Semiannu. Progr. Rep. Feb. 29, 1972*, ORNL-4816.

7. F. J. Witt and J. A. Williams, "Lower Bound Toughness of Irradiated A533 Grade B, Class 1 Steel," *HSST Program Semiannu. Progr. Rep. Feb. 29, 1972*, ORNL-4816.

value range of 130 to 160 ksi $\sqrt{\text{in.}}$ encompasses all material conditions investigated herein.

Fatigue-Crack Propagation of ASTM A533, Grade B, Class 1 Steel

Effect of cyclic frequency

Cyclic frequency has been shown to exert a profound influence upon the elevated-temperature fatigue-crack propagation of some alloys.⁸ Therefore, since reactor operating frequencies are expected to be lower than the test frequencies normally employed in laboratory testing, two survey tests were conducted at HEDL to determine if cyclic frequency was an important variable in the crack propagation behavior of ASTM A533-B steel. Prior results⁹ have indicated that in an air environment, temperatures of 75°F (24°C) and 550°F (288°C) and irradiation at 2.3 to 2.8×10^{19} and 5.3 to 5.7×10^{19} neutrons/cm² ($E > 1$ MeV) had little or no effect on the crack growth behavior of A533-B steel.

The A533-B material employed was from section 02GA of HSST plate 02. Fatigue-crack propagation tests were performed on 1-in.-thick compact-tension specimens (1T CT) in the RW orientation. Specimens were fatigue cycled in load control using a sinusoidal wave form at 1 cpm (0.017 Hz). The stress ratio R was zero. Tests were conducted in an air environment at temperatures of 75°F (24°C) and 550°F (288°C) over a range of ΔK values of approximately 18 to 60 ksi $\sqrt{\text{in.}}$

The results of fatigue cycling A533-B at 1 cpm are compared with 600 cpm at 75°F in Fig. 3.4 and at 550°F in Fig. 3.5 by plots of fatigue-crack growth rate da/dN vs stress intensity factor range ΔK . At both temperatures little or no effect of cyclic frequency is evidenced; in addition, superposition of Figs. 3.4 and 3.5 would demonstrate little or no effect of temperature on the fatigue-crack growth rate at both fatigue cycling

8. L. A. James, "The Effect of Frequency upon the Fatigue-Crack Growth of Type 304 Stainless Steel at 1000°F," *Stress Analysis and Growth of Cracks*, ASTM STP-513, pp. 218-29, 1972.

9. J. A. Williams and L. A. James, "Irradiation Effects on Fracture of Heavy Section Pressure Vessel Steels," *HSST Program Semiannu. Progr. Rep. Aug. 31, 1972*, ORNL-4855.

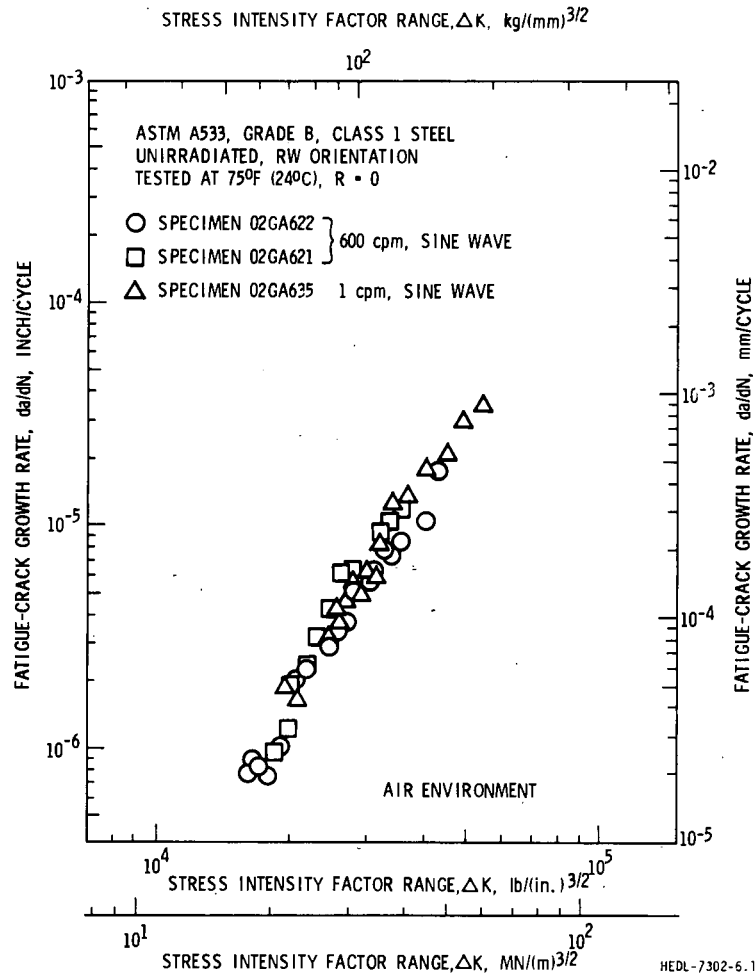


Fig. 3.4. Effect of cyclic frequency in air at 75°F on the fatigue-crack propagation behavior of ASTM A533-B.

frequencies. These results are in agreement with those of Mager and McLoughlin¹⁰ in an air and 550°F water environment at cyclic frequencies between 60 and 600 cpm. Lower cyclic frequencies are reported to affect fatigue-crack growth rate in 550°F pressurized-water environments similar

10. T. R. Mager and V. J. McLoughlin, *The Effect of an Environment of High Temperature Primary Grade Nuclear Reactor Water on the Fatigue Crack Growth Characteristics of A533 Grade B Class 1 Plate and Weldment Material*, WCAP-7776, Westinghouse Nuclear Energy Systems (October 1971).

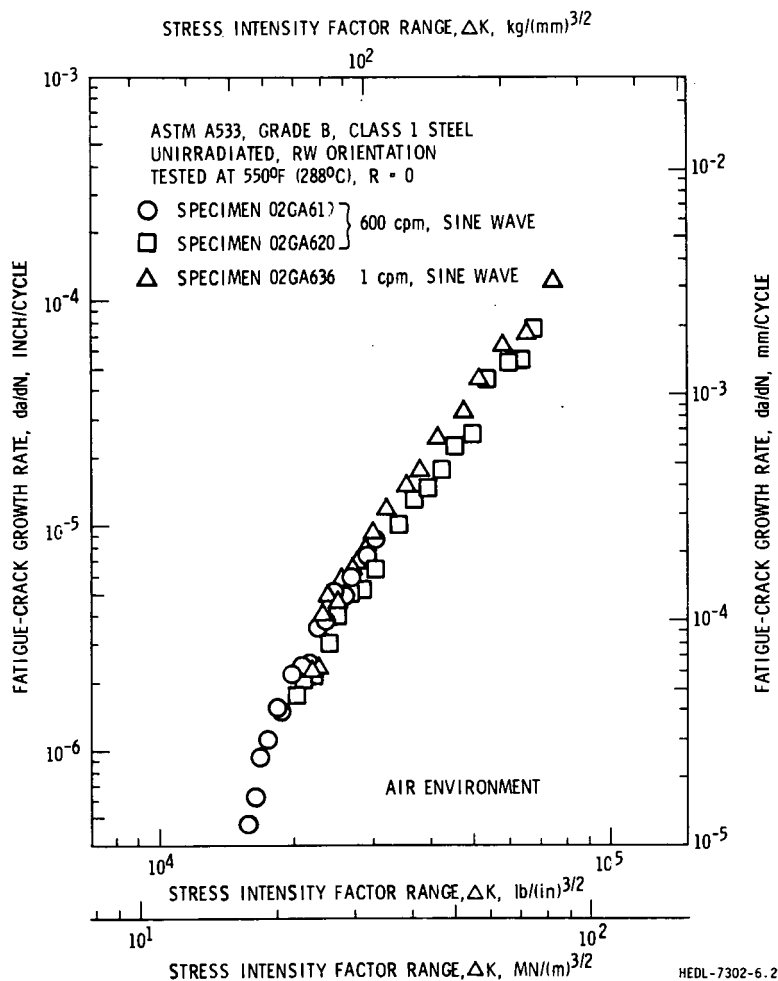


Fig. 3.5. Effect of cyclic frequency in air at 550°F on the fatigue-crack propagation behavior of ASTM A533-B.

to that of water reactors; Kondo et al.¹¹ and, more recently, Mager¹² have observed an increase in fatigue-crack growth rates of unirradiated A533-B at low cyclic frequencies (≤ 1 cpm). The effect of irradiation at low frequency (1 cpm) and high temperature (550°F) in an air environment on the fatigue-crack growth rate will be investigated.

11. T. Kondo et al., "Fatigue Crack Propagation Behavior of ASTM A533-B and A302-B Steels in High Temperature Aqueous Environment," Paper 6, Heavy Section Steel Technology Program Sixth Annual Information Meeting, Oak Ridge, Tenn., Apr. 25-26, 1972.

12. T. R. Mager, *HSST Program Semiannu. Progr. Rep. Aug. 31, 1972*, ORNL-4855.

Effect of stress ratio

The stress ratio ($R = K_{\min}/K_{\max}$) has been shown to influence fatigue-crack growth behavior in ASTM A533-B steel.¹³ Since reactor structural components will likely operate with stress ratios other than those for which tests have been conducted, it is important to characterize crack growth rates in such a way as to normalize the effect of stress ratio.

The most common method of characterizing fatigue-crack growth behavior involves use of the stress intensity factor range ΔK :

$$\frac{da}{dN} = C(\Delta K)^n ,$$

where $\Delta K = K_{\max}(1 - R)$. If, however, one adopts the use of an "effective stress intensity factor" [$K_{\text{eff}} = K_{\max}(1 - R)^m$], rather large variations in R may be accounted for and the results reduced to a single line. This approach has been successfully applied over a wide range of R values to 2024-T3 aluminum alloy,¹⁴ 7075-T6 aluminum alloy,¹⁴ type 304 stainless steel,¹⁵ and type 301 stainless steel,¹⁶ with the resultant values of the exponent m of 0.50, 0.425, 0.50, and 0.667 respectively.

Figure 3.6 illustrates the effect of stress ratio on the fatigue-crack propagation behavior of A533-B tested at 550°F. The data for $R = 0$ are from Ref. 17, and the other data are from Ref. 13. It will be noted

13. P. C. Paris et al., "Extensive Study of Low Fatigue Crack Growth Rates in A533 and A508 Steels," *Stress Analysis and Growth of Cracks*, ASTM STP-513, pp. 141-76, 1972.

14. K. Walker, "The Effect of Mean Stress Ratio During Crack Propagation and Fatigue for 2024-T3 and 7075-T6 Aluminum," *Effects of Environment and Complex Load History on Fatigue Life*, ASTM STP-462, pp. 1-14, 1970.

15. L. A. James, "The Effect of Stress Ratio on the Elevated Temperature Fatigue-Crack Propagation of Type 304 Stainless Steel," *Nucl. Technol.* 14(2), 163-70 (1972).

16. E. K. Walker, "An Effective Strain Concept for Crack Propagation and Fatigue Life with Specific Applications to Biaxial Stress Fatigue," *Proceedings Air Force Conference on Fatigue and Fracture of Aircraft Structures and Materials*, AFFDL-TR-70-144, pp. 225-33, 1970.

17. L. A. James and J. A. Williams, *HSST Technical Report No. 21, The Effect of Temperature and Neutron Irradiation upon the Fatigue-Crack Propagation Behavior of ASTM A533, Grade B, Class 1 Steel*, HEDL-TME-72-133, Hanford Engineering Development Laboratory (1972).

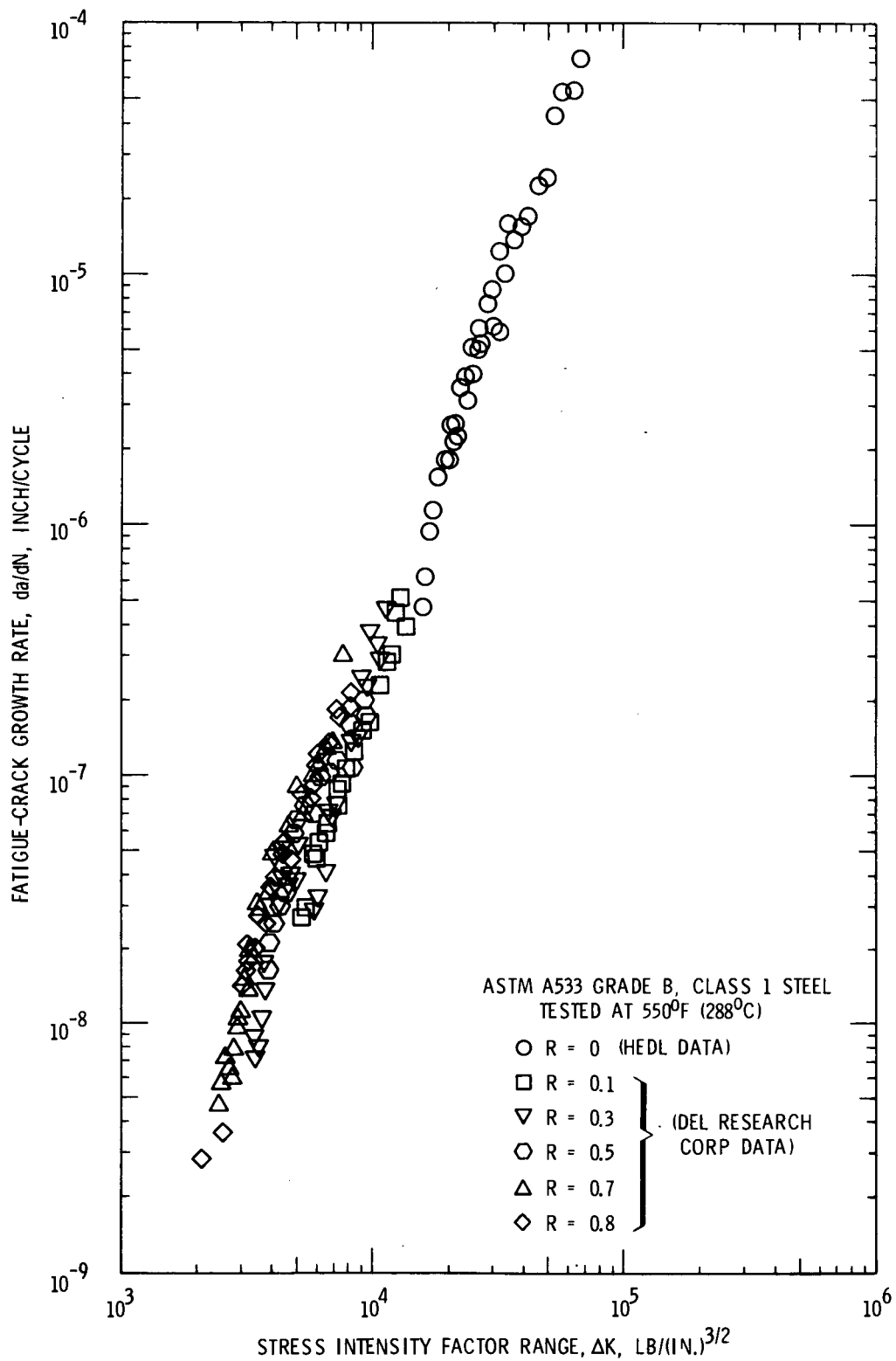


Fig. 3.6. Effect of stress ratio on the fatigue-crack growth behavior of A533-B steel at 550°F.

that, when the crack growth rate is expressed in terms of ΔK , the rates tend to increase with increasing values of R . This is consistent with observations on other materials.¹⁴⁻¹⁶ However, if the growth rate is expressed in terms of the effective stress intensity factor (in this case, the exponent m was found to be 0.75), the data for the various stress ratios converge to what is essentially a single line (see Fig. 3.7). Therefore, tests generated at one value of R may be used to estimate the cracking behavior of a structural component operating at a different value. It is recognized that other empirical relationships exist which would have correlated the data equally well, but the particular relationship used here is quite simple and therefore easy to use.

Fracture Toughness Characterization of Irradiated
A533, Grade B, Class 1 Steel Using 4T
Compact-Tension Specimens¹⁸

T. R. Mager S. A. Legge¹⁹

Six 4T CT specimens are being irradiated in the Battelle Research Reactor (BRR) to midthickness fluence levels of 5×10^{19} neutrons/cm² ($E > 1$ MeV). Three irradiation capsules were fabricated and six 4T CT specimens, two per capsule, were encapsulated. Additional smaller specimens, Charpy V-notch, tensile, and 0.4T CT specimens, were also encapsulated. The three capsules were inserted into the BRR and presently are undergoing neutron bombardment.

Specimen encapsulation

To provide control of the internal temperature distribution of the specimens, they must be encapsulated. Reference 20 summarizes the capsule

18. Work sponsored by HSST program under UCCND Subcontract No. 3720 between Union Carbide Corporation and Westinghouse Electric Corporation.

19. Portions of this program being performed at the Battelle Columbus Laboratories are under the technical direction of Neil E. Miller. W. J. Zielenback is the principal investigator for Battelle Columbus Laboratories for this program.

20. S. A. Legge, T. R. Mager, and P. C. Riccardella, *HSST Program Semiannu. Progr. Rep. Aug. 31, 1972*, ORNL-4855, pp. 25-35.

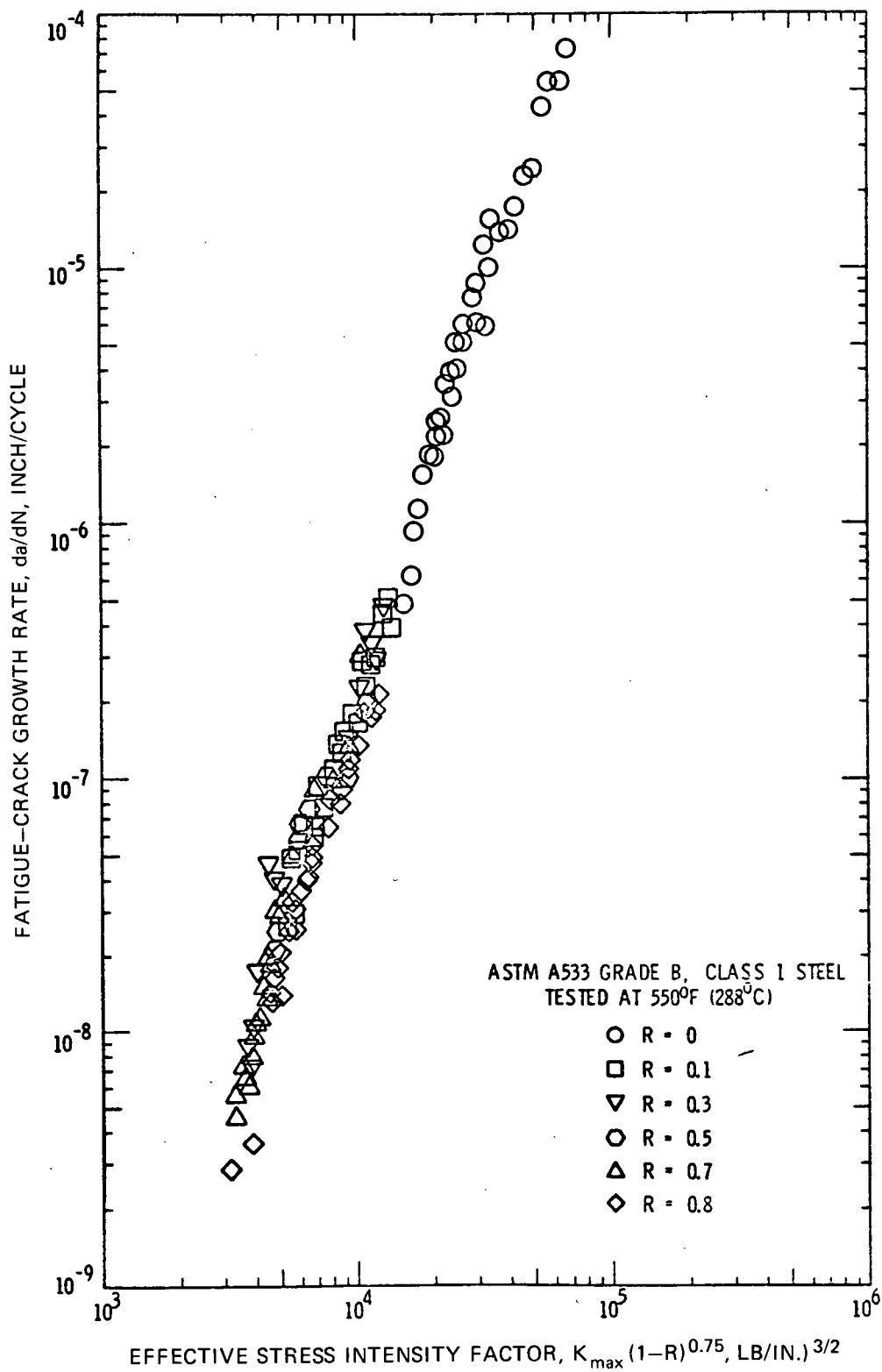


Fig. 3.7. Use of the effective stress intensity factor to correlate stress ratio effects for A533-B steel tested at 550°F.

design considerations, construction, and auxiliary temperature control. A typical irradiation capsule prior to loading is shown in Fig. 3.8, which also shows the heater configuration, the three separately heated zones, and the heater connections to leadouts. The U-tube arrangement at the top of the capsule introduces the He-N₂ gas mixture to the capsule gaps; the tube extending to the bottom of the capsule is the gas exit tube. Figure 3.9 shows the specimens installed in capsule WR with face 1 upward and thermocouples installed into the desired locations, and Fig. 3.10 shows capsule WR with the heater plates installed. Gap spacing pins can be seen in the plate; the dark spots are empty holes not used for pin mountings.

The three irradiation capsules were fabricated and assembled by Battelle. The capsules contained the specimens, dosimeters for monitoring the fluence, and thermocouples for monitoring the temperatures. Each capsule contained two 4T CT specimens and a complement of smaller specimens consisting of Charpy V-notch, tensile, and 0.4T CT specimens. The

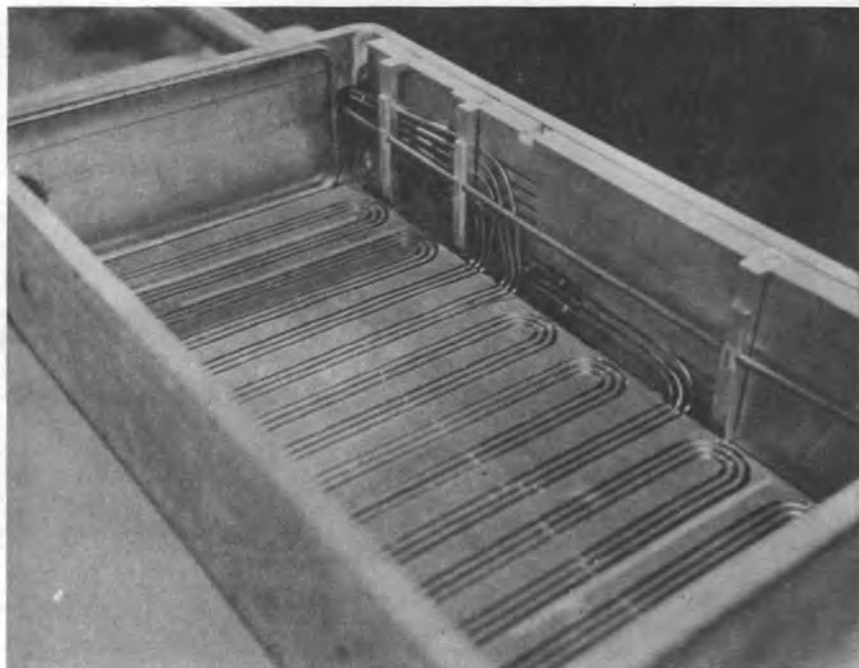


Fig. 3.8. Typical irradiation capsule prior to loading.

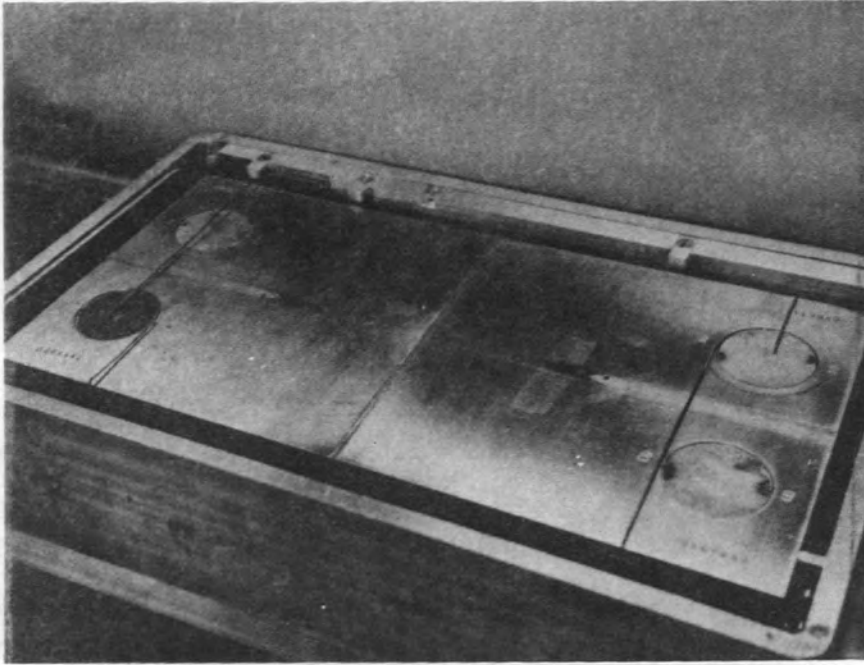


Fig. 3.9. Irradiation capsule WR showing specimens and thermocouples in place.

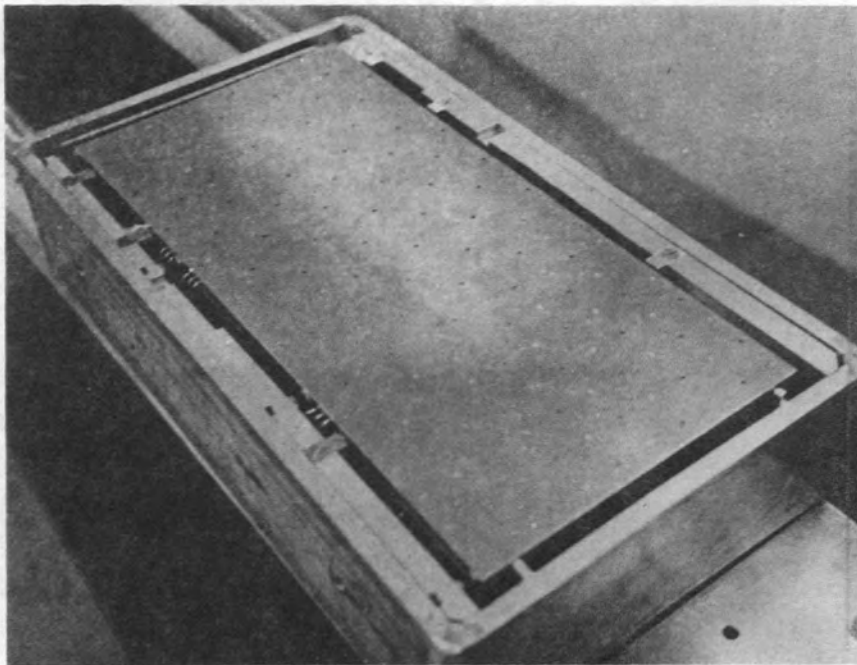


Fig. 3.10. Typical irradiation capsule with heater plate in position.

smaller specimens were first packed into 12 steel containers; four containers were then inserted into each capsule in the 4T CT specimen's loading pin holes. The top of the steel containers can be seen in Fig. 3.9. The fracture toughness specimens loaded into each capsule are identified below.

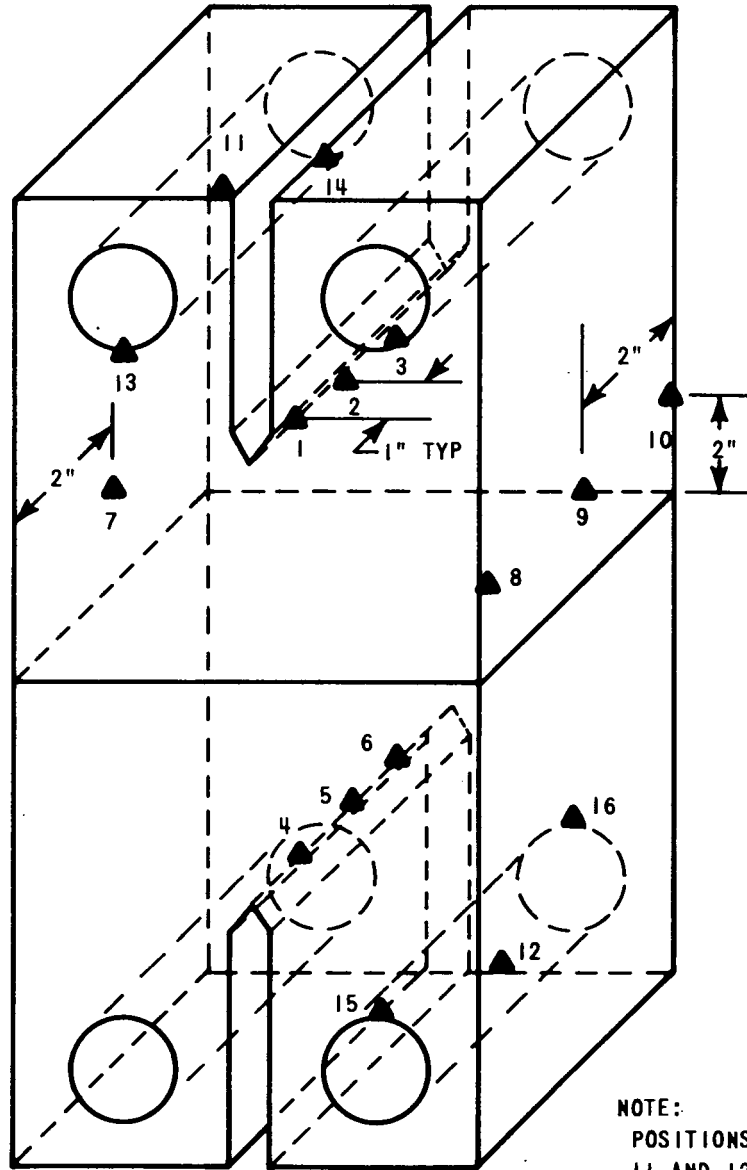
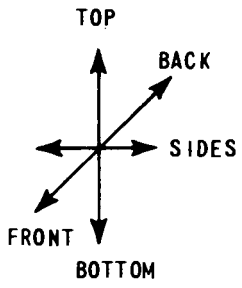
<u>Capsule designation</u>	<u>Specimen identification</u>	<u>Smaller specimen container identification</u>
Weld	W58-1, W58-2	1, ^a 2, 3, ^a 4
RW	W58-3, W58-4	5, ^a 6, 7, ^a 8
WR	O2GA-441, O2GA-442	9, ^a 10, 11, ^a 12

^aDenotes location of U₃O₈ dosimeters.

The thermocouple diagram is reproduced from Ref. 20 and shown as Fig. 3.11. Note that thermocouples 13 and 15 are located in the front surface as shown in Fig. 3.11. The capsules will be rotated periodically to minimize the flux attenuation through the 4-in.-thick specimens. For identification purposes, the surface containing thermocouples 13 and 15 was called face 1 and the opposite surface face 2. The purpose of identifying the two surfaces is to establish which face was nearer the core during a given irradiation cycle.

Specimen irradiation

In the initial reactor startup for each capsule, the reactor power was increased to 2 MW (full power) as rapidly as possible. Specimen temperatures achieved equilibrium levels approximately 1 hr later. Then, 2.5 to 3 kW of electrical heat was supplied to the back face of the capsule which increased specimen temperatures and gave a more uniform temperature pattern through the specimen thickness. About 20 to 30 min were required to achieve an equilibrium condition with auxiliary heat. Nitrogen was then added to the helium flowing through the capsule to raise the specimen temperatures to the desired operating levels. The startup temperature data for each capsule are presented in Figs. 3.12 to 3.14. Thermocouple locations are numbered in each figure. It should be noted that



NOTE:
 POSITIONS NUMBERED
 11 AND 12 ARE DIRECT
 MEASUREMENTS OF SMALL
 SPECIMENS PACKED
 INSIDE THE HOLES.

Fig. 3.11. Thermocouple positions inside capsule.

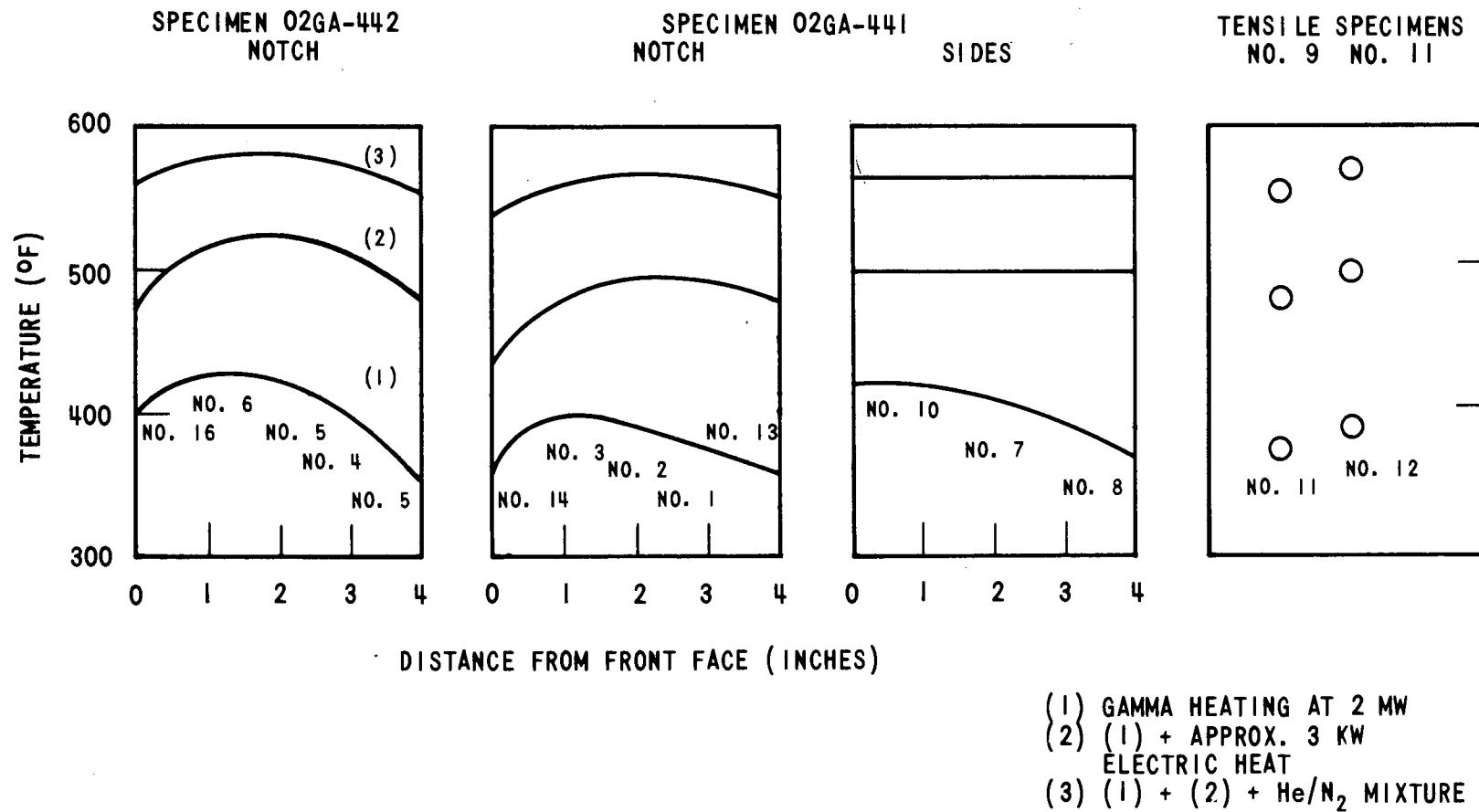
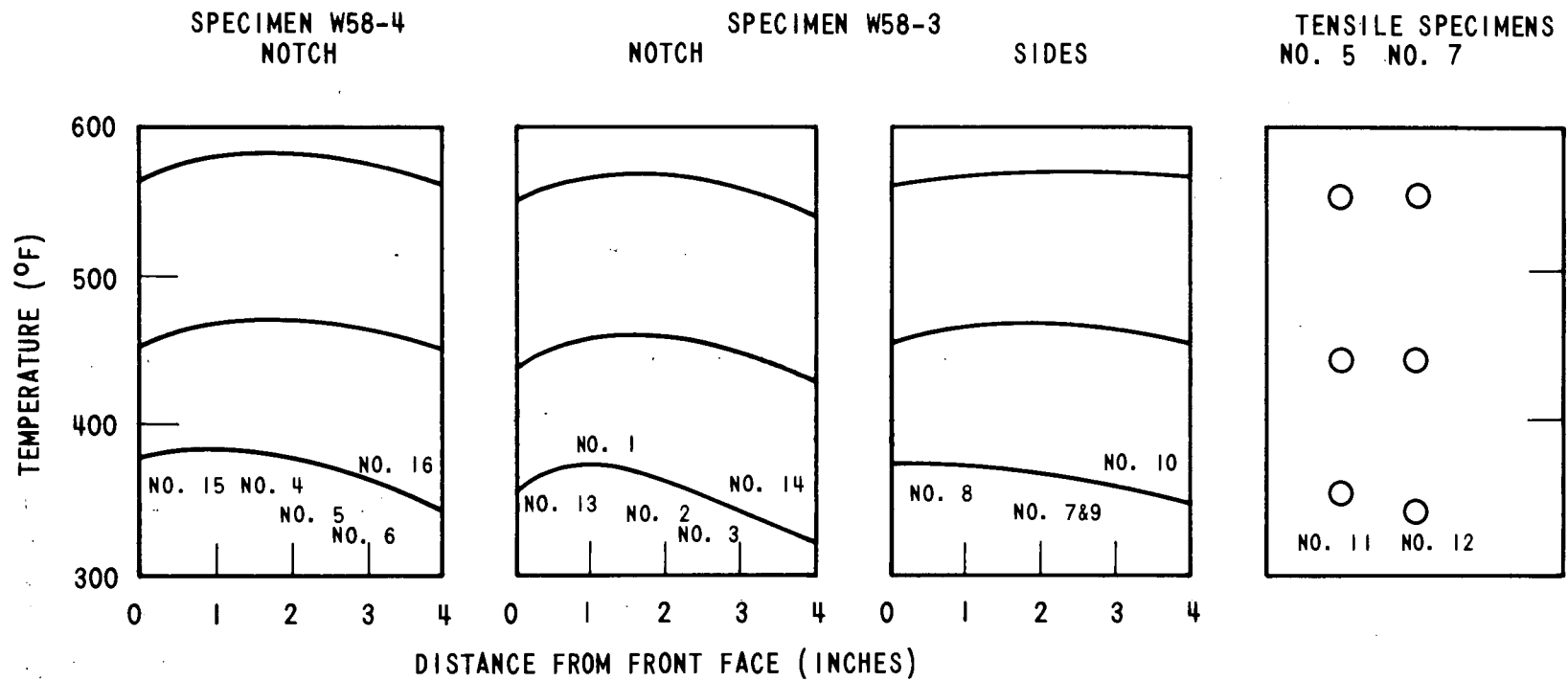
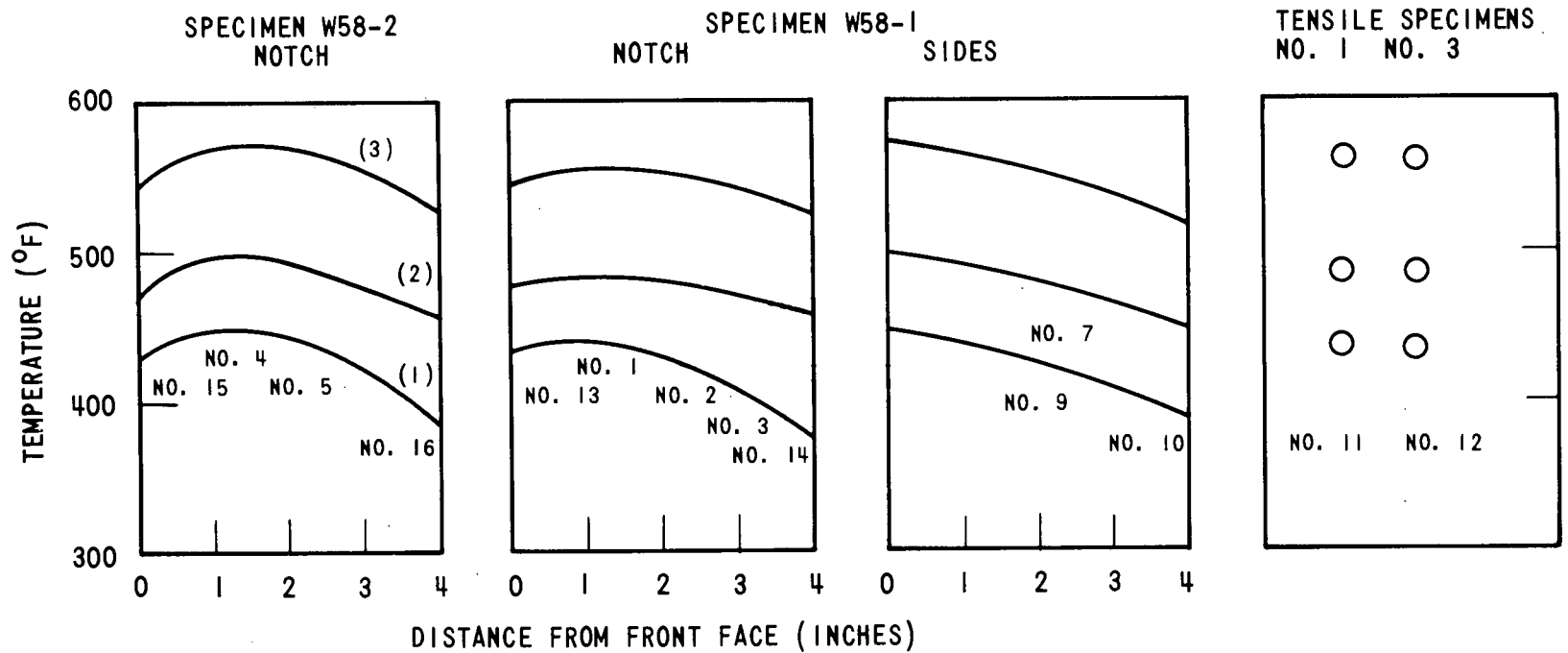


Fig. 3.12. Initial temperature data from capsule WR.



- (1) GAMMA HEATING AT 2 MW
- (2) (1) + APPROX. 2-3/4 KW ELECTRIC HEAT
- (3) (1) + (2) + He/N₂ MIXTURE

Fig. 3.13. Initial temperature data from capsule RW.



- (1) GAMMA HEATING AT 2 MW
- (2) (1) + APPROX. 2 KW
ELECTRIC HEAT
- (3) (1) + (2) + He/N₂ MIXTURE

Fig. 3.14. Initial temperature data from capsule weld.

the notch temperature profiles shown are established from five thermocouples spaced between the front and back surfaces; however, the two surface thermocouples are spaced several inches out of line with the notch thermocouples and may not provide precise profile termination points.

When capsule RW was installed, capsule WR was rotated 180° so that both capsules were positioned with face 1 nearer the core. At that time, capsule WR had been exposed for 418 3/4 hr with face 2 nearer the core. When capsule Weld was installed with face 1 nearer the core, capsules WR and RW had been irradiated 361 1/4 hr, each on face 1. Capsule WR was not rotated when capsule Weld was inserted. With all three capsules in place, the irradiation will continue with the same face nearer the core, and all capsules will be rotated at the same time. Capsule rotation will be scheduled about every 850 hr (two BRR cycles). As the irradiation termination dates approach, capsule rotation schedules will be adjusted to obtain equal exposures on each face.

The specimen temperatures are summarized in Table 3.2. To date, the specimen temperatures were generally at or below the designated maximum of 565°F. When the operating temperatures were at the low extremes of the reported ranges, the temperatures on the specimen surfaces, particularly at the back surface, were approximately 500 to 510°F. A temperature excursion occurred for a duration of no more than 2 hr early in cycle 314 when the reactor automatic control system did not properly compensate for a power change. Peak temperatures of 590 to 600°F were monitored in the lower notches at that time; this condition is not reflected in the reported temperatures in Table 3.2.

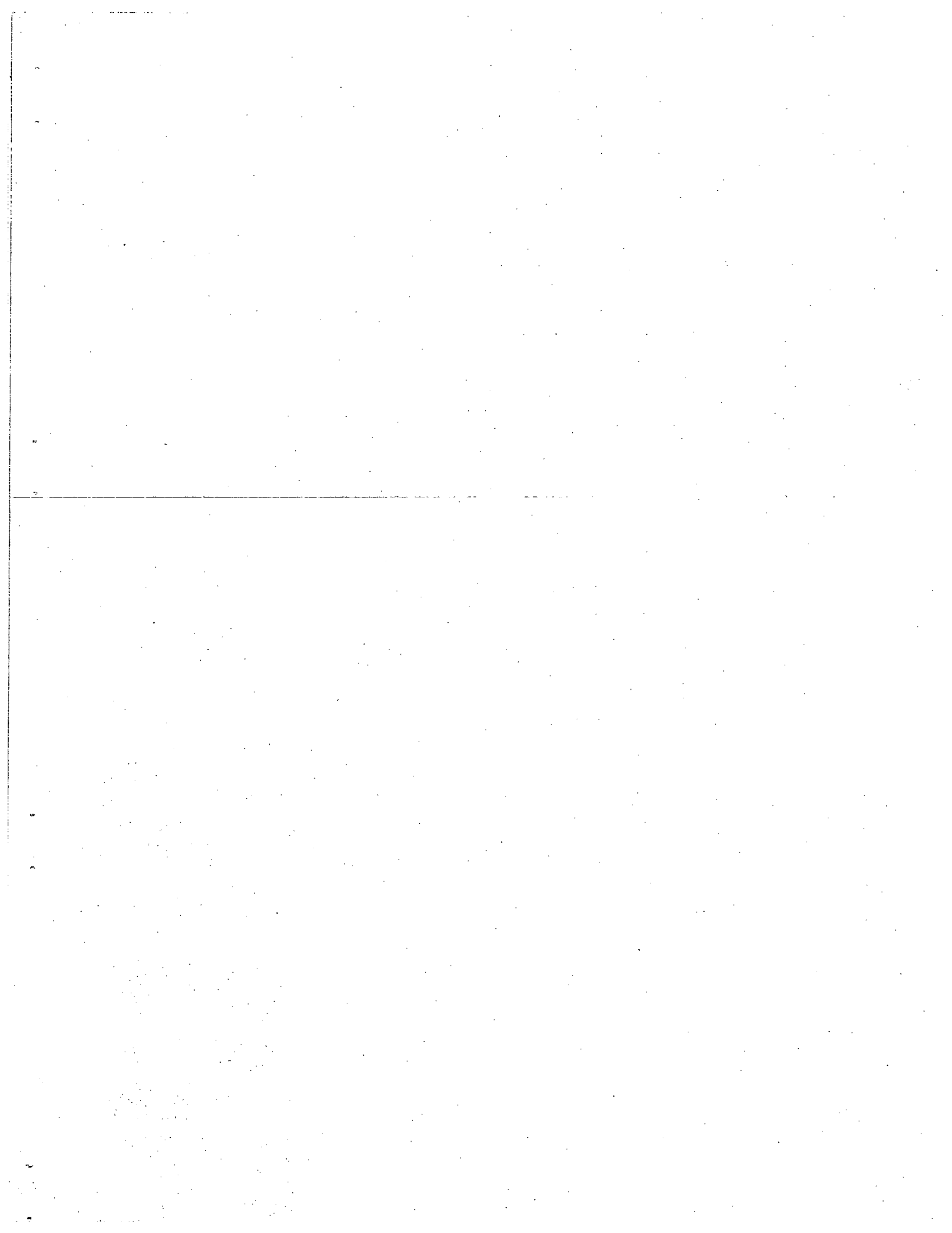
Table 3.2. Average temperatures (°F) in Westinghouse steel capsules

Time period	Capsule WR			Capsule RW			Capsule weld
	10/20-11/6	11/10-11/27	12/1-12/11	11/10-11/19	11/21-11/27	12/1-12/11	12/1-12/11
Face to core	2	1	1	1	1	1	1
Thermocouple No.							
1	570	560	560	560	550	560	560
2	580	570	570	560	550	555	565
3	560	560	560	550	540	540	555
4	580	570	570	560	540	580	585
5	590	570	570	560	540	580	575
6	585	560	560	550	530	570	a
7	580	580	580	560	545	570	575
8	575	555	b	550	540	560	a
9	a	a	a	565	550	565	570
10	575	555	b	555	540	550	530 ^c
11	565	560	565	550	540	550	575
12	570	560	565	530	510	550	575
13	555	550	b	540	530	545	560
14	550	545	b	530	520	525	540
15	560	545	b	540	520	560	555
16	570	535	b	535	515	550	545

^a Thermocouple inoperable or not functioning correctly at start of irradiation.

^b Thermocouple not monitored.

^c A questionable value, since it is much lower than values monitored from TC's 7 and 9 and data from other capsules.



4. PRESSURE VESSEL AND PIPING INVESTIGATIONS

These investigations encompass the complex stress state task, the simulated service test task, and the portion of the specific safety research task that deals with the extent of ductile pipe rupture. No work was performed this reporting period under the complex stress state task. The pressure vessel tests discussed herein, as well as the supporting properties testing and acoustic emission monitoring for the pressure vessel investigations, are part of the simulated service test task.

CHARACTERIZATION OF INTERMEDIATE TEST VESSEL MATERIALS

W. J. Stelzman

Prolongations of intermediate vessels V-2, V-3, and V-4 were studied to obtain tensile, Charpy-V impact, and static lower-bound fracture toughness data. These data were used in conjunction with other data to set the fracture criteria and predict failure as was done for vessel V-1 prior to rupturing the vessel. The mill mechanical properties, mill analyses, welding procedures, and general vessel descriptions were given previously.^{1,2} Vessel V-2, with no longitudinal seam weld and one introduced flaw, was essentially the same as V-1. Both vessels V-3 and V-4 had a

1. C. E. Childress, *HSSST Program Semiannu. Progr. Rep. Aug. 31, 1971*, ORNL-4764, pp. 62-67.

2. C. E. Childress, *HSSST Program Semiannu. Progr. Rep. Feb. 29, 1972*, ORNL-4816, pp. 96-99.

longitudinal, submerged-arc seam weld and one induced flaw in the weld metal; V-4 had an additional flaw in the base metal.

The tensile specimen results were obtained from circumferentially (C) oriented³ 0.178-in.-gage-diam tensile specimens at a strain rate of 0.016 in./min. Yield and ultimate stress results from V-4 base metal at 75°F were identical to those of the V-1 base metal,³ both in magnitude and variation through the vessel wall. Results from V-2 base metal at 78°F indicate that the yield and ultimate stresses are slightly higher than the V-1 and V-4 strengths but follow the same decrease in strength from the outer surface to midthickness. After midthickness, the V-2 stresses remain constant to within about 1/4 in. from the inner surface.

Tensile results from the weld metal indicated a somewhat different through-the-wall distribution than the base metal. Figure 4.1 shows strength values obtained from V-3 weld metal. The outer portion of the weld was deposited first and the inner portion last. The region where

3. W. J. Stelzman, *HSST Program Semiannu. Progr. Rep. Aug. 31, 1972*, ORNL-4855, pp. 38-40.

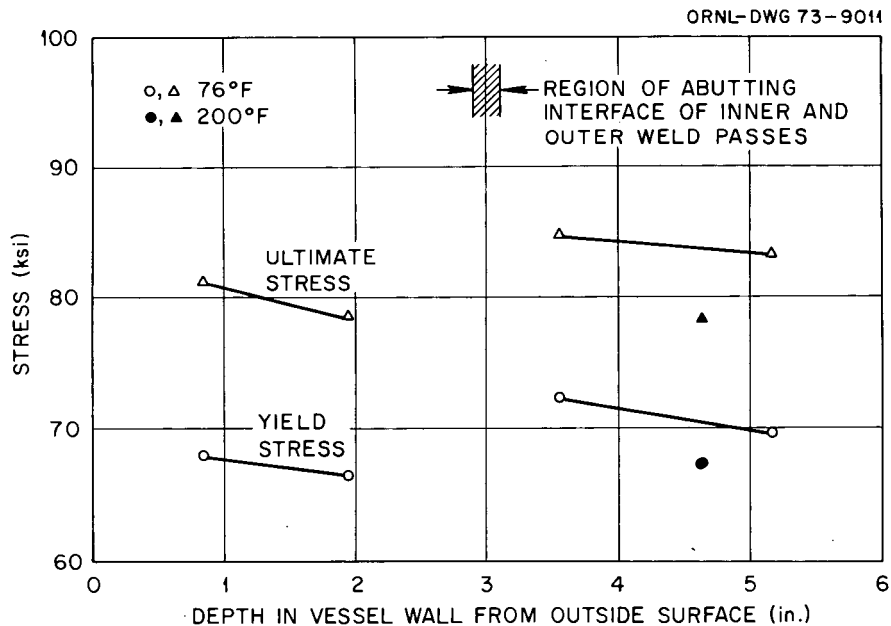


Fig. 4.1. Tensile properties obtained from intermediate vessel V-3 using C-oriented subsized tensile specimens from a 6-in.-thick weld in ASTM A508, class 2 forging steel.

the inner and outer weld passes abutted was determined by surface etching a cross section of the weld to bring out the weld passes. This region is noted in Fig. 4.1. It is evident that the strength values from the outer half of the weld are considerably lower than the base metal values, whereas the strength values from the inner half of the weld are comparable with the base metal results. It was thought that the repairs² to the weld may have been responsible, but the tensile results from V-4 weld metal (Fig. 4.2) show the same type of behavior. The reason for this phenomenon is not apparent at this time.

Standard Charpy-V impact data obtained from 3/8T and 5/8T CA-oriented specimens from V-2 base metal and 2/3T CA-oriented specimens from V-4 base metal agree with the impact data³ obtained from 3/8T and 5/8T specimens of the same orientation from V-1 base metal when the normal scatter expected of Charpy energy data is considered. An energy scan was made from the inner (1T) surface, the outer (OT) surface, and the central (1/4, 1/2, 3/4T) base metal from V-2 at four test temperatures (-50, 0, 50, and

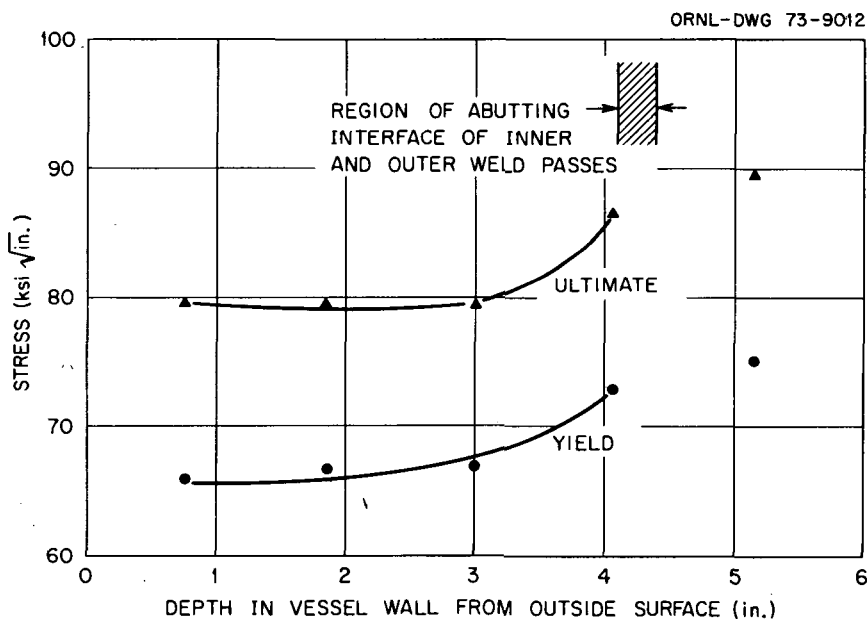


Fig. 4.2. Tensile properties obtained from intermediate vessel V-4 using C-oriented subsized tensile specimens from a 6-in.-thick weld in ASTM A508, class 2 forging steel.

100°F) and in the transition region of the Charpy energy curve. The results were similar to those of the V-1 scan. The outer surface energies agreed with the V-1 data, and no significant differences were noted between the central and inner surface material energies, which were 12 ft-lb lower than the outer surface material energies. Results from V-1 showed a 20-ft-lb difference, indicating that the V-2 inner regions were slightly tougher than the V-1 counterparts.

The Charpy-V impact data from 1/4T and 1/3T AC-oriented specimens from V-2 base metal also agreed with the results from similar depths and orientations in V-1 base metal.

Static fracture toughness data, K_{Icd} , from CA-oriented precracked Charpy V-notch specimens were also obtained for the three vessels. Results from the base metal of V-2 and V-4 are shown in Figs. 4.3 to 4.5, and the results from V-3 and V-4 weld metal are shown in Figs. 4.6 to 4.8. In some instances, a minimum of specimens were available for test, and, in others, a particular temperature or depth range was chosen for principal investigation.

The variations of fracture toughness at several temperatures and at various depths in V-2 base metal are shown in Fig. 4.3. Between 32 and 200°F, the K_{Icd} values appear to be the same for all depths and may decrease with increasing temperature. Below 32°F, the outer surface material exhibits higher K_{Icd} values than either the central or inner surface material, which shows a similar rapid decrease in K_{Icd} values with decreasing temperatures. Figure 4.4 shows these same data plotted to show the variation of K_{Icd} through the wall thickness at several temperatures. At temperatures below 32°F and above 100°F, the inner and outer surface K_{Icd} values appear higher than the central material toughness values; the outer surface K_{Icd} values are also higher than the inner surface toughness. For these temperatures, K_{Icd} appears to become a minimum at about 2/3T. Between 32 and 100°F, the K_{Icd} values are both high and relatively constant through the entire wall.

Figure 4.5 shows the data from V-4 base metal and indicates the same fracture toughness variations with temperature as the V-2 data (Fig. 4.3), except that the V-4 data show additional variations in K_{Icd} values between

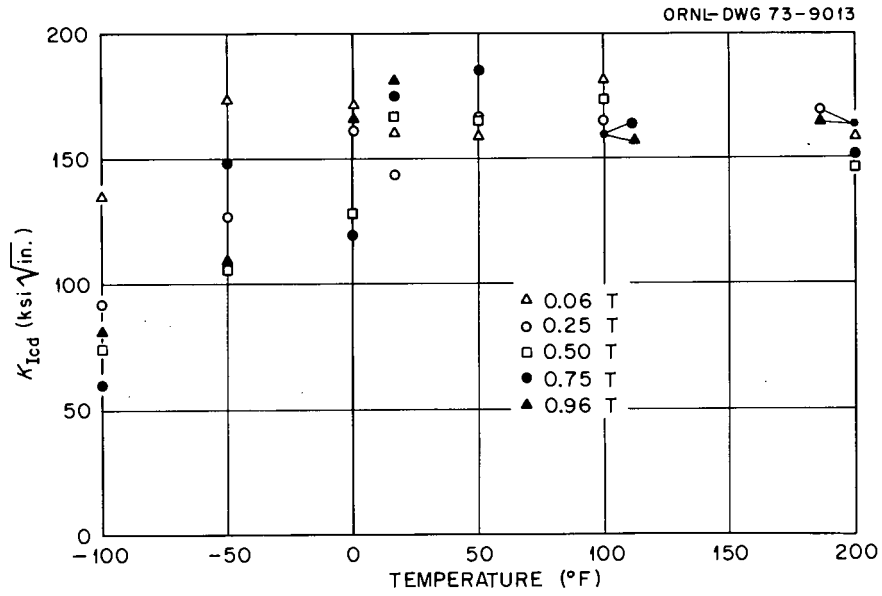


Fig. 4.3. Lower-bound fracture toughness values obtained from intermediate vessel V-2 using CA-oriented precracked Charpy-V specimens from 6-in.-thick ASTM A508, class 2 forging steel.

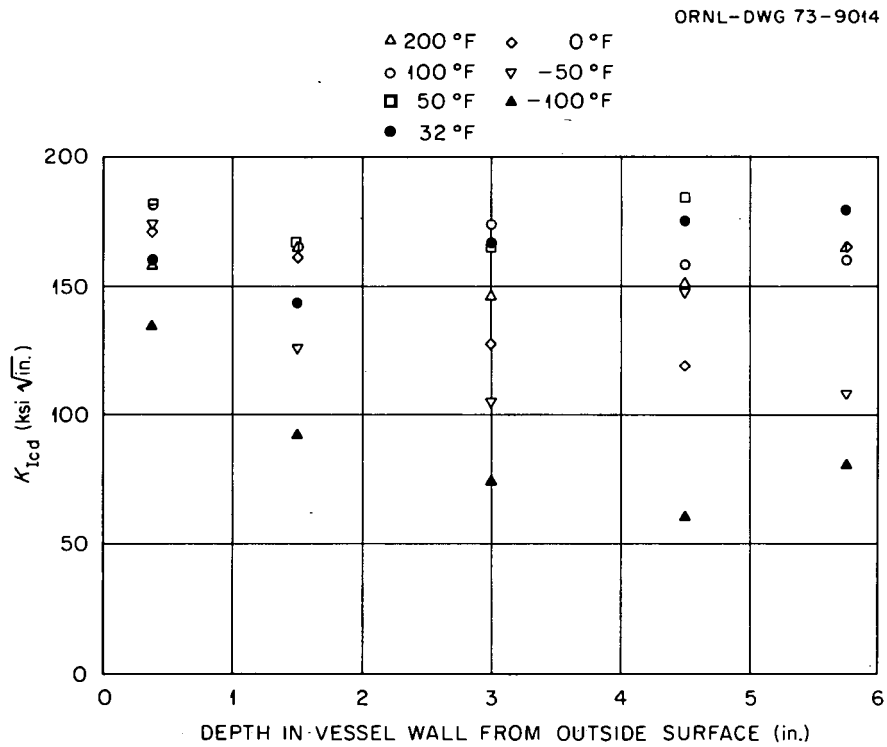


Fig. 4.4. Lower-bound fracture toughness values obtained from intermediate vessel V-2 using CA-oriented precracked Charpy-V specimens from 6-in.-thick ASTM A508, class 2 forging steel.

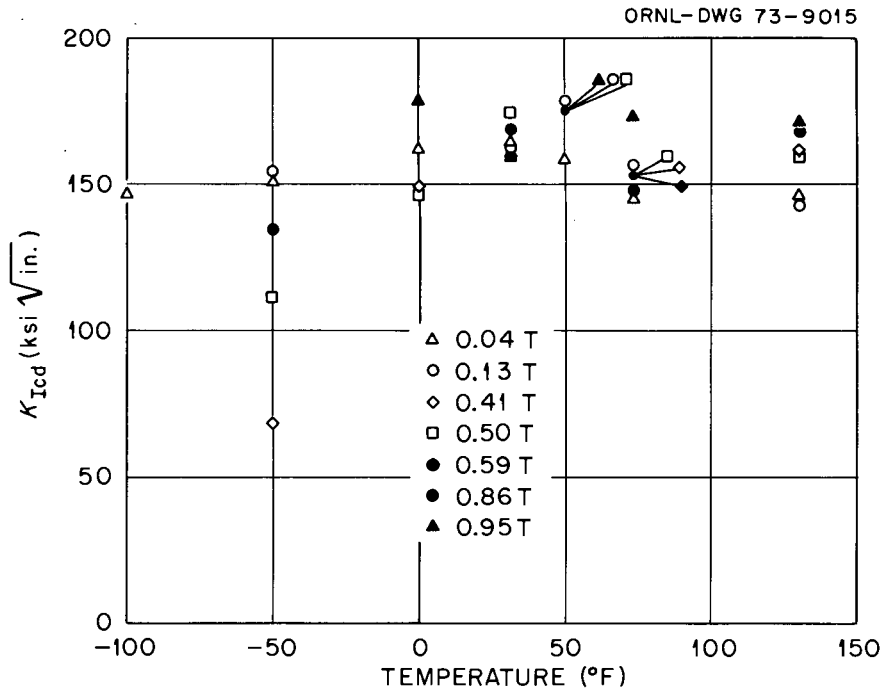


Fig. 4.5. Lower-bound fracture toughness values obtained from intermediate vessel V-4 using CA-oriented precracked Charpy-V specimens from 6-in.-thick ASTM A508, class 2 forging steel.

32 and 75°F. Absence of this variation in the V-2 data may be due to insufficient data or an abnormality in the scatter of the V-4 data.

The variation of K_{Icd} with temperature and depth for submerged-arc weld metal from V-3 and V-4 is shown in Figs. 4.6 to 4.8. A greater data density at -50°F in Fig. 4.6 suggests that V-3 may have higher toughness values at lower temperatures; however, additional K_{Icd} data from V-4 (Fig. 4.7) at -50°F would result in both welds exhibiting a similar behavior, that is, a decrease in K_{Icd} below 32°F and the same toughness plateau above 32°F. Figure 4.8 shows the V-4 data from Fig. 4.7 plotted to show the through-the-weld variations of K_{Icd} at several temperatures. The toughness values are fairly constant through the weld between 0 and 200°F, and insufficient data below 0°F bar any conclusion other than K_{Icd} values are lower. Also, a decrease in toughness near the region of interface between the inner and outer welds is indicated. Higher K_{Icd} values near the surfaces of the weld were not in evidence.

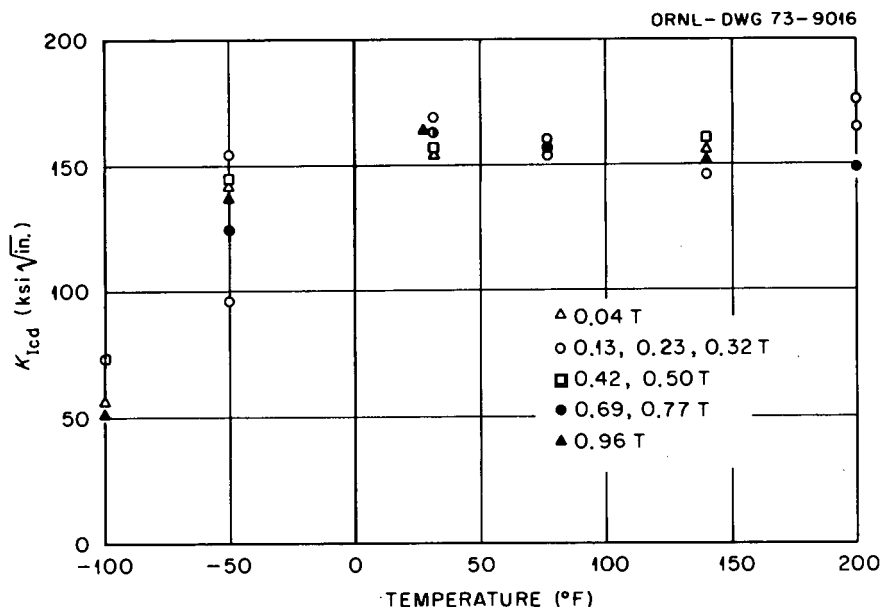


Fig. 4.6. Lower-bound fracture toughness values obtained from intermediate vessel V-3 using CA-oriented precracked Charpy-V specimens from a 6-in.-thick weld in ASTM A508, class 2 forging steel.

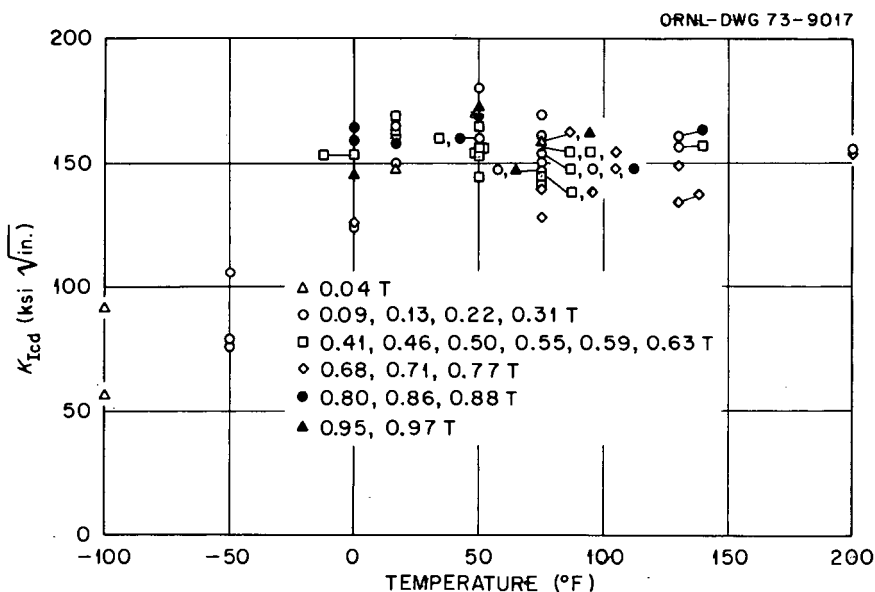


Fig. 4.7. Lower-bound fracture toughness values obtained from intermediate vessel V-4 using CA-oriented precracked Charpy-V specimens from a 6-in.-thick weld in ASTM A508, class 2 forging steel.

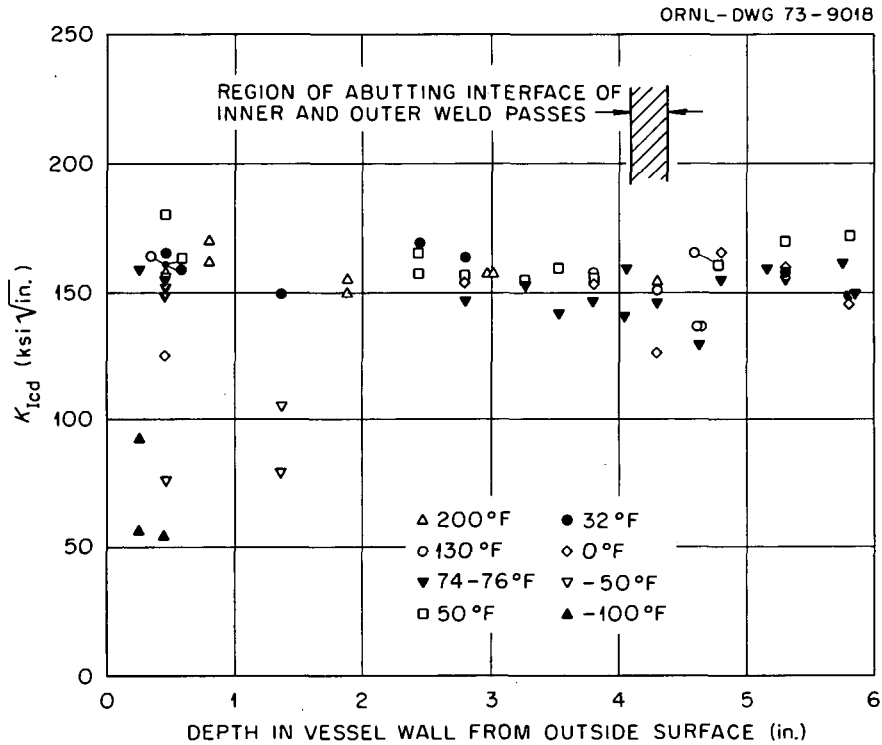


Fig. 4.8. Lower-bound fracture toughness values obtained from intermediate vessel V-4 using CA-oriented precracked Charpy-V specimens from a 6-in.-thick weld in ASTM A508 class 2 forging steel.

In addition to completing the V-2, V-3, and V-4 studies, materials from intermediate vessels V-5 and V-6, other steels, and other product forms are being investigated and should provide similar data.

FRACTURE TOUGHNESS CHARACTERIZATION OF HSST
INTERMEDIATE PRESSURE VESSEL MATERIAL⁴

P. C. Riccardella L. R. Singer

Introduction

In order to demonstrate the capability to predict failure of large, heavy-walled pressure vessels under service-type loading conditions, the HSST program includes a series of pressure vessel tests which are intermediate between conventional laboratory tests and a full-scale vessel.

4. Work sponsored by HSST program under UCCND Subcontract No. 3196 between Union Carbide Corporation and Westinghouse Electric Corporation.

The intermediate pressure vessels contain a cylindrical test course approximately 54 in. long and 6 in. thick. The third and fourth vessels contained longitudinal welds in the test course for comparison of weldment vs base metal behavior. To characterize the material properties of these test vessels, 24-in. prolongations of the test courses (including the weldments) were removed prior to welding on the heads. This section describes the fracture toughness testing of the forging prolongations from the third and fourth vessels.

Specimen Fabrication

Forty-two compact-tension specimens were machined from the forging prolongations from the third and fourth pressure vessels, V-3 and V-4. Sixteen specimens were machined from the weldment region of the third vessel prolongation (Fig. 4.9). These specimens included six 0.394T CT specimens, nine 0.85T CT specimens, and one 3T CT specimen. Ten specimens were machined from the weldment region of the fourth vessel (Fig. 4.10), including nine 0.85T CT specimens and one 4T CT specimen. Also, sixteen specimens were machined from the base metal region of the fourth vessel (Fig. 4.11), including ten 0.85T CT specimens and six 4T CT specimens. The base metal specimens included both center thickness and outside surface specimens. All the specimens were fatigue precracked according to the methods specified in Ref. 5.

Test Program

Specimen test temperatures were specified during the test program in order to determine test temperatures which would yield failures in the desired fracture regimes (frangible, transitional, or ductile). Test temperatures of 130°F for the third vessel and 75°F for the fourth vessel were selected, based on this material characterization study.

These test temperatures are in the temperature range where very large specimens (greater than 6T CT) would be necessary to perform valid fracture toughness testing according to the ASTM recommended procedure.⁵ For

5. Tentative Method of Test for Plane-Strain Fracture Toughness of Metallic Materials, ASTM E399-70T.

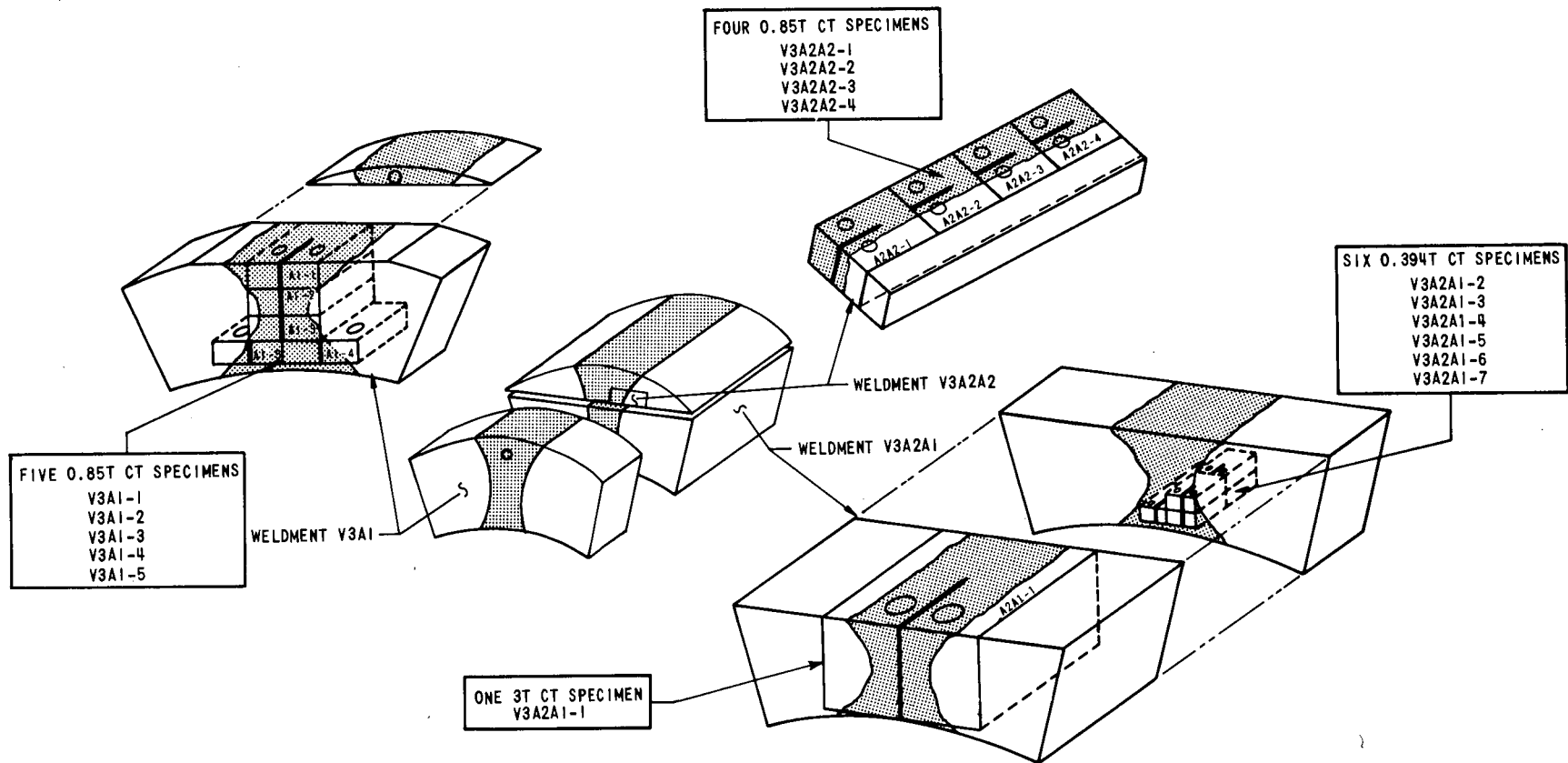
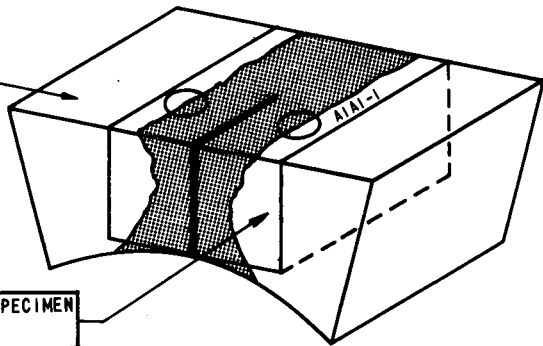
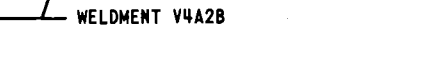
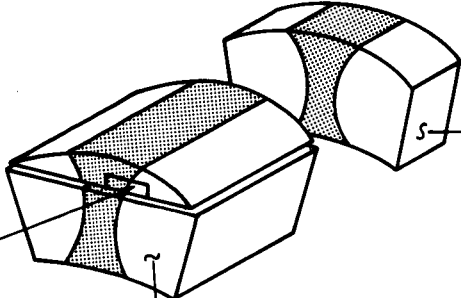
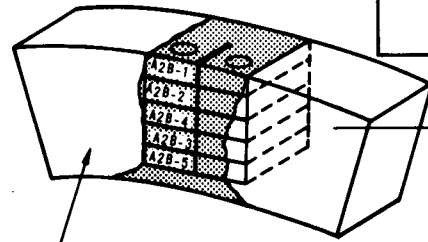
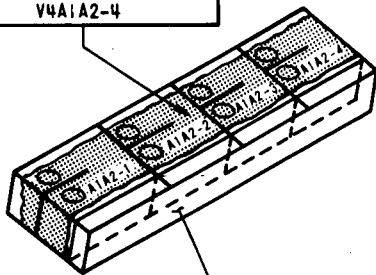


Fig. 4.9. Machining of fracture toughness specimens from HSST intermediate pressure vessel V-3 weldment.

FOUR 0.85T CT SPECIMENS
V4A1A2-1
V4A1A2-2
V4A1A2-3
V4A1A2-4

FIVE 0.85T CT SPECIMENS
V4A2B-1
V4A2B-2
V4A2B-3
V4A2B-4
V4A2B-5



WELDMENT V4A1A2

WELDMENT V4A2B

WELDMENT V4A1A1

ONE 4T CT SPECIMEN
V4A1A1-1

WELDMENT V4A2B

Fig. 4.10. Machining of fracture toughness specimens from HSST intermediate pressure vessel V-4 weldment.

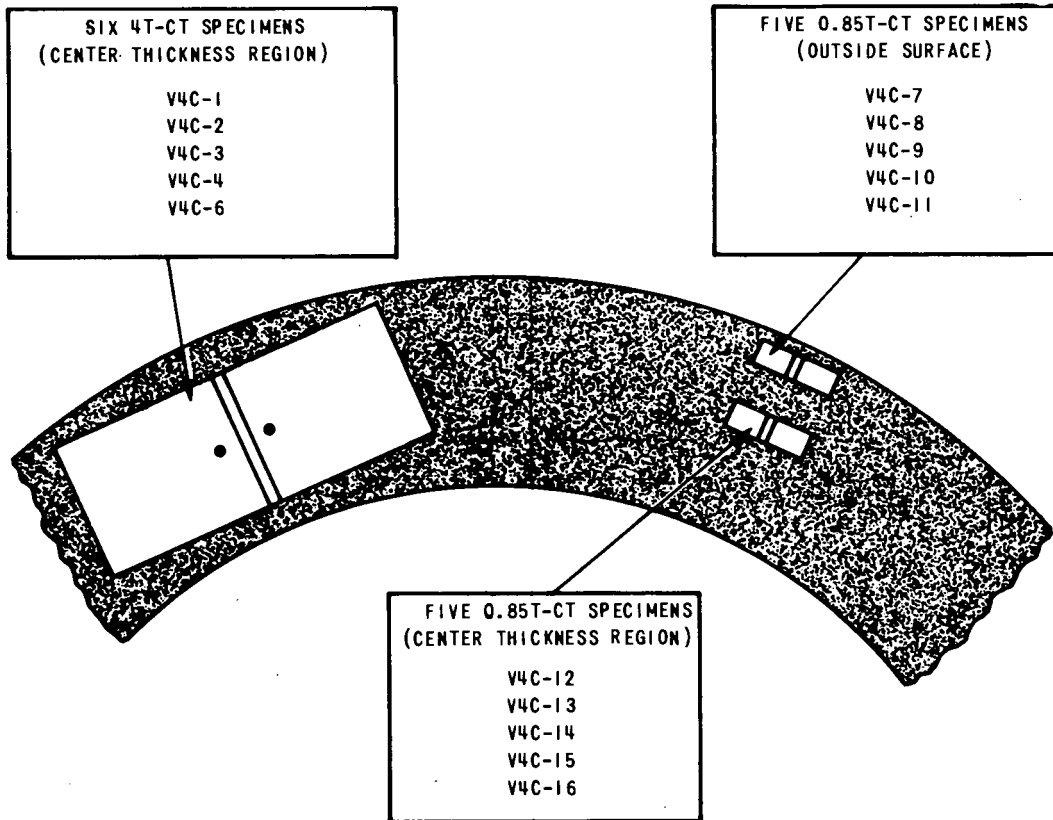


Fig. 4.11. Machining of fracture toughness specimens from HSST intermediate pressure vessel V-4 base metal.

this reason, the equivalent-energy concept⁶ was used to interpret the data in terms of lower-bound values of the actual fracture toughness.

Test Results

The results of these tests are summarized in Tables 4.1 to 4.3. Table 4.1 gives the fracture toughness data for the weldment material from the third pressure vessel, Table 4.2 covers the weldment material from the fourth pressure vessel, and Table 4.3 covers the base metal from this vessel. The toughness data from these tables are illustrated graphically as a function of temperature in Figs. 4.12 to 4.14 respectively.

6. F. J. Witt, "A Procedure for Determining Bounding Values on Fracture Toughness K_{Ic} at Any Temperature," HSST 5th Annual Information Meeting, Paper 13, March 1971.

Table 4.1. Fracture toughness results determined from testing 3T, 0.850T, and 0.394T compact-tension specimens from HSST V-3 weldment

Specimen No.	Test temp. (°F)	Crack length (in.)	Maximum load (lb)	Energy to maximum load (in.-lb)	P_Q (lb)	Energy to P_Q (in.-lb)	K_{Icd} (ksi $\sqrt{\text{in.}}$)
0.394T CT specimens (weldment V3A2A1)							
V3A2A1-2	-100	0.414	1,850	16.3	1,000	5.0	55.0
V3A2A1-3	-50	0.418	2,510	61.1	1,000	4.8	110.0
V3A2A1-4	+32	0.421	2,320	197.3	1,000	5.0	197.0
V3A2A1-5	+75	0.405	2,490	152.2	1,000	4.7	166.3
V3A2A1-6	+130	0.410	2,275	197.5	1,000	4.4	198.5
V3A2A1-7	+200	0.410	2,250	159.0	1,000	4.8	171.5
0.850T CT specimens (weldment V3A1)							
V3A1-1	-50	0.881	5,800	64.8	4,000	30.7	53.0
V3A1-4	+32	0.918	8,270	133.3	4,000	32.8	86.7
V3A1-2	+100	0.886	11,380	963.4	4,000	28.2	215.1
V3A1-3	+130	0.883	11,000	780.6	4,000	30.6	184.6
V3A1-5	+130	0.800	11,590	1,034.1	4,000	29.3	221.4
0.850T CT specimens (weldment V3A2A2)							
V3A2A2-4	±0	0.926	9,800	263.0	4,000	32.2	113.3
V3A2A2-3	+32	0.911	9,540	232.1	4,000	31.5	104.4
V3A2A2-2	+130	0.878	11,600	838.3	4,000	33.8	180.5
V3A2A2-1	+200	0.880	11,200	553.0	4,000	31.4	152.4
3T CT specimen (weldment V3A2A1)							
V3A2A1-1	+130	3.356	113,500	11,680.0	40,000	554.0	287.0

Table 4.2. Fracture toughness results determined from testing 0.850T and 4T compact-tension specimens from HSST V-4 weldment

Specimen No.	Test temp. (°F)	Crack length (in.)	Maximum load (lb)	Energy to maximum load (in.-lb)	P_Q (lb)	Energy to P_Q (in.-lb)	K_{Icd} (ksi $\sqrt{\text{in.}}$)
0.850T CT specimens (weldment V4A2B)							
V4A2B-3	+32	0.878	11,200	1,734.5	4,000	27.4	289.5
V4A2B-5	+50	0.883	10,350	342.7	4,000	27.6	129.3
V4A2B-4	+50	0.871	11,350	541.7	4,000	26.0	164.1
V4A2B-1	+50	0.881	11,100	1,348.8	4,000	27.8	255.0
V4A2B-3	+75	0.887	11,600	361.4	4,000	27.6	133.7
0.850T CT specimens (weldment V4A1A2)							
V4A1A2-1	-50	0.887	9,900	228.8	4,000	26.0	112.7
V4A1A2-2	+32	0.876	11,150	930.1	4,000	24.0	226.3
V4A1A2-3	+50	0.888	10,600	1,231.7	4,000	26.0	262.0
V4A1A2-4	+130	0.863	10,850	1,475.3	4,000	26.2	266.0
4T CT specimen (weldment V4A1A1)							
V4A1A1-1	+75	3.963	197,500	9,600.0	80,000	1,136.0	194.4

Table 4.3. Fracture toughness results determined from testing 0.850T and 4T compact-tension specimens from HSST V-4 base metal

Specimen No.	Test temp. (°F)	Crack length (in.)	Maximum load (lb)	Energy to maximum load (in.-lb)	P_Q (lb)	Energy to P_Q (in.-lb)	K_{Icd} (ksi $\sqrt{\text{in.}}$)
0.805T CT specimens (outside surface)							
V4C-7	-150	0.871	4,750	40.7	4,000	15.2	44.0
V4C-8	-50	0.853	12,250	369.4	4,000	23.2	139.0
V4C-9	± 0	0.872	11,975	723.4	4,000	30.8	174.0
V4C-10	+50	0.867	11,900	1,176.8	4,000	28.3	230.4
V4C-11	+100	0.864	11,750	1,182.0	4,000	25.3	243.0
0.850T CT specimens (center thickness region)							
V4C-12	+32	0.855	12,200	1,054.1	4,000	26.4	220.3
V4C-13	+50	0.883	11,600	1,394.5	4,000	26.0	269.0
V4C-16	+50	0.855	12,000	1,483.3	4,000	27.1	258.0
V4C-14	+75	0.881	11,650	1,624.8	4,000	27.8	280.0
V4C-15	+130	0.878	11,300	1,080.6	4,000	29.8	220.1
4T CT specimens (center thickness region)							
V4C-1	+32	4.120	208,000	12,972.0	80,000	1,504.0	209.9
V4C-2	+50	4.138	214,000	15,436.0	80,000	1,428.0	235.0
V4C-5	+50	4.166	199,500	12,400.0	80,000	1,572.0	203.0
V4C-3	+75	4.139	221,000	20,260.0	80,000	1,520.0	261.0
V4C-6	+75	4.205	218,000	23,808.0	80,000	1,564.0	286.0
V4C-4	+130	4.156	222,000	31,752.0	80,000	1,432.0	338.6

Although the data from these tests are comparable with data previously obtained for steels of this type,^{7,8} there are some differences. The tests on vessel V-4 indicate that the toughness of the weldment material is less than that of the base metal, while the converse has generally been true in the past. Comparison of the weldment data for these two vessels with the base metal data for the first and second HSST intermediate pressure vessels⁹ indicates significantly more scatter in weldment than in base

7. T. R. Mager, "Experimental Verification of Lower Bound K_{IC} Values Utilizing the Equivalent Energy Concept," HSST 6th Annual Information Meeting, Paper 23, April 1972.

8. W. O. Shabbits, W. H. Pryle, and E. T. Wessel, *Heavy Section Fracture Toughness Properties of A533 Grade B, Class 1 Steel Plate and Submerged Arc Weldment*, HSST Program Technical Report No. 6 (December 1969).

9. *HSST Program Semiannu. Progr. Rep. Aug. 31, 1972*, ORNL-4855.

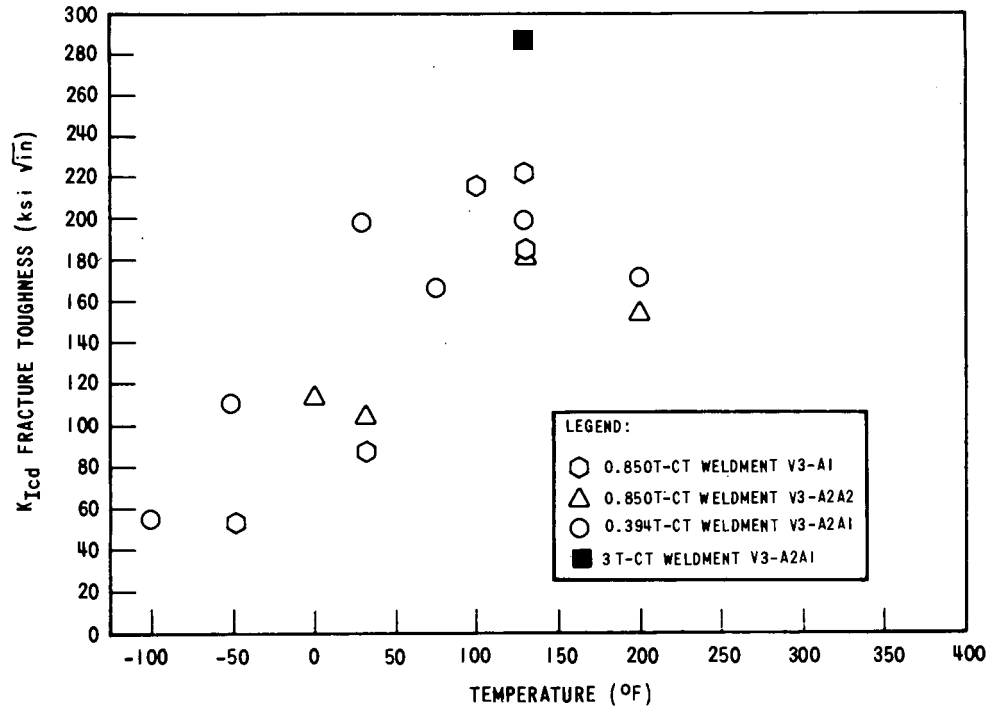


Fig. 4.12. Fracture toughness data for HSST intermediate pressure vessel V-3 weldment material.

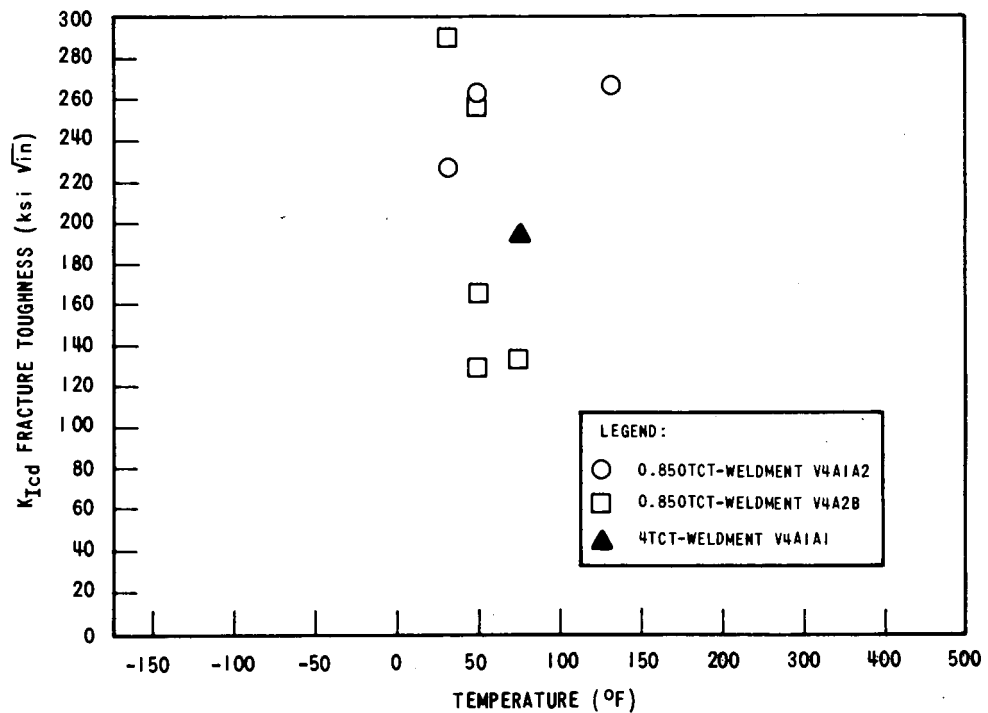


Fig. 4.13. Fracture toughness data for HSST intermediate pressure vessel V-4 weldment material.

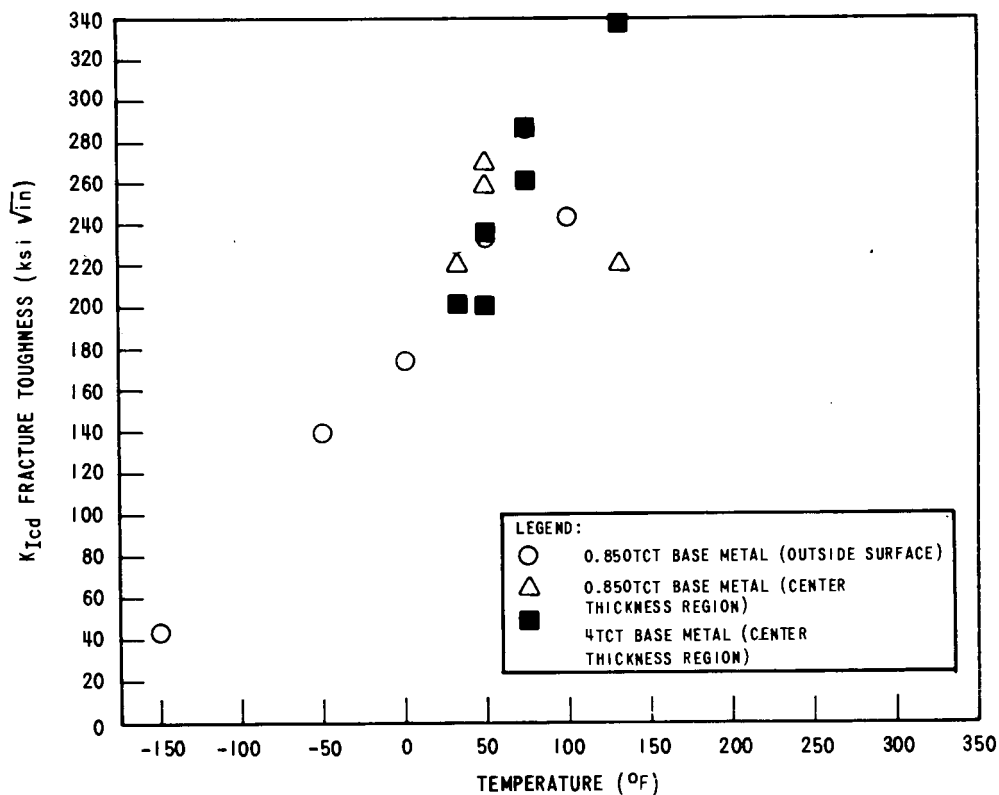


Fig. 4.14. Fracture toughness data for HSST intermediate pressure vessel V-4 base metal.

metal. However, this scatter is a function of location through the thickness, as may be noted from Fig. 4.10.

FRACTOGRAPHY STUDY OF FAILURE IN INTERMEDIATE TEST VESSEL V-1

D. A. Canonico

The intermediate test vessels are fabricated from a cylindrical center section, a hemihead bottom, and a top transition piece. The material from which these pieces are made is ASTM A508, class 2 forging steel. The components are joined by submerged-arc welding of the circumferential joints. A fatigue-sharpened, semielliptical flaw approximately 8 in. long and 2 5/8 in. deep was placed at the midpoint of the center cylindrical section of vessel V-1. The flaw is oriented perpendicular to the tangent and parallel to its axis.

The first vessel, V-1, was internally pressurized to destruction on June 30, 1972. It was tested at 130°F and failed at a pressure of 28,800 psi. The vessel underwent approximately 1% strain prior to failure and failed by splitting longitudinally.

Fracture Propagation

The fracture propagated to the top head in the upward direction and around the bottom hemihead in the downward direction. The upward propagation of the crack ran through the circumferential weld that joined the transition piece to the cylindrical test section and terminated at the interface between the transition piece and the bolted-on cover plate. The downward propagation path was through the circumferential weld that joins the bottom hemihead to the center cylindrical test section. The crack continued around the bottom and terminated near the circumferential weld, approximately 180° from where it first entered the bottom hemihead.

Because of the nature of the failure, we decided to conduct an extensive study of the fracture surface. The scanning electron microscope (SEM) in the Metals and Ceramics Division of ORNL was employed. Initially, we attempted to extract fracture surface replicas without disturbing the failed vessel. However, the rough texture of the fracture did not allow this nondestructive approach, so we decided that oxyacetylene burning and saw cutting was the most expedient and least expensive technique available for obtaining samples. The flame cut was made approximately 8 in. away from the fracture surface, which is more than ample to assure that the flame-cutting operation would have no effect. A photograph of the fracture surface prior to sawing is shown in Fig. 4.15, where the original man-made flaw is quite evident. The circumferential weld that joined the bottom hemihead to the cylindrical test section is easily seen at the left side of the photograph. (It is located at the change in contour.) The circumferential weld at the upper end of the cylindrical test section is not evident; however, it too is located at the geometric change in section size at the right side of the photograph.



Fig. 4.15. Photograph of fracture surface from intermediate test vessel V-1.

Fractography Study

Several regions of the fracture surface shown in Fig. 4.15 were studied. One is located in the transition piece; others are located in the cylindrical test section and the hemihead.

Figure 4.16 shows the results of the SEM study of the region just adjacent to the man-made flaw. Two areas within this region were studied. (The corner of the flaw can be seen.) From the appearance of the fracture surface, we concluded that this region exhibited a dimpled mode of failure.

A region just under the steel rope shown in Fig. 4.15 was also investigated. This location exhibits a change in appearance and coloration. The dark "ductile" coloration seems to terminate in a V, and chevron lines, lighter in color, appear to originate from its apex. This is usually indicative of an initiation site for fracture propagation. Figure 4.17 contains the results of the fractography study of this region. Two areas were studied; the first, located close to the center of the fracture surface, was within an area that was similar (visually) to the regions shown in Fig. 4.16. It has a fracture appearance nearly identical to those previously discussed. The second area studied was from outside the V-shaped area and in the lighter (shinier) area. The fracture surface of this area is different from that of Fig. 4.16; this area exhibits a fracture surface identical to that seen in a low-energy (cleavage) failure.

Additional regions were studied, which included regions approximately 3 in. from the circumferential welds in the top transition piece and the bottom hemihead. Both exhibit cleavage fracture. Regions in the cylindrical test section approximately 3 in. from the two circumferential welds were also found to exhibit cleavage fracture appearances.

In summary, the fractography study revealed that the region around the man-made flaw exhibited a fracture appearance that is indicative of tough behavior (dimpled). This mode of failure continues for some distance in either direction away from the man-made flaw to a point where it undergoes a transition from dimple to cleavage. This cleavage fracture continues and is found in both the bottom hemihead and in the top transition piece.

ITV V1 ASTM A508 CL 2

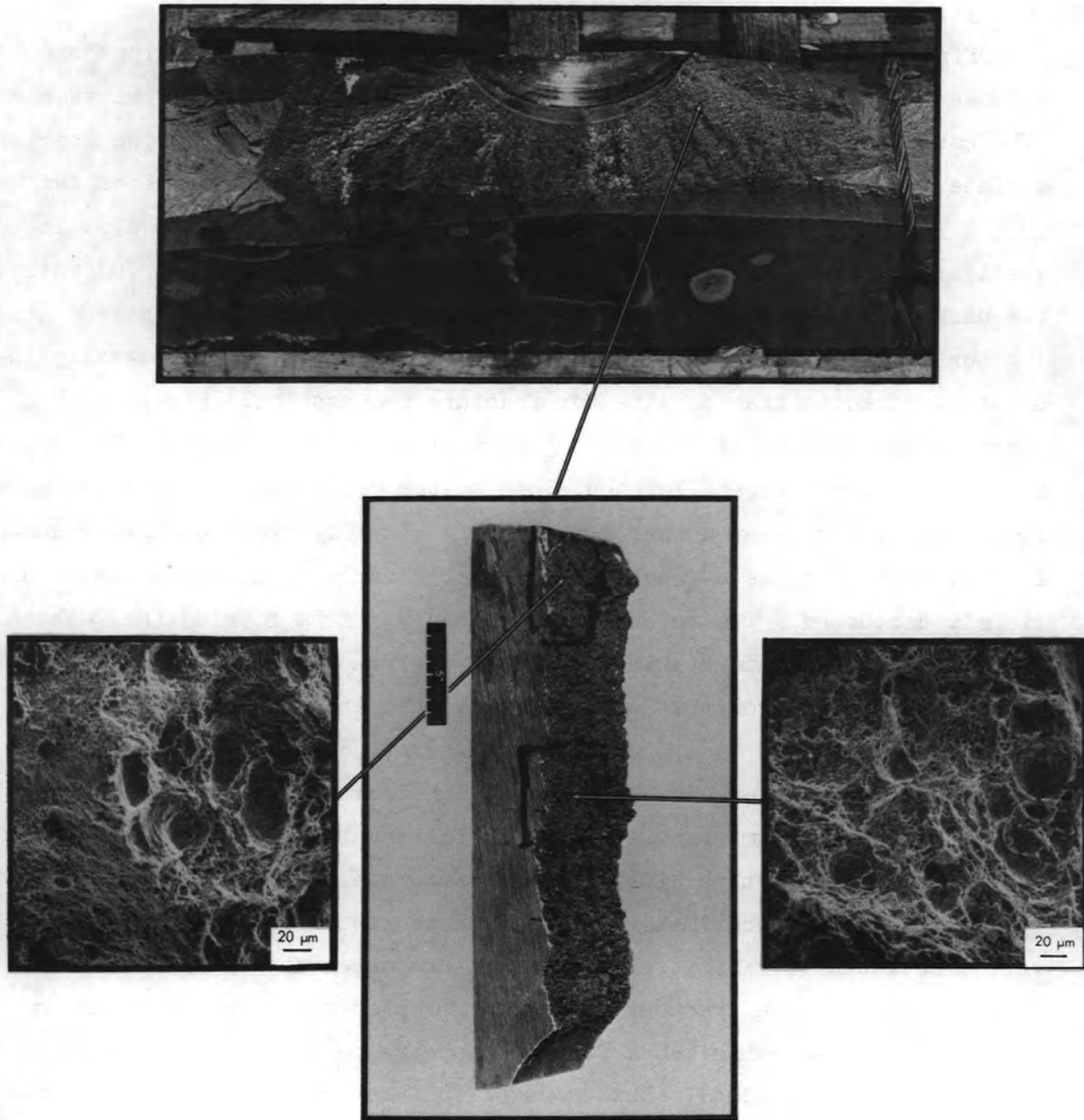


Fig. 4.16. Results of scanning electron microscopy study of fracture surface near the machined flaw. The two areas shown illustrate dimple mode of failure.

ITV VI ASTM A508 CL 2

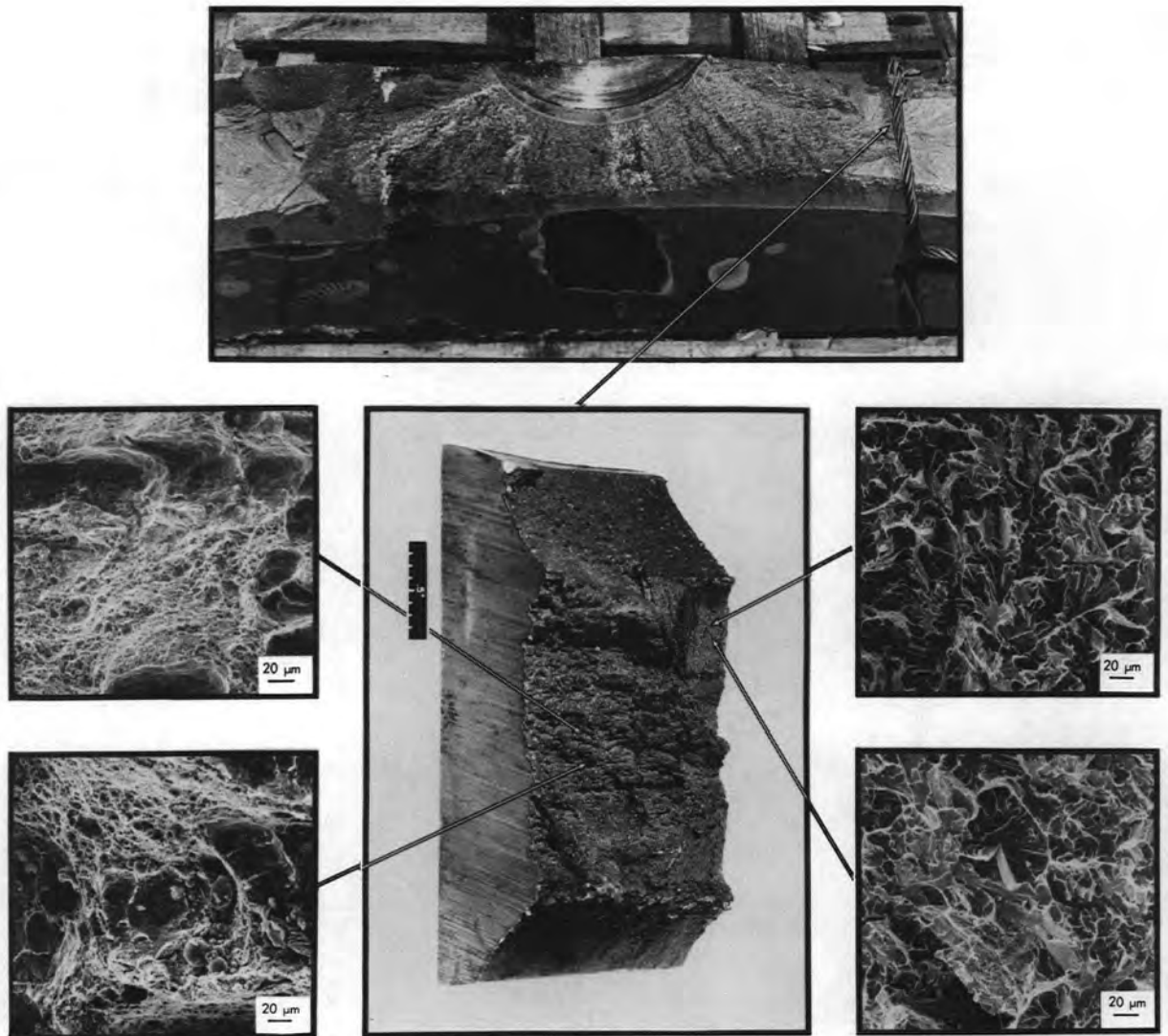


Fig. 4.17. Results of scanning electron microscopy study of region where failure mode changed from dimple to cleavage. SEM photomicrographs on left are dimples; those on the right show the cleavage mode of failure.

PROCUREMENT OF INTERMEDIATE TEST VESSELS

C. E. Childress

Three of the first six intermediate test vessels (V-1, V-2, and V-3) have been completed and found to be acceptable.¹⁰ A general description

10. C. E. Childress, *HSST Program Semiannu. Progr. Rep. Feb. 29, 1972*, ORNL-4816, pp. 96-99.

of all the vessels and the orientation of the shell courses within the original ingots is shown in Figs. 4.18 and 4.19.

Vessels V-4 and V-6 (and completed vessel V-3) contained longitudinal weld seams (V-6 contains two longitudinal weld seams 180° apart). On

ORNL-DWG 70-10047A

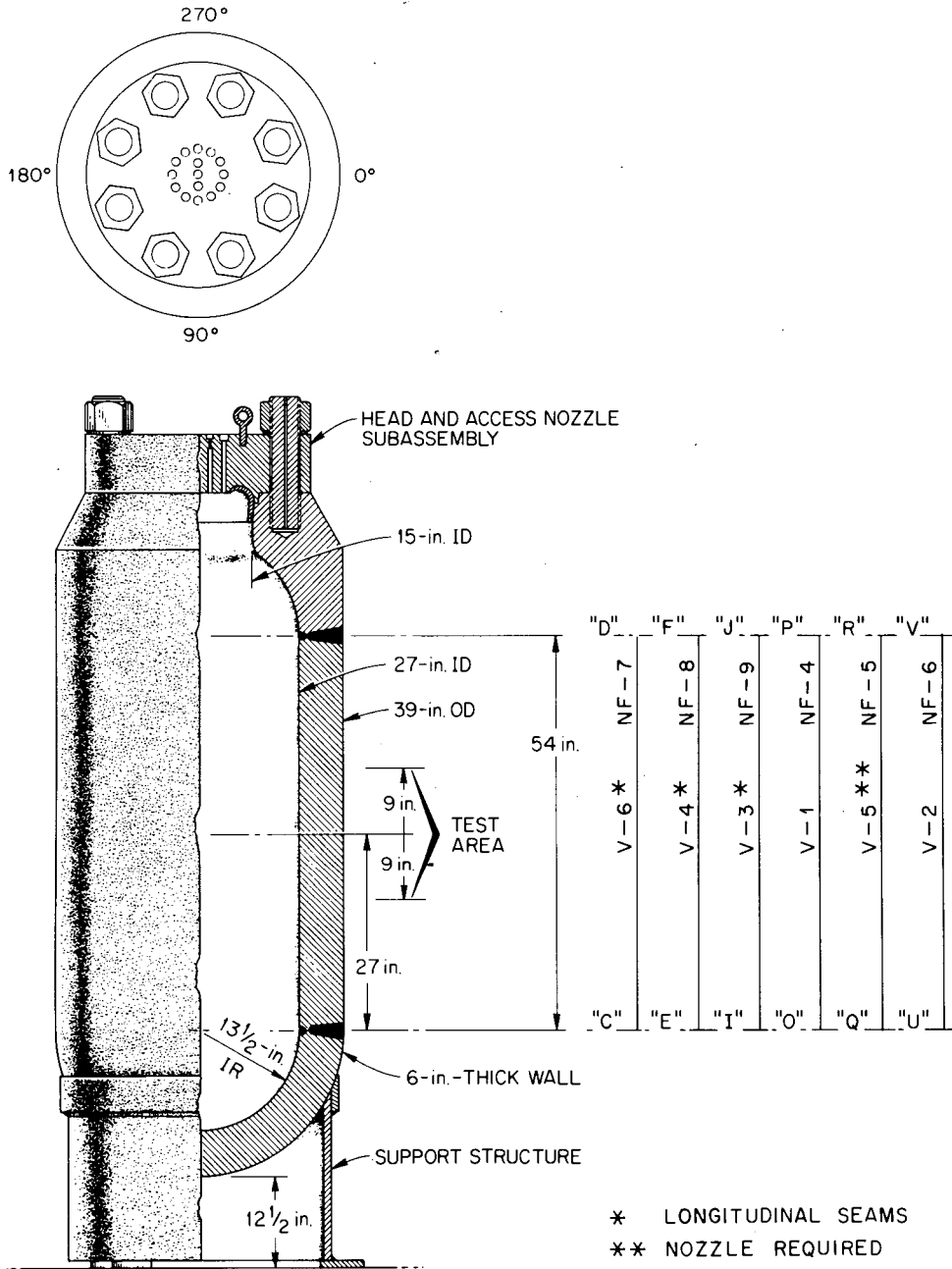


Fig. 4.18. Orientation of shell courses for intermediate test vessels.

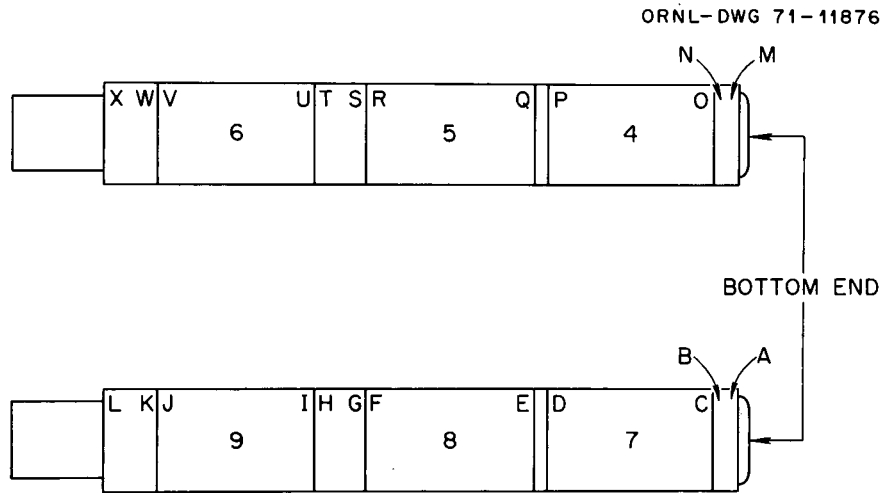


Fig. 4.19. Identification of shell courses by National Forge.

completion of these welds, radiographic inspection showed that they were unacceptable. They were then cut out and rewelded. Accordingly, the joint design for the longitudinal seams is somewhat at variance with (larger than) that shown previously (Fig. 4.25 of Ref. 11). It should be noted that no subsequent repairs were necessary to either of the longitudinal seams after the defective welds were cut out and rewelded.

Considerable difficulty was encountered in obtaining acceptable circumferential welds. The hemispherical head-to-shell seams of vessels V-5 and V-6 were the only welds that did not require repairs. In some cases, four repair attempts were necessary before the welds were acceptable.

In a few cases, the weld defects were found by radiographic inspection, but in most cases the welds failed to meet the ultrasonic inspection requirements. Each of the welds was inspected ultrasonically in accordance with the technique defined in Paragraph N-625 of Section III ASME Nuclear Code. The Taylor Forge test procedure specified that all shear-wave indications producing signals equal to the height of the distance amplitude correction (DAC) curves or straight beam indications causing 100% loss of back-surface reflection are rejectable. The reference block used for instrument calibration is shown in Fig. 4.20. All the

11. C. E. Childress, *HSSST Program Semiannu. Progr. Rep. Aug. 31, 1971*, ORNL-4764, pp. 62-67.

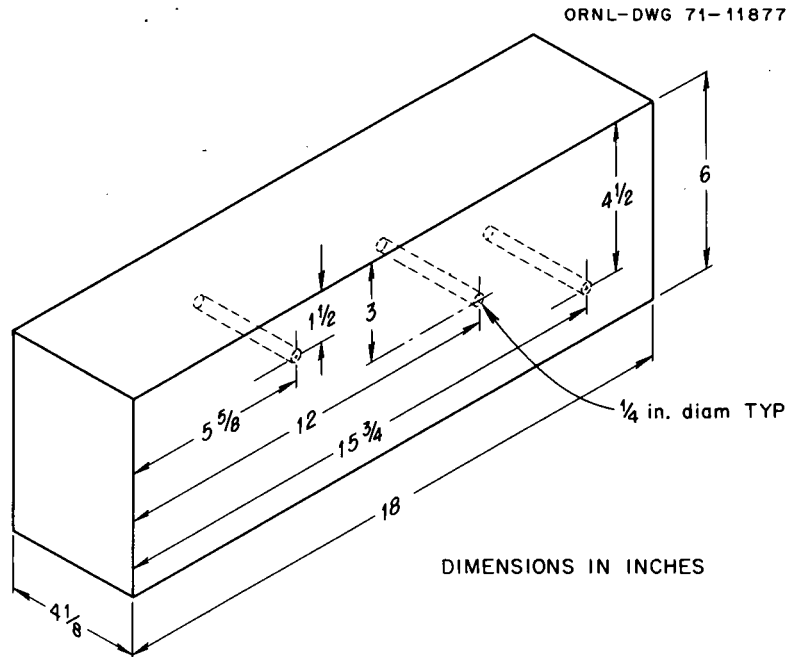


Fig. 4.20. Ultrasonic reference standard.

rejectable indications were found by shear-wave inspection, most of them near the $3/4T$ level.

Vessel V-4 contained the fewest repairs of all vessels discussed in this section and was free of "rejectable" indications on final inspection. As many as four repair attempts were made on the circumferential seams of V-5 and V-6, after which rejectable ultrasonic indications were still being found (four in the top circumferential seam of V-5 and one each in the top and middle girth seams of V-6). In consideration of the fact that further repairs could be more detrimental than helpful and to expedite delivery, we decided to accept V-5 and V-6 with these imperfections.

As noted previously, most of the defects found by ultrasonic inspection were not detectable by radiography. However, Taylor Forge reported that they observed the grinding in some of the repair areas and that they could actually see the defects as they were uncovered. They reported that the defects appeared to be small "stringer-like" inclusions that were very tight and usually $1/2$ to $3/4$ in. long and $1/8$ to $3/4$ in. high.

In all cases, porosity was observed immediately before grinding into a "stringer."

Each vessel successfully withstood a hydrostatic pressure test of 12,500 psi on completion of final postweld heat treatment (PWHT). Following ultrasonic inspection, the welds of each vessel were inspected with magnetic particles on both OD and ID surfaces. The vessels were then helium leak tested by pressurizing with a mixture of helium and nitrogen. In each case the leak rate was less than the minimum requirement of 5.8×10^{-5} std cc/sec.

Four additional vessels, similar to the first six except that the shell courses will be made from A533 grade B, class 1 plate, have been ordered.

TESTING OF 6-IN.-THICK INTERMEDIATE TEST VESSELS

R. W. Derby

Three additional 6-in.-thick intermediate test vessels (V-2, V-3, and V-4) were instrumented and pressurized to failure. The results from these tests are summarized below.

Vessel V-2

Vessel V-2 was a duplicate vessel, insofar as possible, of vessel V-1. The only desired difference in this test from that of vessel V-1 was the test temperature.¹² The extensive properties data from the prolongation of vessel V-2 have already been summarized in this chapter and in Ref. 13.

The test of vessel V-2 was initiated on September 28, 1972, at a nominal test temperature of 32°F. A picture of vessel V-2 fully instrumented is shown in Fig. 4.21. The wood frame is part of a mirror device set up to allow the crack monitor cameras to view the vessel flaw remotely.

12. R. W. Derby, *HSST Program Semiannu. Progr. Rep. Aug. 31, 1972*, ORNL-4855, pp. 44-55.

13. P. C. Riccardella et al., *HSST Program Semiannu. Progr. Rep. Aug. 31, 1972*, ORNL-4855, pp. 40-44.

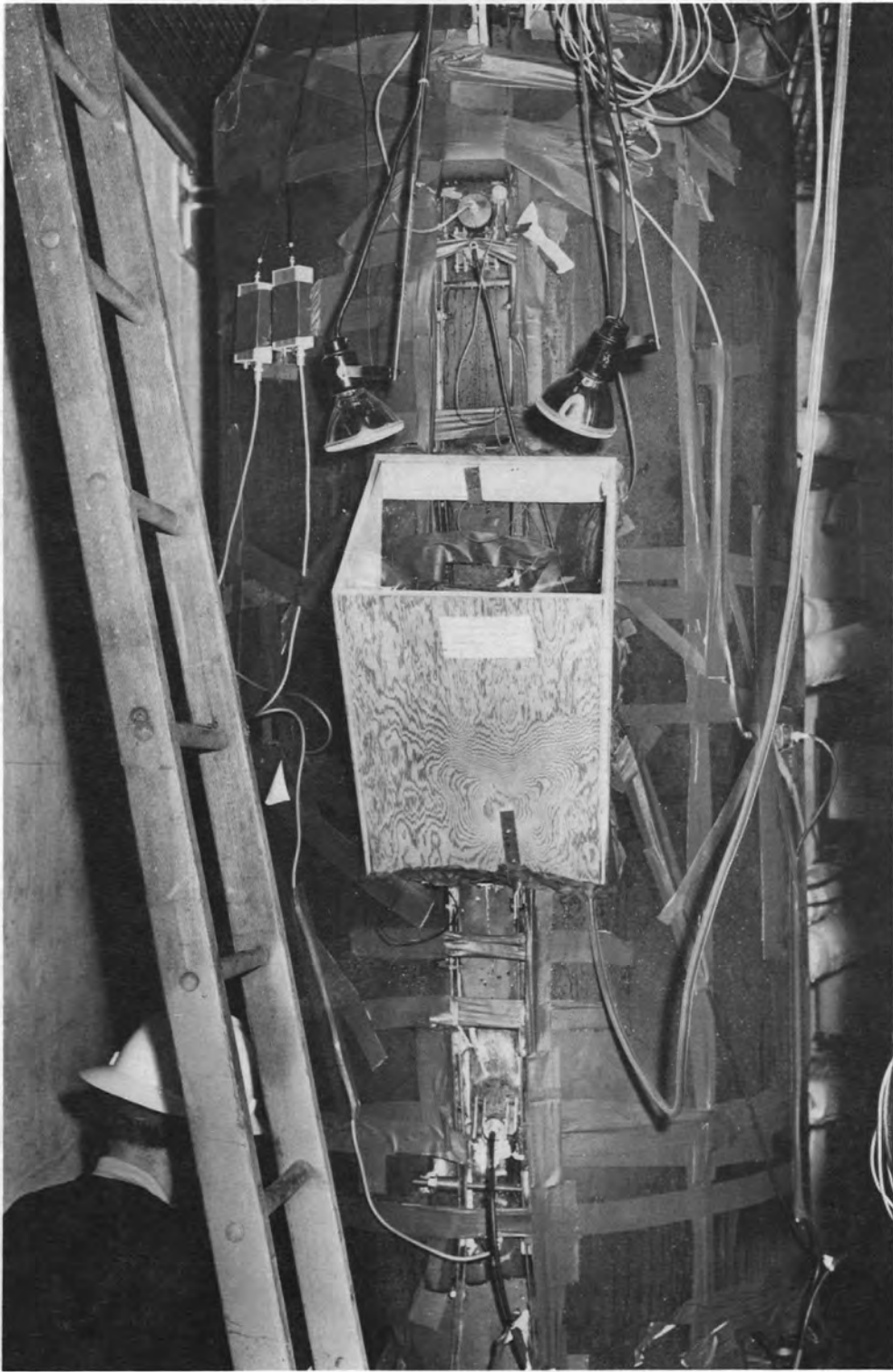


Fig. 4.21. Intermediate test vessel V-2 fully instrumented and ready for testing.

Vessel V-2 was pressurized to a predetermined pressure, and a hold period was taken for obtaining and evaluating pertinent data. During the test the pressurizer developed a leak in the seals, first on one side and then on the other, and no greater pressure could be obtained. At the termination of the first pressurization cycle, a pressure of about 24,500 psi had been reached. The seals in the pressurizer were replaced, and the test was reinitiated. The vessel failed at a pressure of 27,900 psi. The temperature in the flaw at failure was 30°F.

The experimental pressure-strain curve obtained during the test of vessel V-2 of the outside surface circumferential strain 180° from the flaw is given in Fig. 4.22. As may be seen, gross yielding through the vessel wall was just initiating.

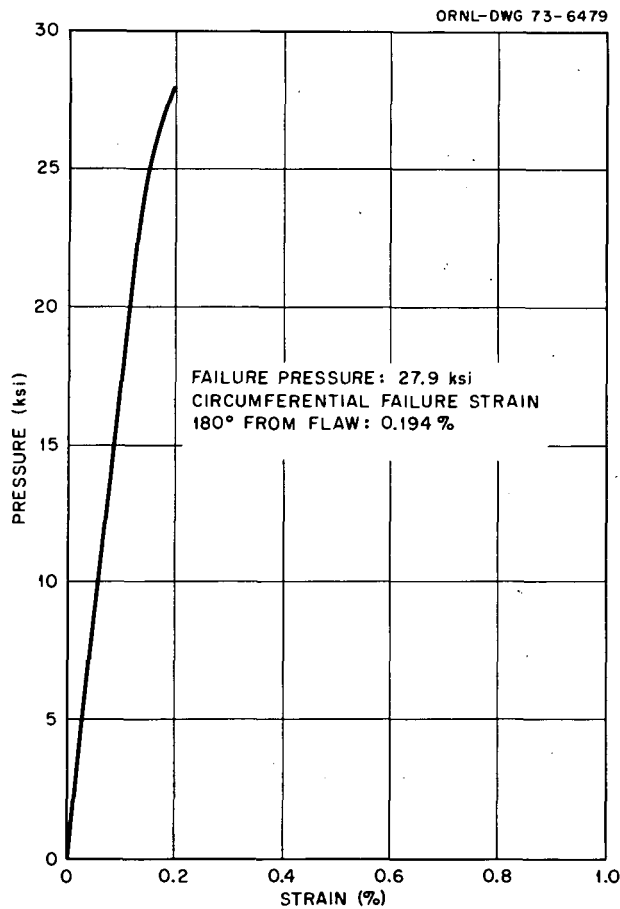


Fig. 4.22. Pressure-outside surface circumferential strain curve 180° from flaw - intermediate test vessel V-2.

Considerably greater strain existed in the region of the flaw. Outside surface data near the flaw are given in Fig. 4.23, which shows that a strain of 0.8% was obtained very close to the flaw. A comparison of results from various internal gages, given in Fig. 4.24, again shows that gross yielding of the vessel was commencing with strains directly under the flaw less than the nominal strain.

The results from the crack-opening-displacement measurements are given in Fig. 4.25.

In summary, the results of the strain measurements show that gross yielding had begun on both the inside and outside of the vessel at failure, whereas yielding was well under way close to the flaw. Thus the failure was not a "brittle fracture" in the traditional sense; that is,

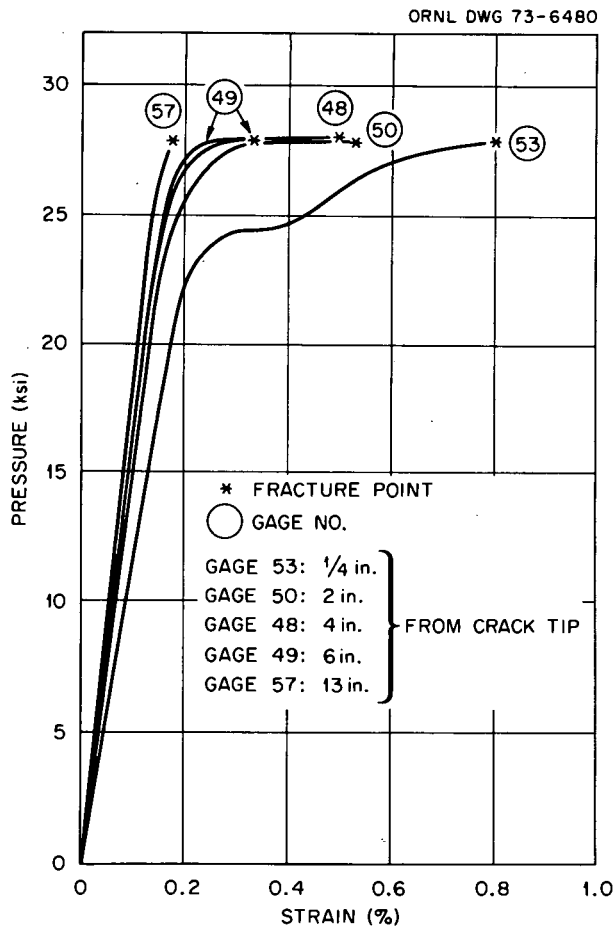


Fig. 4.23. Pressure—outside surface circumferential strain curves in line with flaw — intermediate test vessel V-2.

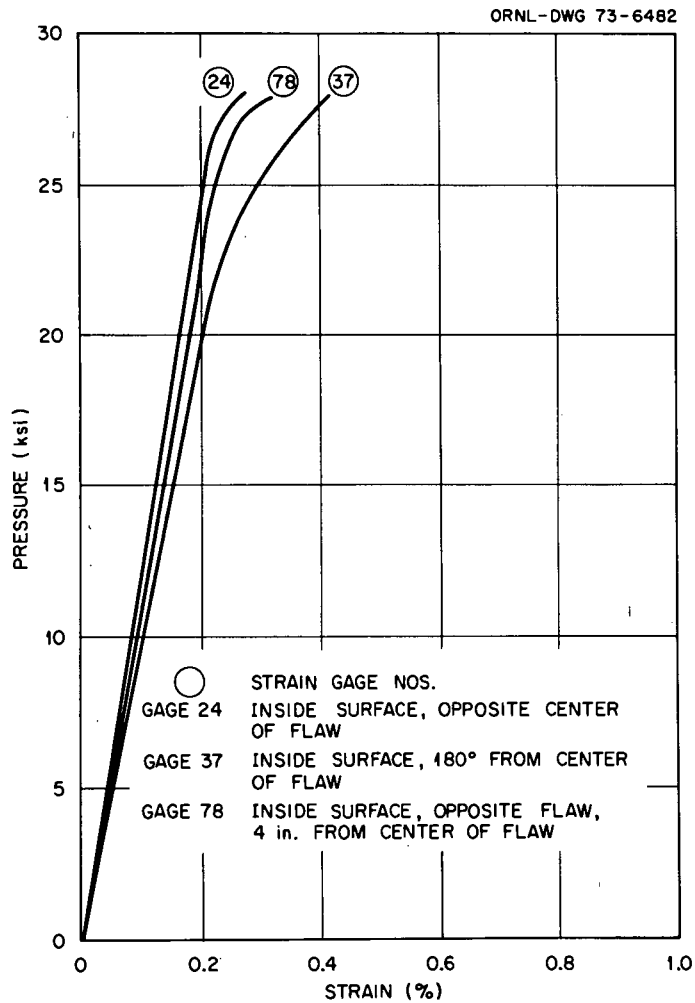


Fig. 4.24. Comparison of pressure-inside surface circumferential strain curves - intermediate test vessel V-2.

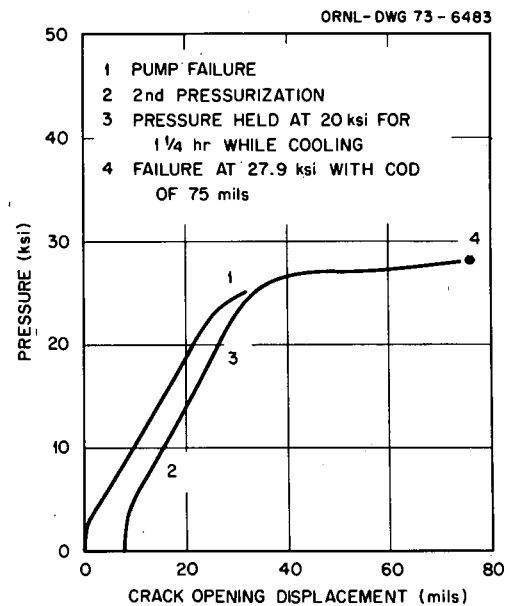


Fig. 4.25. Crack opening displacement vs pressure - intermediate test vessel V-2.

it did not occur below general yielding and was accompanied on a local level by significant plastic strains.

The propagation characteristics of vessel V-2 at fracture were as expected — catastrophic and complete with degrees of fragmentation. An annotated photograph of the vessel in the test pit immediately after the test is shown in Fig. 4.26 (note the flaw). One large fragment is seen to have been formed. In general, the vessel had many cracks, indicating the near generation of additional fragments. The vessel after removal from the test pit is shown in Fig. 4.27, in which the fragments of one of the model vessels tested at -55°F may also be seen.

Vessel V-2 was again monitored during pressurization by acoustic emission devices by Southwest Research Institute. A final report on the results from both vessels V-1 and V-2 is in preparation.

Extensive predictions and calculations of the behavior of vessels V-1 and V-2 were made. Complete discussions of all the test results, calculations, and complementary results, including acoustic emission data, are reported for vessels V-1 and V-2 in Ref. 14.

Vessel V-3

Intermediate test vessel V-3 was a duplicate of vessels V-1 and V-2 except it contained a submerged-arc longitudinal weld seam. A sharp flaw, supposedly the same size as was in the prior vessels, was placed on the outside surface of the weld seam midway along the length of the cylindrical course. Materials properties data on the weld metal were presented previously in this chapter. A test temperature of 130°F was selected.

Vessel V-3 was tested to failure on November 8. The maximum pressure reached was 31,000 psi, and the gross section outside surface circumferential strain 180° from the flaw was 1.47%. A plot of this pressure-strain curve is given in Fig. 4.28. The pressure-strain curves 17 in. from the center of the vessel (one 180° from the flaw in base metal

14. R. W. Derby et al., *Test of 6-in.-thick Pressure Vessels; Series 1: Intermediate Test Vessels V-1 and V-2*, ORNL-4895 (in publication).

PHOTO 3647-72

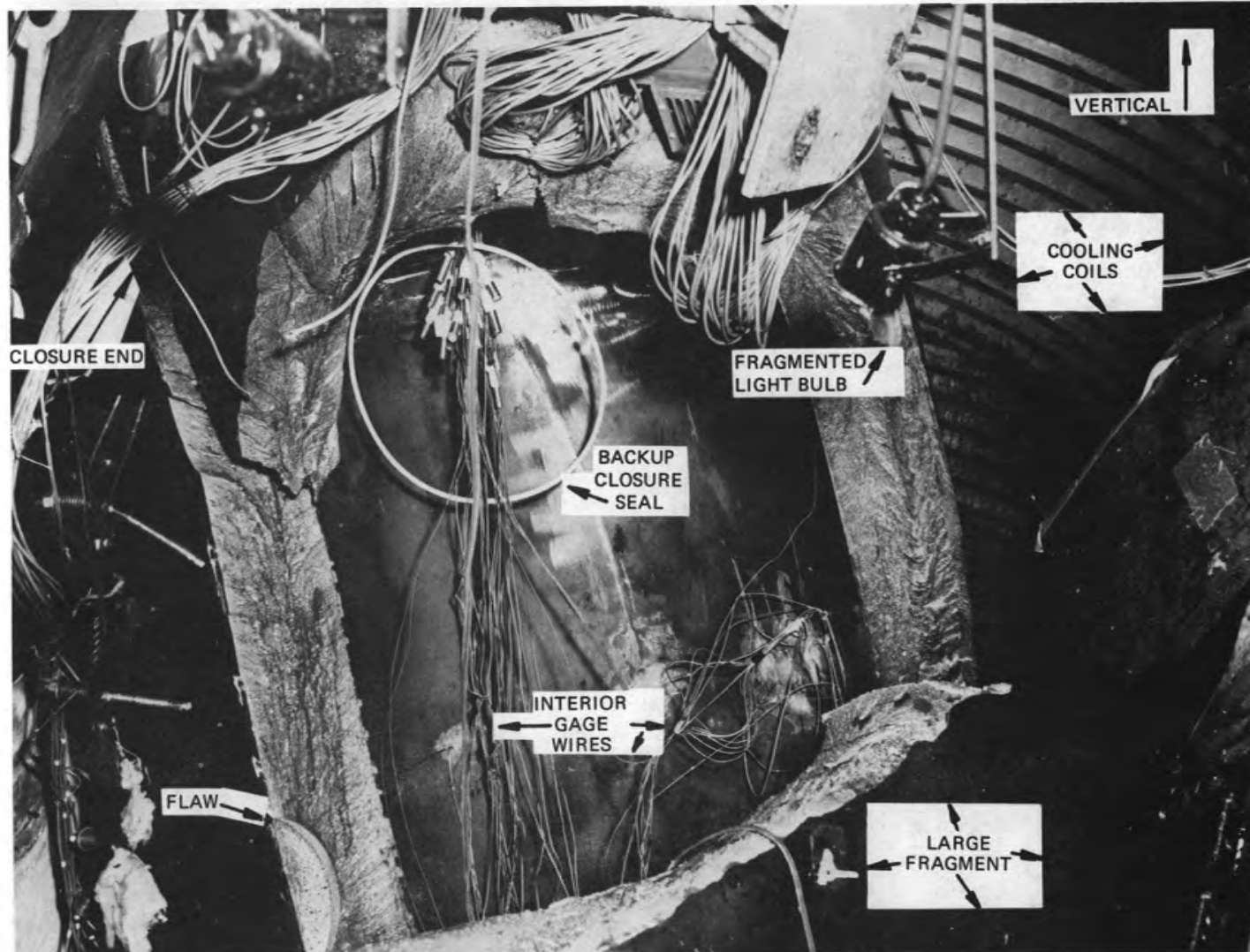


Fig. 4.26. Intermediate test vessel V-2 immediately after fracture.

PHOTO 4060-73



Fig. 4.27. Intermediate test vessel V-2 removed from test pit after fracture. Fragments of a small model vessel tested at -55°F are shown in foreground.

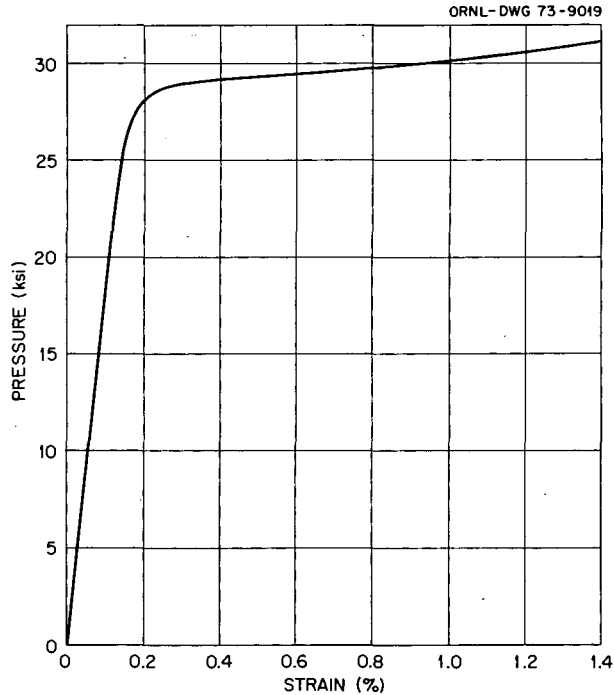


Fig. 4.28. Plot of pressure—outside surface circumferential strain curve 180° from flaw — intermediate test vessel V-3.

and the other aligned with the flaw in weld metal) are compared in Fig. 4.29. This comparison shows that the behavior of the weld metal (about a 1-in.-wide longitudinal strip) in the vessel is somewhat different from that in the base metal in the elastic region, but that the weld metal conforms to the plastic behavior of the base metal after considerable yielding has occurred. Typical pressure-strain plots at various locations along the weld seam are given in Fig. 4.30. The plot of crack-opening-displacement vs pressure is given in Fig. 4.31.

A photograph of the fracture surface is given in Fig. 4.32. The fracture propagated in the heat-affected zone on base metal in a flat fracture mode with shear lips similar to that in vessel V-1. The first three fractured vessels are shown in Fig. 4.33.

Following the fracture of vessel V-3, it was found that the fatigued crack was slightly longer (8.50 in.) and considerably shallower (2.11 in.) than those in vessels V-1 and V-2. This flaw size was sufficiently different from that anticipated (8.25 in. long by 2.55 in. deep) that the

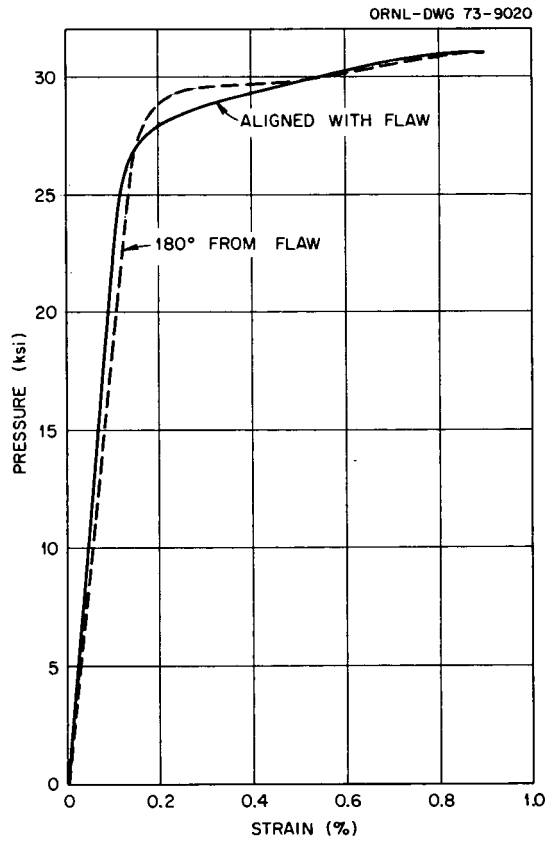


Fig. 4.29. Comparison between pressure—outside surface circumferential strain curves 17 in. from center line of vessel, one located 180° from flaw in base metal and one aligned with flaw in weld metal — intermediate test vessel V-3.

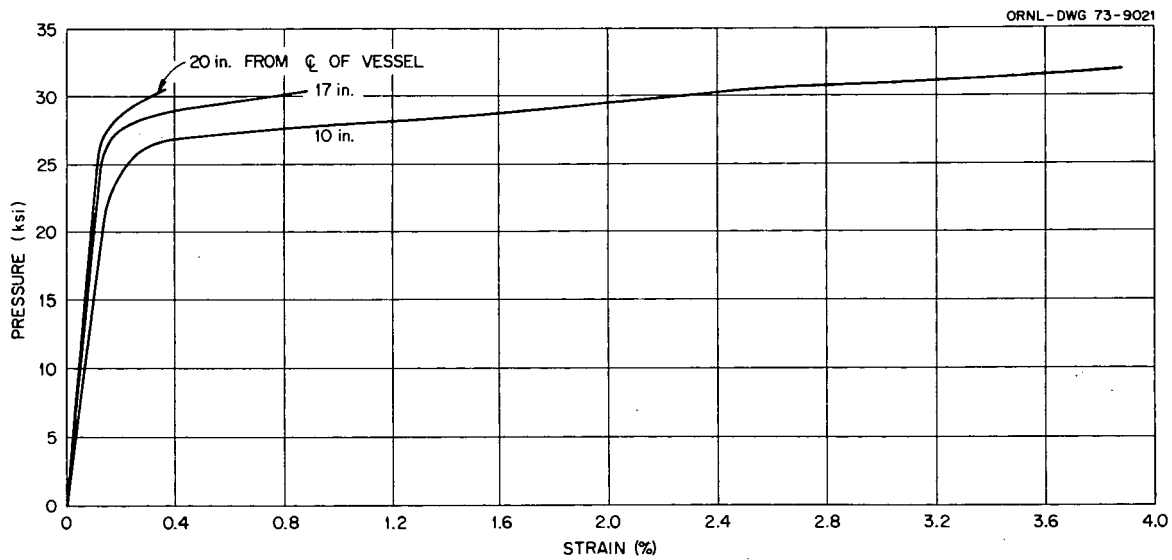


Fig. 4.30. Pressure—outside surface circumferential strain plots at various locations in weld seam aligned with flaw — intermediate test vessel V-3.

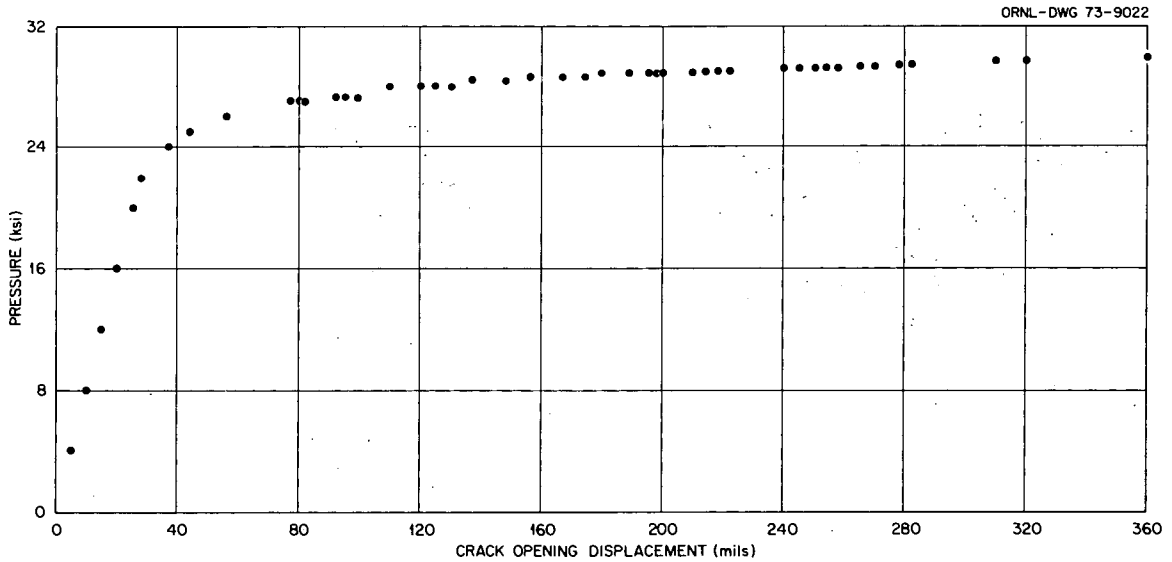


Fig. 4.31. Plot of pressure-crack opening displacement for intermediate test vessel V-3.

fracture calculations based on the anticipated flaw size are not expected to be accurate. Acoustic emission monitoring was performed on this vessel by Westinghouse Electric Corporation and will be summarized in a later report.

Vessel V-4

Intermediate test vessel V-4 was a duplicate of vessel V-3. Two sharp flaws, each supposedly the same size as those in vessels V-1 and V-2, were placed on the outside surface of the vessel midway along the cylindrical course. One flaw was in the weld seam and one in base metal 90° away. Materials property data for both weld and base metal were presented previously in this chapter. A test temperature of 75°F was selected.

Vessel V-4 was tested to failure on December 20. The maximum pressure was 26,500 psi, and the gross section circumferential strain away from the flaw was 0.17%. Failure occurred at the flaw in the weld. The failure strain was lower than anticipated; however, upon examination of the fracture, the flaw in the weld was found to be 3 in. deep instead

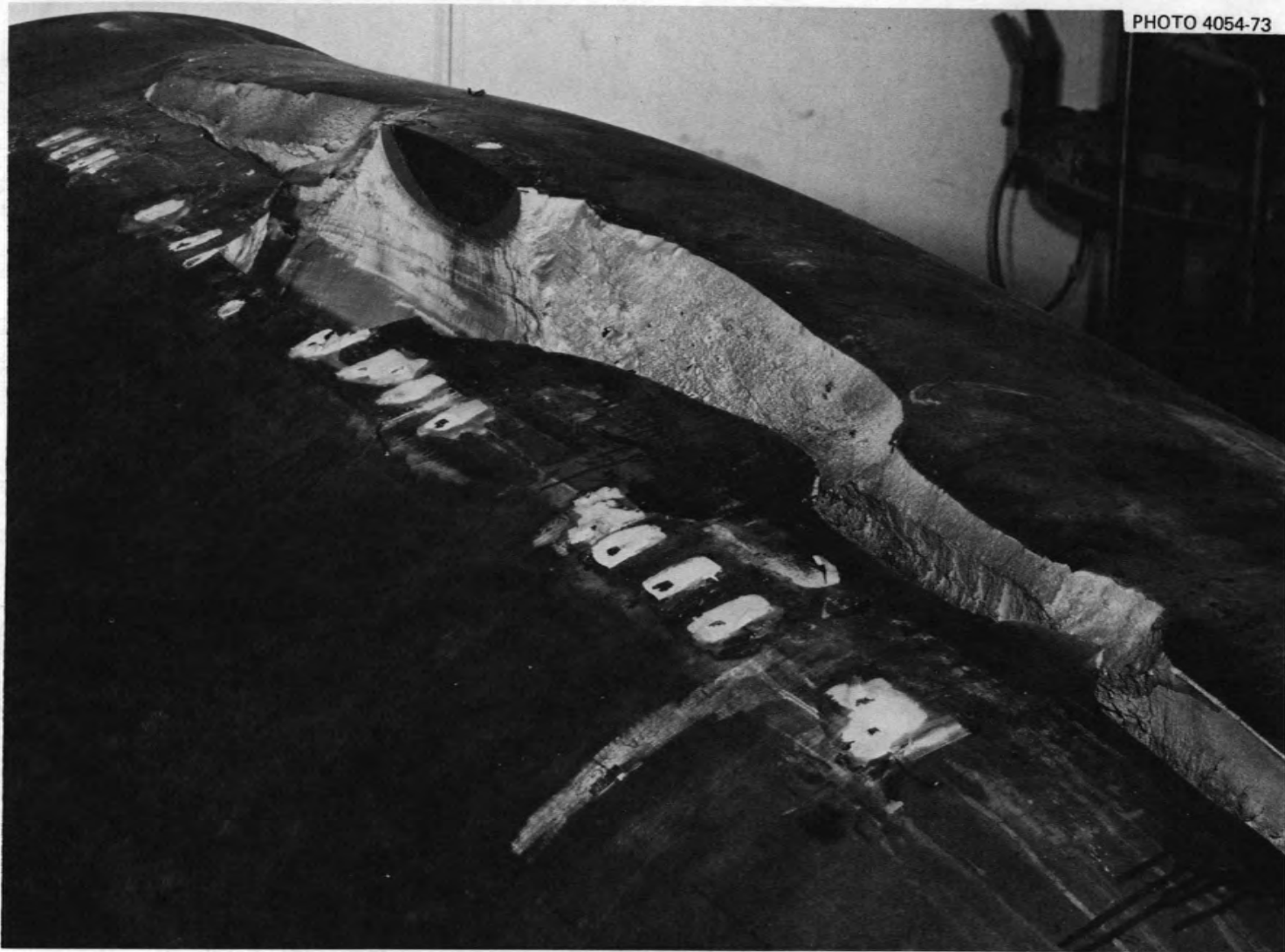


Fig. 4.32. Fracture region of intermediate test vessel V-3.

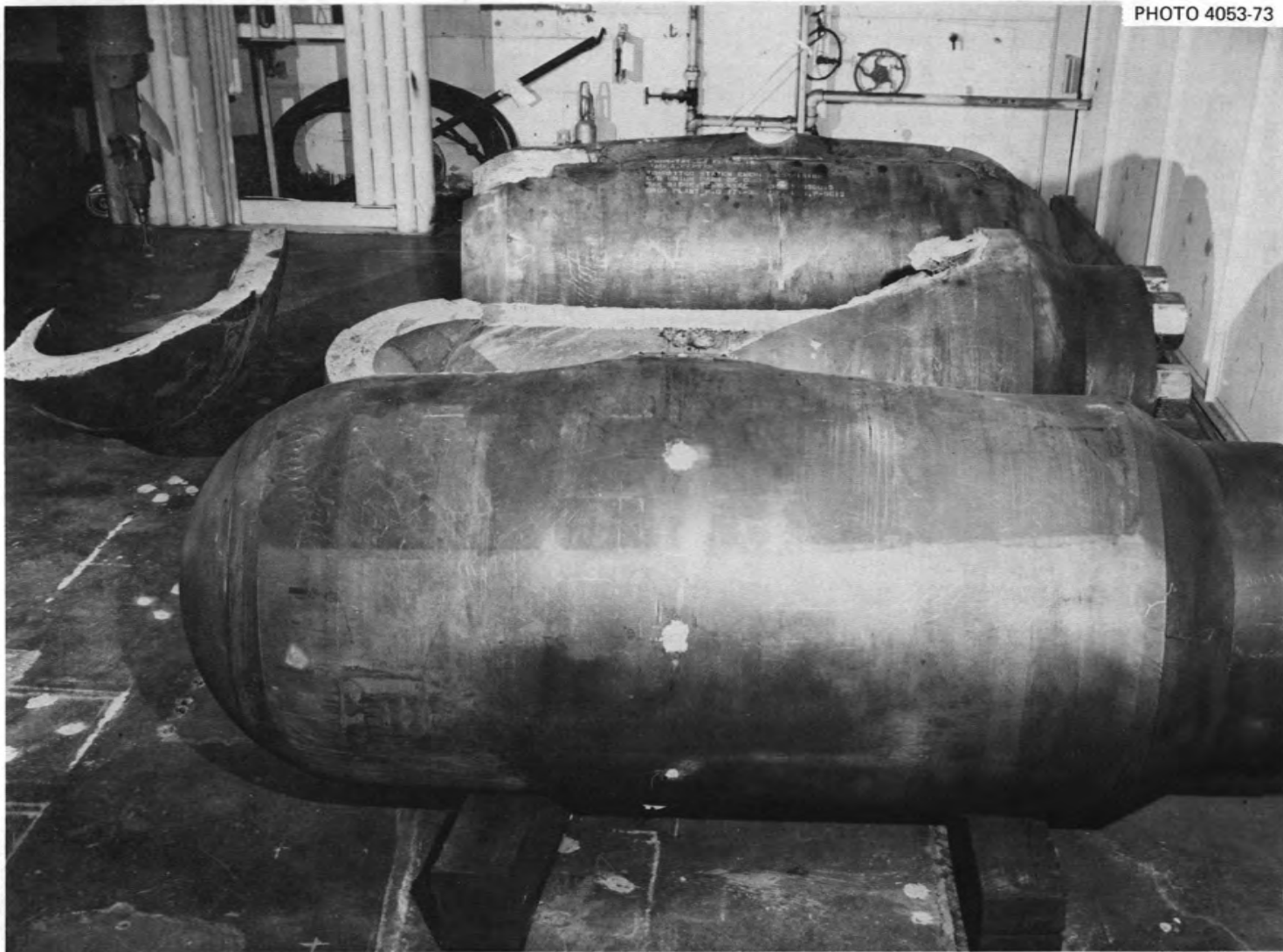


Fig. 4.33. Picture of the first three fractured intermediate test vessels.

of the desired depth of about 2.5 in. Subsequent investigations revealed that the base metal flaw was also about 3 in. deep.

Plots of the pressure—nominal outside surface circumferential strains at different locations along a longitudinal element are given in Fig. 4.34. Similar plots aligned with both flaws are given in Figs. 4.35 and 4.36. As seen the behavior of vessel V-4 was similar to that of vessel V-2; however, V-4 exhibited less ductility local to the flaw. The crack opening displacements were less than 0.1 in. for each flaw.

Figure 4.37 shows vessel V-4 after fracture along with a model tested at 0°F that exhibited a similar fracture. The cracks propagated in a flat mode the full length of the cylindrical course and well into the hemispherical head.

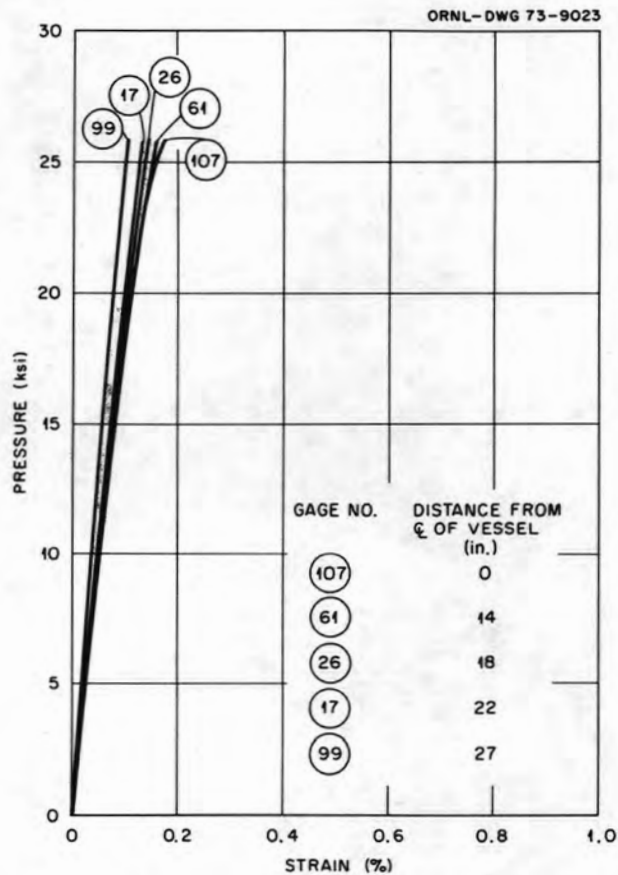


Fig. 4.34. Plot of pressure—outside surface circumferential strain along an axial element remote from the flaws as a function of distance from the center line — intermediate test vessel V-4.

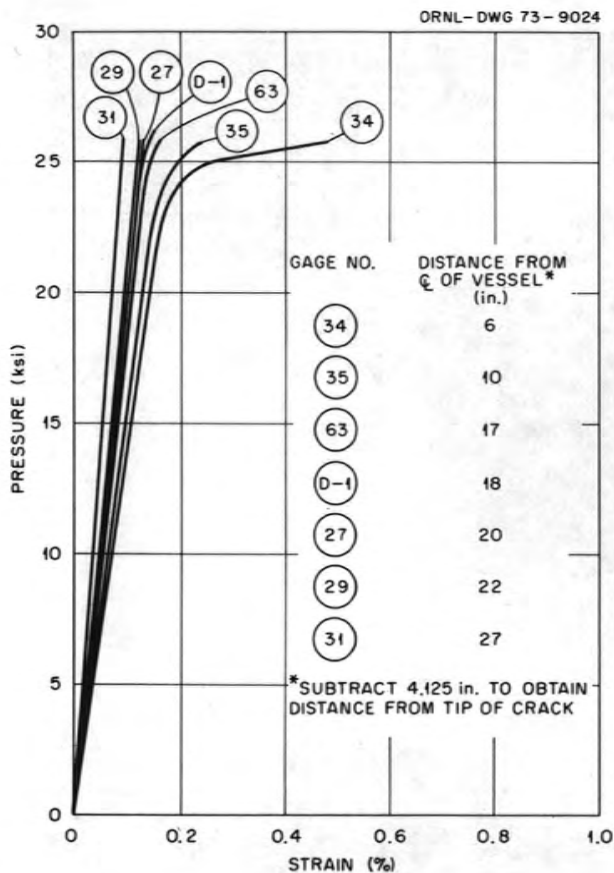


Fig. 4.35. Plot of pressure—outside surface circumferential strain aligned with the flaw in the weld metal — intermediate test vessel V-4.

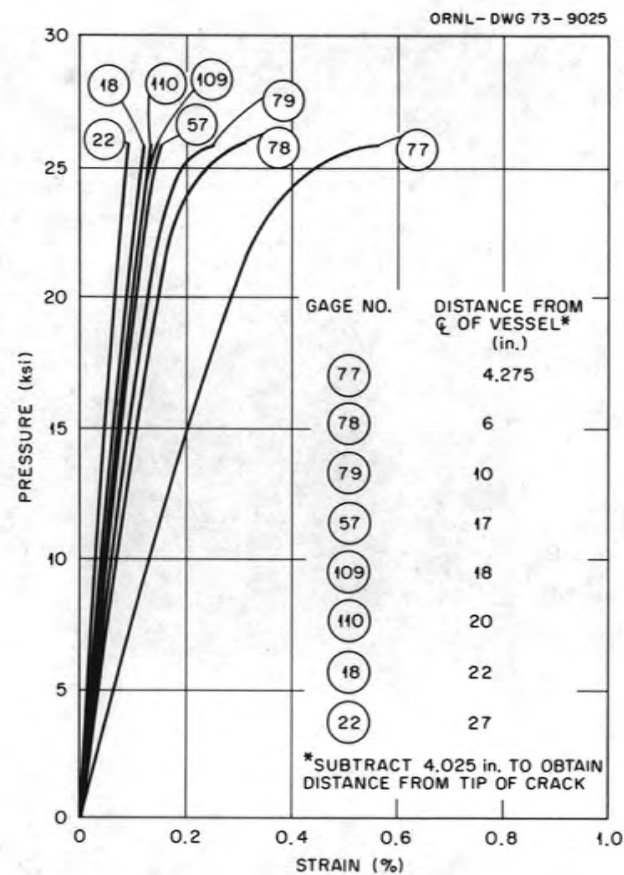


Fig. 4.36. Plot of pressure—outside surface circumferential strain aligned with the flaw in the base metal — intermediate test vessel V-4.



Fig. 4.37. Intermediate test vessel V-4 removed from test pit after fracture.

Summary of Results and Future Plans

The results from the first four vessel tests are summarized in Table 4.4. The next vessel scheduled for testing is vessel V-6, which contains both longitudinal and girth welds in the cylindrical course. Additional research is in progress to develop more accurate techniques for monitoring crack growth during the fatigue sharpening of the flaw.

INVESTIGATION OF MODE III CRACK EXTENSION IN REACTOR PIPING¹⁵

R. J. Podlasek
Battelle Columbus Laboratories

This report summarizes the results of a research program investigating the nature and extent of mode III - tearing shear fractures in nuclear reactor piping. The study was started in April 1972, and to date, four full-scale rupture experiments have been conducted. The results of the first two experiments were presented in a previous progress report.¹⁶ The results of the last two experiments and a discussion of all four experiments are given here.

Introduction

The results of a previous investigation¹⁷ examining the fracture behavior of nuclear reactor piping indicated that if the saturation pressure stress level was below a threshold level,¹⁸ axial ductile cracks would not propagate. However, the results of one experiment (experiment 32) indicated that it may be possible to propagate a tearing shear crack

15. Work sponsored by HSST program under UCCND Subcontract 3678 between Union Carbide Corporation and Battelle Columbus Laboratories.

16. R. J. Podlasek, *HSST Program Semiannu. Progr. Rep. Aug. 31, 1972*, ORNL-4855, pp. 64-72.

17. R. J. Eiber et al., *Investigation of the Initiation and Extent of Ductile Pipe Rupture*, BMI-1908 (June 1971).

18. The threshold level was experimentally determined to be approximately 12,000 psi for A106-B pipe. Since that time, an empirical formulation has been developed to predict this level for other pipe sizes and materials.

Table 4.4. Summary of test results - V-1 through V-4

Vessel No.	Date	Temperature (°F)	Burst pressure (kpsi)	Gross strain (%)	Flaw location	Flaw depth (in.)	Flaw length (in.)
V-1	June 30	130	28.7	0.90	Base metal	2.56	8.25
V-2	September 28	32	27.9	0.19	Base metal	2.53	8.30
V-3	November 8	130	31.0	1.47	Longitudinal weld seam	2.11	8.50
V-4	December 20	75	26.5	0.17	Longitudinal weld seam	3.00	8.25

which spirals around the pipe at a saturation pressure stress level below the threshold level. In this previous research program, experiment 32, in which tearing shear fracture was obtained, was conducted at 545°F. The test specimen consisted of a 10-ft length of 7.5-in.-OD by 0.500-in. wall, A106-B pipe with two 36-in.-OD by 1.0-in.-wall reservoirs 5 ft long attached to each end and a side heating loop of 8-in.-OD pipe connecting the two reservoirs. The axial flaw which was placed in the center of the 7.5-in.-OD pipe was 20 in. long and 85% through the wall. In this experiment, a tearing shear fracture propagated for approximately one-half of the test specimen length.

The first experiment in the current research investigation was designated as experiment 35. The objective of this experiment was to determine if extensive tearing shear fracture propagation could be obtained in a straight specimen without reservoirs. Using material from the same joint of pipe as experiment 32 and the same flaw geometry, a test specimen for experiment 35 was fabricated. Experiment 35 was conducted at the same temperature and pressure as experiment 32 (545°F and 1640 psi). In the experiment, the fracture propagated axially 14 in. in one direction, with 1 in. of tearing shear fracture at the end, and 13 in. in the other direction, with 5 in. of tearing shear fracture at the end.

It was suspected that a longer initial flaw might aid in extending the length of the mode III fracture; thus experiment 36 was fabricated using the same material and flaw depth, but the initial flaw length was doubled. This test specimen failed at a temperature of 575°F and a pressure level of 1754 psig. The results of this experiment were similar to those of experiment 35. The crack extended axially 16.5 in. in one direction and 20.0 in. in the other direction, and 1 in. of tearing shear fracture was observed at each end.

In pipe rupture experiments using subcooled water as the pressurizing medium, as the rupture opening in the pipe develops, the pressure decays from the failure pressure to the saturation pressure corresponding to the water temperature. In the experiments using 20-ft test sections without reservoirs, it is believed that the decompression to the saturation pressure occurred rapidly. However, in the case of experiment 32, it is suspected that, due to the reservoirs supplying additional

pressured water to the test section, the rate of pressure decay was significantly slower. Consequently, the pressure in the pipe during the test with the reservoir may have been greater on a relative basis. With this possibility in mind, experiment 37 was designed.

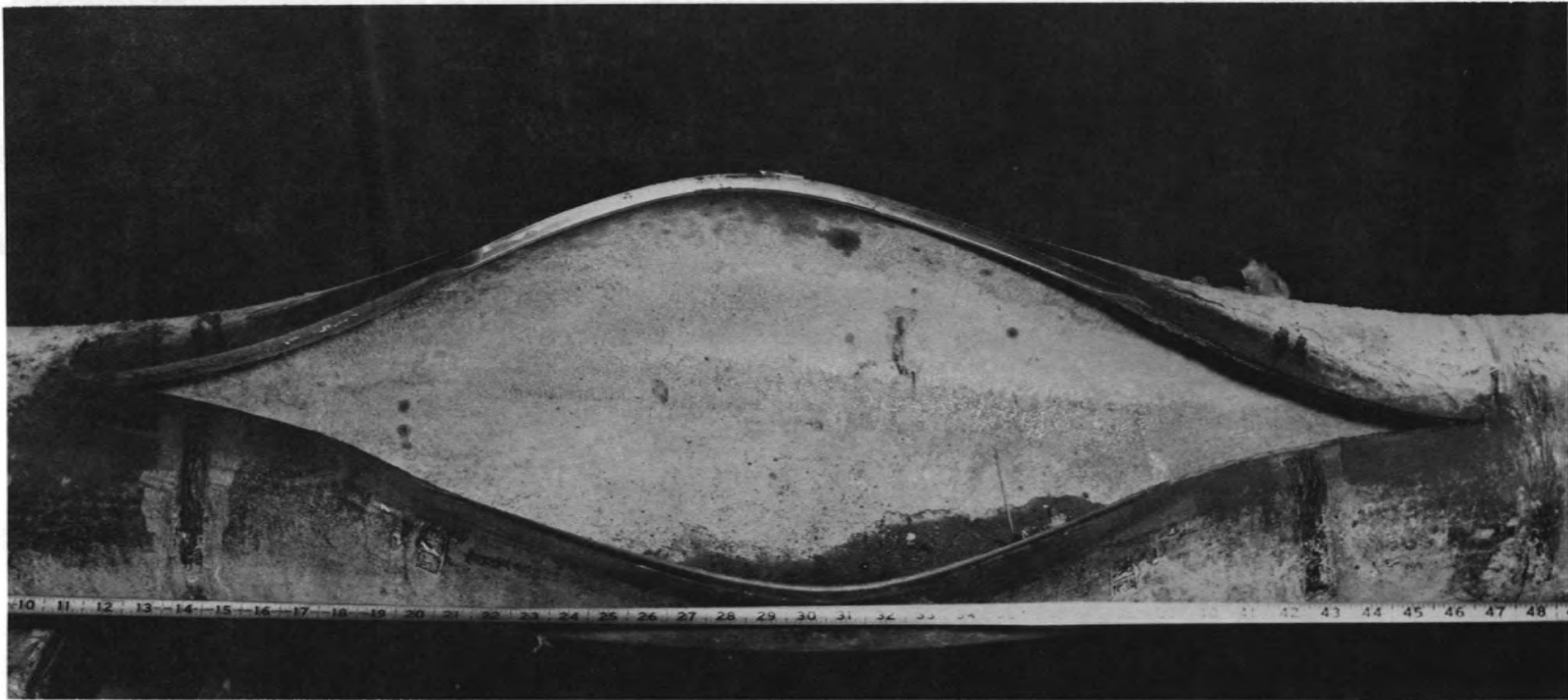
Results of Experiments 37 and 38

The objective of experiment 37 was to determine if a tearing shear fracture would be obtained when the saturation pressure increased to the failure pressure of experiment 32. Since the material used for the previous experiments was exhausted, a new length of A106-B pipe was purchased for this experiment. The results of the materials property tests on this newly acquired pipe indicated that the material was similar to that used in the previous experiments. The flaw geometry for experiment 37 was identical to that for experiment 32, and the failure temperature was designed to be 610°F (saturation pressure of 1640 psi). This saturation pressure was the same as the failure pressure in experiment 32.

While heating to 610°F, the test specimen in experiment 37 failed prematurely at 575°F and at a saturation pressure of 1230 psi. As shown in Fig. 4.38, the crack propagated axially 9.5 in. in one direction and 10.5 in. in the other. No tearing shear fracture occurred. It is believed that the lower than desired failure pressure occurred because the material beneath the extremely deep notch (85% through the wall) had a slightly different flow stress.

Based on the results of experiment 37, the flow stress of the new material was determined to be 45.5 ksi. Using a flow stress of 45.5 ksi and a desired pressure of 1940 psi, a 20-in.-long, 78% through-the-wall flaw was specified for a repeat specimen, experiment 38. This specimen was fabricated in the same manner as the previous specimens.

Test specimen 38 failed at 1830 psi and 610°F; the saturation pressure was 1660 psi. The failure hoop stress was 11.9 ksi, and the saturation pressure hoop stress was 10.8 ksi. As shown in Fig. 4.39, the crack propagated axially 40 in. in one direction and 38.5 in. in the other, but no tearing shear fracture resulted.



97

7131

Fig. 4.38. Photograph showing the results of experiment 37. The failure pressure was 1230 psi, and the temperature was 575°F.

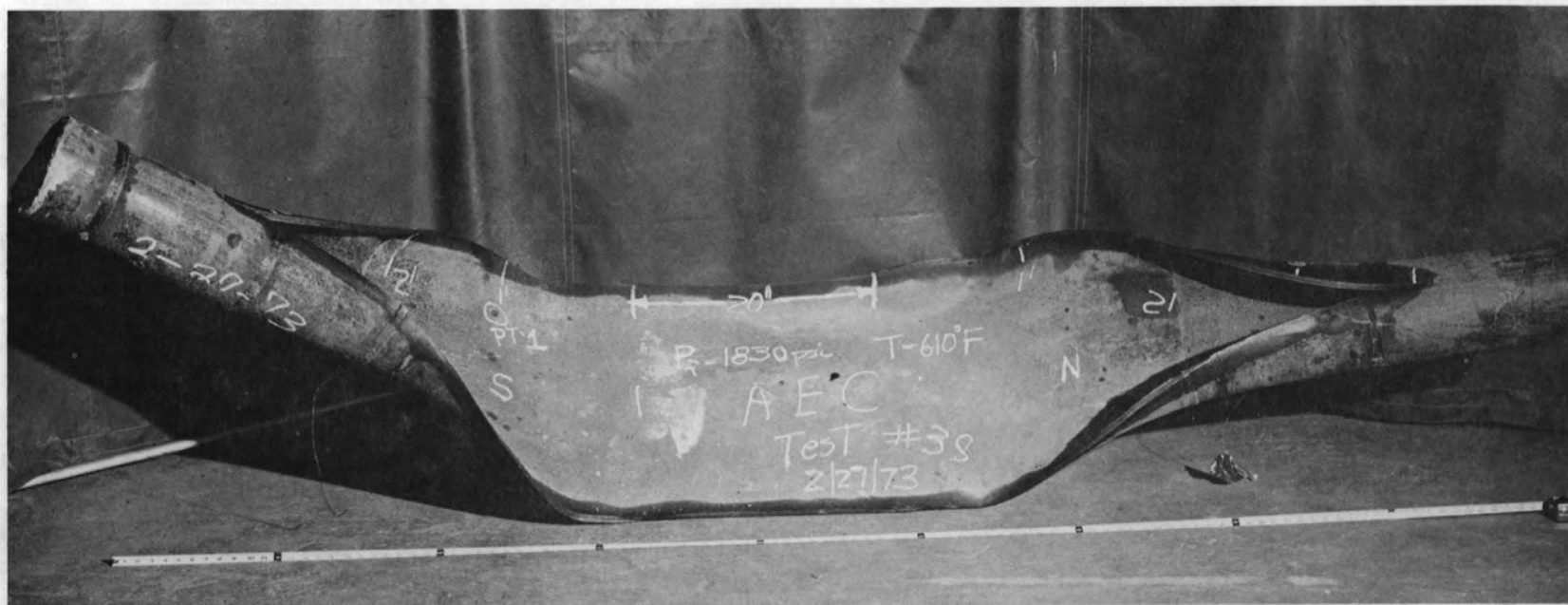


Fig. 4.39. Photograph showing the results of experiment 38. The failure pressure was 1830 psi, and the temperature was 610°F.

Future Work

Table 4.5 is a summary of the data from experiment 32 and the four experiments conducted in this phase. As seen in the table, the parameters of crack length, saturation pressure, and failure pressure were varied. The results of the four experiments conducted with 20-ft test specimens without reservoirs were not successful in duplicating the results of experiment 32, where an extensive mode III fracture was obtained. These results suggest that extensive mode III fracture from internal pressure stress alone may not be possible. It appears that the reservoirs present in experiment 32 may be necessary to obtain extensive mode III fracture propagation.

It is possible that in experiment 32 with reservoirs that the exiting pressurized water from the reservoir to the pipe produced a significant axial thrust that caused an additional axial tensile stress on the pipe. Thus, in experiment 32 the crack propagated in a biaxial stress field, where the nominal circumferential stress was the hoop pressure stress and the nominal axial stress was the sum of one-half the hoop stress and the stress from the axial thrust resulting from water exhausting from the reservoirs.

Plans are under way to perform additional work to clarify the conditions under which unstable mode III fracture is possible. The future work will focus on identifying the parameters which cause a long tearing shear fracture to propagate. The available literature related to the decompression of subcooled water will be examined to estimate the magnitude of the axial thrust expected during the test and to determine the influence of the size of the reservoir. It is believed that this information will enable a better understanding of the state of stress accompanying tearing shear fracture. Utilizing the results of the literature study and the previous experiments, another experiment will be designed. The specific test geometry and test parameters will be selected after the completion of the literature study.

Table 4.5. Summary of experimental results A106-B 7.5-in.-OD by 0.500-in.-wall pipe

Experiment	Reservoir	Flaw length (in.)	Flaw depth (in.)	Failure pressure (psi)	Failure temp. (°F)	Saturation pressure (psi)	Failure hoop stress (ksi)	Saturation hoop stress (ksi)	Remarks
32	Yes	20	0.419	1640	545	1058	11.0	7.1	Extensive mode III fracture propagation
35	No	20	0.419	1640	545	1058	11.0	7.1	Longitudinal fractures 14 and 13 in. long
36	No	40	0.419	1745	575	1270	12.4	9.0	Longitudinal fractures 20 and 16.5 in. long
37	No	20	0.429	1230	575	1230	8.6	8.6	Longitudinal fractures 10.5 and 9.5 in. long
38	No	20	0.391	1830	610	1660	11.9	10.8	Longitudinal fractures 40 and 38.5 in. long